

TECHNISCHE UNIVERSITÄT MÜNCHEN

Fakultät für Medizin

Natural-origin biopolymers and stem cells in chondral and osteochondral repair

Elisabeth Veronika Maria Amann

Vollständiger Abdruck der von der Fakultät für Medizin der Technischen Universität München zur Erlangung des akademischen Grades einer Doktorin der Medizin genehmigten Dissertation.

Vorsitz: Prof. Dr. Gabriele Multhoff

Prüfer der Dissertation: 1. Priv.-Doz. Elizabeth Rosado-Balmayor, Ph.D.

2. Priv.-Doz. Dr. Peter Prodingner

3. apl. Prof. Dr. Hans W. Gollwitzer

Die Dissertation wurde am 25.01.2021 bei der Technischen Universität München eingereicht und durch die Fakultät für Medizin am 07.12.2021 angenommen.

Table of contents

Table of contents	2
Abbreviations	4
Introduction	6
Cartilage tissue: Biology and function	6
Clinical problem	7
Current solutions	8
Limitations	10
Tissue engineering approach to cartilage regeneration.....	12
Aim of our study	13
Materials and methods	14
Outline	14
Production of gels and scaffolds.....	15
Chemical and morphological characterisation of the scaffolds.....	15
Cell isolation, co-culture and seeding on gels/scaffolds	18
Cell attachment, toxicity, viability and proliferation on gels and scaffolds.....	19
Evaluation of cell differentiation: ALP-activity, GAG-quantification, gene expression	21
Histology	22
Biomechanics	24
Oxygen levels of cell-loaded gels	25
Bioactivity assay of the scaffolds.....	25
Statistical evaluation.....	26
Discussion	27
Summary and Outlook.....	30
Summaries of publications included in this thesis.....	32
Summary of publication #1 - Hyaluronic acid facilitates chondrogenesis and matrix deposition of human adipose derived mesenchymal stem cells and human chondrocytes co-cultures	32
Summary of publication #2 - A graded, porous composite of natural biopolymers and octacalcium phosphate guides osteochondral differentiation of stem cells	33
References	35
List of figures	44

Acknowledgements	45
Appendix.....	46
Full research article “Hyaluronic acid facilitates chondrogenesis and matrix deposition of human adipose derived mesenchymal stem cells and human chondrocytes co-cultures ”	46
Elsevier permit for reuse	61
Full research article “A graded, porous composite of natural biopolymers and octacalcium phosphate guides osteochondral differentiation of stem cells”	62
Advance Healthcare Materials permit for reuse	80

Abbreviations

μCT	microcomputed tomography
AC	articular cartilage
ACI/ACT	autologous cartilage implantation/transplantation
ACs	articular chondrocytes
ALP	alkaline phosphatase
AMSCs	adipose derived mesenchymal stem cells
ANOVA	analysis of variance
BMSCs	bone marrow derived mesenchymal stem cells
CHI	chitosan
COL	collagen
DAB	3,3-diaminobenzidine
DMEM	Dulbecco's Modified Eagle Medium
DPBS	Dulbecco's Phosphate-Buffered Saline
dsDNA	double-stranded deoxyribonucleic acid
ECM	extracellular matrix
EDS	energy-dispersive X-ray spectroscopy
FCS	fetal calf serum
FTIR	fourier-transformed infrared spectroscopy
FTIR-ATR	fourier-transformed infrared spectroscopy with attenuated total reflection
GAG	glycosaminoglycan
H&E	hematoxylin and eosin staining
HA	hyaluronic acid
ICP-OES	inductively coupled plasma optical emission spectroscopy
LDH	lactate dehydrogenase
MACI/MACT	matrix-induced autologous cartilage implantation/transplantation
MMP-13	matrix metalloproteinase 13
MSCs	mesenchymal stem cells
MTT	3-(4, 5-dimethylthiazol-2-yl)-2, 5-diphenyltetrazoliumbromide
OA	osteoarthritis

OAT	osteocondral autograft transfer
OCP	octacalciumphosphate
P/S	penicillin/streptomycin
PCR	polymerase chain reaction
RNA	ribonucleic acid
ROI	region of interest
SBF	simulated body fluid
SDOCA	sterilized and decellularized osteochondral allografts
SEM	scanning electron microscopy
TGF	transforming growth factor
TRIS	tris(hydroxymethyl)-aminomethan
XRD	x-ray diffraction

Introduction

Cartilage tissue: Biology and function

Articular cartilage (AC), also known as hyaline cartilage, is a specialised connective tissue that provides an important buffer function in joints. It absorbs both vertical and shear stress and reduces and passes them to the subchondral bone. The most important role of AC, therefore, is the ability of osmotic swelling of the proteoglycans in a defined mesh of collagen fibrils. (Poole 1997; Becerra et al. 2010)

AC is constructed of extensive extracellular matrix (ECM) and only a few cells. There is no innervation or vascularisation for a blood supply or lymphatic transport. Nutrition and oxygen supply occur solely via diffusion. (Medvedeva et al. 2018; Chen et al. 2017; Poole 1997; Schumacher et al. 1994) Consequently, there is no possibility for an early repair of defects by generating a blood clot or providing tissue reconstruction by infiltrating monocytes or macrophages. (Becerra et al. 2010) Therefore, AC, displays a very limited self-regeneration capacity.

Native cartilage tissue is constructed in four layers. From the top to the subchondral bone, the superficial, transitional (middle), deep (radial) and calcified zones are present. (Becerra et al. 2010; Poole 1997) The transitional zone constitutes an important boundary between the non-calcified and calcified regions of the cartilage tissue. (Meirer et al. 2011) Articular chondrocytes are the only cell type that are present in AC, and their cell mass constitutes less than 5% of the wet weight. (Chen et al. 2017; Schumacher et al. 1994; Xia et al. 2014) The structural unit of the cartilage, known as the chondron, contains chondrocytes and the associated hydrodynamic peri-cellular matrix. Chondrons serve as mechanical units able to absorb forces by changing their shape. Furthermore, they play an important role in cartilage metabolism and ECM distribution. (Poole 1997) The chondrocyte shape changes between the different tissue layers. While flat cells are present at the surface, round cells populate the middle part. In the deep and calcified zones, the round-shaped chondrocytes are arranged in vertical columns. (Becerra et al. 2010; Lorenzo, Bayliss, and Heinegard 1998; Poole 1997)

The ECM consists mainly of water, collagen, proteoglycans and glycoproteins. The ECM distribution is layer-dependent, and the major part of the wet weight is water (65–80%). (Chen et al. 2017; Xia et al. 2014) The next largest element is represented by collagens and constitutes approximately 10–20%. Although up to 15 different collagen types can be found in AC, the large majority is collagen type II. (Eyre, Brickley-Parsons, and Glimcher 1978; Chen et al. 2017) Some collagen types, for example types I and III, are only expressed during degeneration and de-differentiation of chondrocytes, respectively. (Pei, Yu, and Qu 2000) The arrangement of the collagen fibrils is essentially parallel in the superficial layer, randomly arranged in the middle layer and concomitantly to the cell columns in the deep layer. (Schumacher et al. 1994; Lorenzo, Bayliss, and Heinegard 1998) Approximately 10% of the wet weight consists of proteoglycans, the major one thereof being aggrecan. (Heinegard and Oldberg 1989) Proteoglycans and type II collagen are the main constituents of the tissue structure. A small amount of the ECM consists of glycoproteins, particularly laminin. The amount of glycoproteins in AC diminishes during tissue degeneration. (Noyes and Stabler 1989)

In summary, AC is a rather complex tissue and constitutes a major challenge in tissue engineering.

Clinical problem

The clinical problem investigated was osteoarthritis (OA), an important field in orthopaedic surgery. OA is a degenerative disease with an increasing global incidence and a high economic impact. (Huang et al. 2018; Martel-Pelletier et al. 2016) Full-thickness cartilage defects are an early stage or precursor of OA. (Niemeyer et al. 2016) Such lesions can occur from trauma, osteochondrosis dissecans or idiopathically as in primary OA. (Brittberg et al. 1994; Cicuttini et al. 2005)

Symptomatic OA is reported in 10–15% of all subjects aged over 70 years, women even more than men. (Felson et al. 1995) Reported symptoms include pain, limited joint movement and tender joints. (Becerra et al. 2010; Martel-Pelletier et al. 2016) Radiographic results rarely correlate with the individual symptoms of the patient because cartilage tissue is known to be aneural. Neural innervation and thus pain detection occur at the periosteum, capsule, synovia, part of the meniscus and

ligaments. (Felson 2004; Burr and Gallant 2012) The most affected joints are the knee, hip, distal interphalangeal joint, proximal interphalangeal joint and spine. (Felson 2004)

The intrinsic cause of primary OA is a combination of general susceptibility for OA and local factors in the joints, including alterations in shape and alignment. (Felson and Zhang 1998; Berenbaum et al. 2018; Martel-Pelletier et al. 2016) General susceptibility can be caused by variations in collagens, enzymes, cytokines or growth factors. (Felson 2004; Felson and Zhang 1998) Furthermore, extrinsic determinants influence the incidence of the disease. These include excessive overweight, poor muscle strength or overuse by sport exercise or the job. (Felson 2004; Felson and Zhang 1998; Anderson and Felson 1988; Croft et al. 1992; Berenbaum et al. 2018; Martel-Pelletier et al. 2016)

The basic biological problem is the loss of integrity and damage of the AC structure. (Becerra et al. 2010; Felson 2004) Degradation of cartilage matrix leads to water deposit in this tissue that manifests in swelling. This in turn leads to an altered biomechanical property and further cartilage damage. (Felson 2004) The change in cartilage structure and mechanical properties lead to a reaction of the underlying bone tissue, including subchondral sclerosis and osteophyte formation. (Felson 2004; Burr and Gallant 2012) The development of the disease is very individual and dynamic. (Felson 2004)

In an end-stage of the disease, OA leads to major symptoms, disability and frailty. (Meessen et al. 2018; Driban et al. 2016)

Current solutions

OA treatment is currently based on numerous different methods. There are treatments with and without medication as well as invasive treatments, including injections, cartilage repair treatments and endoprosthesis. (Jordan et al. 2003) The first steps in treatment include patient education, diet for weight loss, physical exercise such as cycling and other lifestyle modifications. Additionally, physical therapy may be indicated that includes quadriceps exercise for knee stabilisation. (Huang et al. 2018) These treatment options may be followed by or combined with treatment with pain killers like non-steroidal anti-inflammatory drugs or paracetamol. (Jordan et al. 2003)

Invasive treatments include intra-articular injection of corticosteroids, new cartilage-repair treatments and arthroplasty as ultima ratio. (Jordan et al. 2003; Medvedeva et al. 2018) The commonly used strategies, including pharmacological treatment and steroid injection, only address the symptoms and not the cartilage defects. Additionally, they are accompanied by the risk for potential side effects. (Bert and Bert 2014)

Clinically used cartilage-repair treatments include microfracture, osteochondral autograft transfer (OAT), autologous chondrocyte implantation / transplantation (ACI/ACT) and matrix-associated autologous chondrocyte implantation / transplantation (MACI/MACT). (Medvedeva et al. 2018)

Microfracture is a technique to create connection channels between the cartilage defect and the bone marrow underneath. These channels enable the migration of bone marrow mesenchymal stem cells (BMSCs) into the defect to promote cartilage healing. Microfracture can be performed via an arthroscopic procedure without any additional instruments. Therefore, the technique is readily performed, low-cost, safe and has a low complication rate. (Medvedeva et al. 2018; Hunziker 2002; Mithoefer et al. 2009)

OAT, also known as mosaicplasty, is a surgical procedure where autologous osteochondral grafts are transferred into the cartilage defect. As autologous grafts, cylinders from cancellous bone covered with AC are taken from non-weight-bearing areas. (Erol and Karakoyun 2016; Dall'Oca et al. 2017; Sherman, Thyssen, and Nuelle 2017) It is an inexpensive procedure with only a single operation and rapid defect healing. (Sherman, Thyssen, and Nuelle 2017) An alternative to an autograft is allograft transplantation. However, allografts display the risk for infection and transmitting diseases. (Ng and Bernhard 2017; Frank et al. 2017) OAT has shown promising long-term results for smaller to medium-sized defects in various studies. (Andrade et al. 2016; Dall'Oca et al. 2017)

Cell-based therapies are normally applied for larger defects; a size of ≥ 4 cm². (Niemeyer et al. 2016) These approaches include different techniques, like autologous chondrocyte implantation (ACI) or its further development, the matrix-associated autologous chondrocyte transplantation (MACI).

The ACI technique was initially developed by Mats Brittberg and colleagues in 1994. (Brittberg et al. 1994) In a first step, AC is harvested from non-weight-bearing areas of

the joint. Chondrocytes are isolated from the harvested cartilage tissue, cultivated and transplanted into the defect in a second operation. The implantation normally occurs 2 to 3 weeks after chondrocyte isolation. Therefore, the defect is covered by a small piece of autologous periosteum, and the chondrocytes are inserted beneath it. (Brittberg et al. 1994) A further development of ACI is the use of a bio-absorbable collagen membrane instead of the periosteal flap. This may reduce the complication of periosteal hypertrophy. (Zhang, Cai, and Lin 2016)

MACI represents a further development of the ACI technique. Previously harvested and cultivated articular chondrocytes are seeded on a three-dimensional matrix prior to implantation. Hyaluronan or collagen-based matrices are examples of the scaffolds used. (Schinhan et al. 2013; Aldrian et al. 2014) Promising results were reported from animal and human studies. (Schinhan et al. 2013; Schuette, Kraeutler, and McCarty 2017; Aldrian et al. 2014)

Limitations

Microfracture: Satisfactory results were reported from patients younger than 30 – 40 years but there remains no convincing data for patients suffering with global OA. (Hunziker 2002; Mithoefer et al. 2009) The microfracture technique is limited to small defects of $<4\text{cm}^2$, like osteochondrosis dissecans, because it creates fibrocartilage rather than hyaline AC. (Hunziker 2002; Albright and Daoud 2017; Mithoefer et al. 2009) While this technique can be applied to fill small defects, the resulting biomechanical properties differ from the original cartilage tissue. (Aldrian et al. 2014) Recently published data demonstrated a reduced pain level and increased joint mobility 6 months after microfracture in OA patients. Nevertheless, the patients' condition regressed to the prior condition at least after 18 months. (Nguyen et al. 2017) Furthermore, it is doubtful whether this technique is effective in patients with limited regeneration potential and a reduced number and viability of BMSCs. (Hunziker 2002)

OAT: In the OAT procedure, cartilage is harvested from healthy regions in the joint. This creates a new defect and leads to significant donor-site morbidity. (Andrade et al. 2016; Sherman, Thyssen, and Nuelle 2017) In particular, knee-to-ankle transplantations can lead to pain, crepitation or stiffness in an initially healthy joint. (Andrade et al. 2016) The use of a cylindrical form for the graft leads to small gaps

between the cylinders that are again filled with insufficient fibrocartilage. A further development is the use of honeycomb patterns to avoid these gaps. (Erol and Karakoyun 2016) However, the outcome depends of the quality of the donor cartilage. (Erol and Karakoyun 2016) Furthermore, the size of the defect is limited because only a few areas in the joint could be used as a possible donor site. (Niemeyer et al. 2016; Sherman, Thyssen, and Nuelle 2017) This constitutes a particular problem for larger cartilage defects. (Erol and Karakoyun 2016) Allogenic grafts avoid donor-side morbidity. However, they pose further challenges, including tissue availability and/or immunologic reactions. (Medvedeva et al. 2018; Yabumoto et al. 2017; Dall'Oca et al. 2017)

ACI/MACI: A disadvantage of ACI and MACI is that a minimum of two operations are needed for cell harvesting and implantation after cultivation. These techniques are quite complex procedures and require surgical training to achieve reliable results. (Zhang, Cai, and Lin 2016; Aldrian et al. 2014) Furthermore, a longer rehabilitation time is needed for ingrowth and tissue formation. (Jones and Cash 2019) Both techniques involve high costs and display the problem of de-differentiation of the harvested cells during cultivation, which may lead to hypertrophy and fibrocartilage formation. (Medvedeva et al. 2018; Zhang, Cai, and Lin 2016)

Typical complications of the ACI technique are hypertrophy of the periosteal patch or insufficiency of the newly formed tissue with limited biomechanical properties. Furthermore, chondrocyte injection leads to insufficient control of the distribution or leakage of the cells in the defect. (Zhang, Cai, and Lin 2016; Schuette, Kraeutler, and McCarty 2017) Limitations of the MACI technique are detachment or dislocation of the matrix in the defect, among others. (Schuette, Kraeutler, and McCarty 2017) Failure rates of MACI were reported to be up to 28% in a 5 year follow up. (Schuette, Kraeutler, and McCarty 2017) Even less satisfactory clinical outcomes with a failure rate of >50% after 15 years were described in a long-term follow-up study. It is reported not to be possible to avoid the need for a joint replacement operation, but at least MACI delays the need for this. (Andriolo et al. 2019)

Tissue engineering approach to cartilage regeneration

Tissue engineering is an innovative approach in regenerative medicine. This method is based on the combination of biomaterials, cells and different bioactive agents.

Biomaterials: The aim of a scaffolding biomaterial is to mimic the structure and components of the native ECM to provide the cells with a favourable environment. Therefore, mostly natural materials are used. Important properties are biocompatibility, a surface that offers good cell attachment, porosity for a homogenous cell distribution and permeability to oxygen and nutrients. Favoured materials are different proteins, collagens or polysaccharides. (Vinatier and Guicheux 2016)

Cells: The only cell population in AC are chondrocytes. These cells can be isolated from non-weight-bearing areas of the joint. Chondrocytes are a well-investigated cell population, but include all the previously discussed negative aspects, including limited availability and de-differentiation during cultivation. To reduce or replace the need for chondrocytes, MSCs have been used in cartilage tissue engineering. These multipotent cells retain the ability to differentiate into various cell types. The main sources for MSCs are bone marrow and adipose tissue. (Vinatier and Guicheux 2016) In particular, adipose-derived MSCs are the preferred cell type because of an almost unlimited availability, minimally invasive procedure for harvesting and an abundant amount of cells per cm³ tissue. (Gimble, Katz, and Bunnell 2007) Recent studies demonstrated that the combination of articular chondrocytes (ACs) and MSCs may offer several advantages for cell-based approaches. (Ahmed et al. 2014) It was described that there is less hypertrophy and calcification of the newly formed tissue as well as a superior cell viability and improved biomechanical properties. (Ahmed et al. 2014; Nazempour and Van Wie 2016)

Bioactive factors: Different types of compounds can be used for additional cell stimulation. These molecules offer the stem cells additional stimulus for proliferation and differentiation. Growth factors, like transforming growth factor β (TGF- β), are widely used and investigated. (Blaney Davidson, van der Kraan, and van den Berg 2007) Additionally, different mechanical stimuli or three-dimensional cultivation are used to improve the engineered tissue. Furthermore, a hypoxic environment can preferentially direct cell differentiation towards chondrogenesis and thus improve cartilage formation. (Nagel-Heyer et al. 2006)

Aim of our study

As previously described in this thesis, current OA treatment is complicated and limited. The aim of our study was to analyse and improve new strategies of tissue engineering to intervene in early stages of primary OA with localised lesions.

In a first step, we aimed to improve the quality of cartilage regeneration by developing a special three-dimensional collagen gel and evaluate different possible co-culture conditions of ACs and adipose derived mesenchymal stem cells (AMSCs). On the one hand, this attempted to mimic the natural environment and properties of healthy cartilage as closely as possible, particularly in terms of biomechanical features and oxygen distribution. On the other hand, we aimed to reduce the number of chondrocytes needed and simultaneously improve the tissue quality by combining the two cell types.

Because OA not only affects the cartilage but also the subchondral bone, the next step of this study was to target repair treatments to different types of tissues of relevance, that is, cartilage and bone, on a single scaffold. In a second project, we, therefore, developed an intelligent layered three-dimensional scaffold to be able to concurrently create different distinct tissues and the connecting interface. First, the scaffolds were comprehensively characterised. Then the guided stem cell differentiation was evaluated using AMSCs.

Materials and methods

Outline

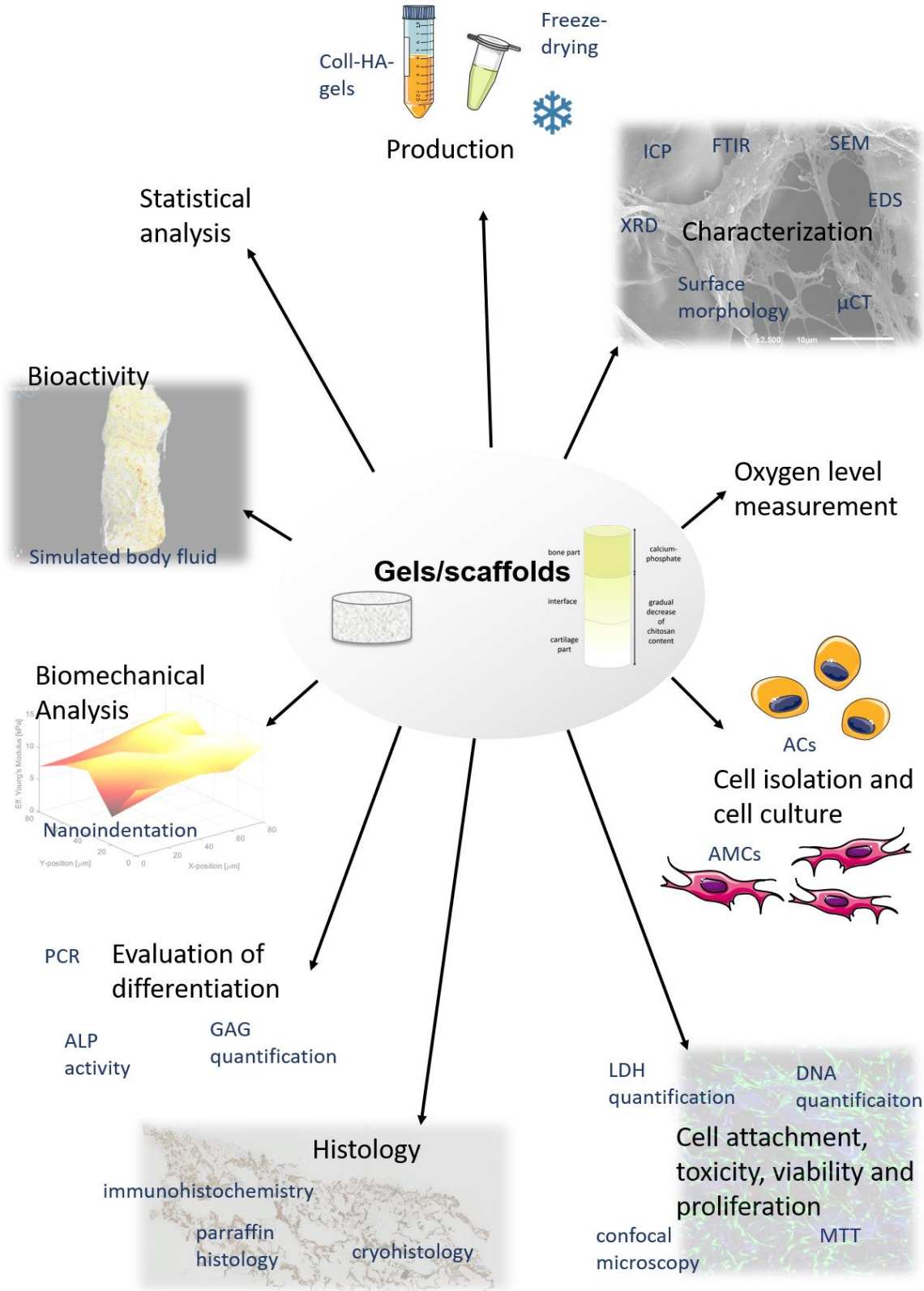


Figure 1: Overview of methods used in the study

Production of gels and scaffolds

Production of collagen-hyaluronic acid gels: The hyaluronic acid (HA) solution was obtained by dissolving 100 mg HA sodium salt (Sigma Aldrich, St. Louis, MO, USA) in 10 ml Dulbecco's Phosphate-Buffered Saline (DPBS). Following sterilisation, the solution was stored at 4°C until further use. The collagen gels were produced by adding 1 part 10× Dulbecco's Modified Eagle Medium (DMEM) (Sigma-Aldrich) and 1 part 20 mM L-Glutamine (Sigma-Aldrich) to 8 parts PureCol type I bovine collagen solution (Advanced BioMatrix, Carlsbad, CA, USA). The components were mixed carefully, and the gels were formed by pipetting 500 µl of the solution into 48-well-plates. For the different gel compositions, the collagen gel solution was supplemented by 1 or 5% HA. Cells were added to the different gel compositions by dissolving cells in the L-Glutamine solution prior to mixing the components. For all experiments, a cell density of 1×10^5 cells/500 µl was used.

Production of collagen (COL)- chitosan (CHI)- octacalcium phosphate (OCP) scaffolds: Scaffold production was performed by means of a layer-by-layer lyophilisation process. The bone layer consisted of equal amounts of CHI and COL (both Sigma Aldrich), supplemented by 2% OCP. Following freezing of the bone layer approximately -25 °C, the next layer was added. The interface layer consisted of equal amounts of CHI and COL without OCP. The procedure was continued by adding the third layer (cartilage layer). The final solution consisted of a ratio of 1:3 of CHI/COL. The final scaffold was obtained by a 48 h lyophilisation process, punched cylinders of 3 or 5 mm diameter and sterilised using ethylene oxide (inpac Medizintechnik GmbH, Birkenfeld, Germany).

Chemical and morphological characterisation of the scaffolds

Surface morphology: Depth of field microscopy and evaluation of the surface topography were performed using a digital microscope (Keyence VHX-900F, Osaka, Japan). A flat surface was achieved by axial cutting of the scaffold. Images of the scaffolds' surface were obtained and a morphological analysis of the surface of each layer was performed.



Figure 2: Digital microscope picture with full depth of field of 3-layered scaffold

Microcomputed tomography (μ CT): Scaffold porosity, pore size and wall thickness were analysed using μ CT (SkyScan 1176, Bruker, Billerica, Massachusetts, USA). Staining of the sample was performed with iodine vapour for 12 h. Scanning was performed at 40 kV, 600 μ A and with a resolution of 9 μ m. As the reconstruction programme, the NRecon software (Version 1.6.9.18, Bruker) was used. For the analysis of porosity, pore size and wall thickness, a region of interest (ROI) was defined in each layer (bone, interface and cartilage). Calculations and presentations were performed using CTAnalyser software (Version 1.17.7.2, Bruker). Different greyscale thresholds were used to distinguish the collagen structure, calcium phosphate deposit and hydroxyapatite particles. All these components were identified using different colours in the μ CT images. The greyscale dataset was divided in different phases using the multi-level Otsu method. Volume rendering of the scaffold was performed using CTVoxel (Version 3.3, Bruker).

SEM and EDS: Scanning electron microscopy (SEM) is a commonly used technique to assess the morphological surface properties of different samples with high resolution. The three-layered COL-CHI-OCP-scaffold were imaged at low and high magnifications. Therefore, an overview as well as detailed images were obtained (JSM-6010LV, JEOL, Tokyo, Japan). Furthermore, uncoated scaffolds were used to detect the different elements by energy-dispersive X-ray spectroscopy (EDS) (INCAx-Act, PentaFET Precision, Oxford Instruments, Abingdon, England). All three layers were analysed by defining different ROIs. Additionally, a colour-coded element mapping of the entire scaffold surface was performed. To obtain images, all scaffolds were treated with a platinum coating by ion sputtering. Backscattered electron imaging and secondary electron imaging were applied as techniques for different surface presentations.

FTIR: Chemical compounds of different materials can be detected by fourier-transformed infrared spectroscopy (FTIR) with attenuated total reflection (FTIR-ATR IR Prestige-21 spectrometer Shimadzu, Kyoto, Japan). The bone, interface and cartilage layers of the COL-CHI-OCP were analysed before and several times after treatment with simulated body fluid (SBF) (days 1, 3 and 7). A spectral range of 400 – 4000 cm^{-1} was used.

XRD: X-ray diffraction (XRD) is an x-ray-based method to detect crystalline phases of materials. Thin-film XRD (D8 Advance, Bruker, Rheinstetten, Germany) was used for the blank scaffold as well as samples from the different time points of the bioactivity experiments. The 2θ scan method was used, with a 1° incident beam angle using a Cu $K\alpha$ X-ray line and a scan speed of $0.05^\circ/\text{min}$.

ICP: Ion detection in fluid was performed using inductively coupled plasma (ICP) optical emission spectroscopy (ICP-OES, JY2000-2, Jobin Yvon, Horiba, Japan), following the manufacturer's instructions. SBF solutions with or without scaffolds were analysed for the concentrations of Ca and P after 1, 3 and 7 days of incubation time. Prior to analysis the solutions were filtered, diluted in 1% HNO_3 (1:10) and stored at -20°C .

Cell isolation, co-culture and seeding on gels/scaffolds

Both described studies were approved by the ethical committee of the University Hospital “Klinikum rechts der Isar” (Technical University of Munich) and in accordance with the Declaration of Helsinki. All patients gave their informed written consent prior to the surgical procedure.

Isolation of human AMSCs: Stem cell isolation was performed according to a published protocol. (Schneider et al. 2017) In brief, small pieces of the fat tissue were washed using DPBS in several centrifugation steps. The obtained fat solution was added to collagenase solution (0.8 mg/ml in DPBS of collagenase type II, Biochrom GmbH, Berlin, Germany) and incubated in a water bath at 37 °C for 30 min. The reaction was terminated by adding pre-warmed cell culture medium (high glucose DMEM, 10% foetal calf serum (FCS), 1% penicillin/streptomycin (P/S), Sigma-Aldrich) to fill the incubation tube. Following centrifugation, the pellet was resuspended in culture medium and poured through a 40 µm cell strainer (BD Falcon, Franklin Lakes, NJ, USA). The cell density in the culture flasks was 3000 cells/cm². The culture medium was changed twice weekly, and the cells were used in passage 2 or 3.

Isolation of human ACs: Chondrocyte isolation was performed using human femur heads from hip replacement procedures. To obtain cartilage tissue of high quality, the femur heads alone from femur neck fractures were used. Therefore, femur heads from endoprosthesis surgery with primary arthrosis were excluded. Furthermore, no patients with OA or malign bone tumor disease (primary bone tumor or metastasis) were included in our study. Small pieces of the cartilage were cut from the femur head, washed thoroughly and mixed with a prepared digestion solution (0.15% collagenase type II in high glucose DMEM, supplemented with 1% P/S). The mixture was incubated at 37°C over night under constant stirring. Following the incubation, the solution was filtered (100 µm cell strainer) and centrifuged. The obtained cell pellet was dissolved in pre-warmed culture medium (low glucose DMEM, 10% FCS, 1% P/S). A seeding density of 7500 cells/cm² was used and the culture medium was changed twice weekly. The chondrocytes were used at passage 2.

Cell attachment, toxicity, viability and proliferation on gels and scaffolds

SEM: The cell appearance and arrangement on the scaffold was analysed by SEM microscopy after 2, 3 and 5 weeks of culture. For this, the cultivated scaffolds were treated with 2.5% glutaraldehyde in a sodium cacodylate buffer. Subsequently, several washing steps with this buffer were performed followed by incubation in different ethanol (EtOH) concentrations (30 – 100%). Immersion in hexamethyl-disilazane was used for sample drying. Uncoated samples were used for EDS analysis, while for SEM analysis, sputter coating was used.

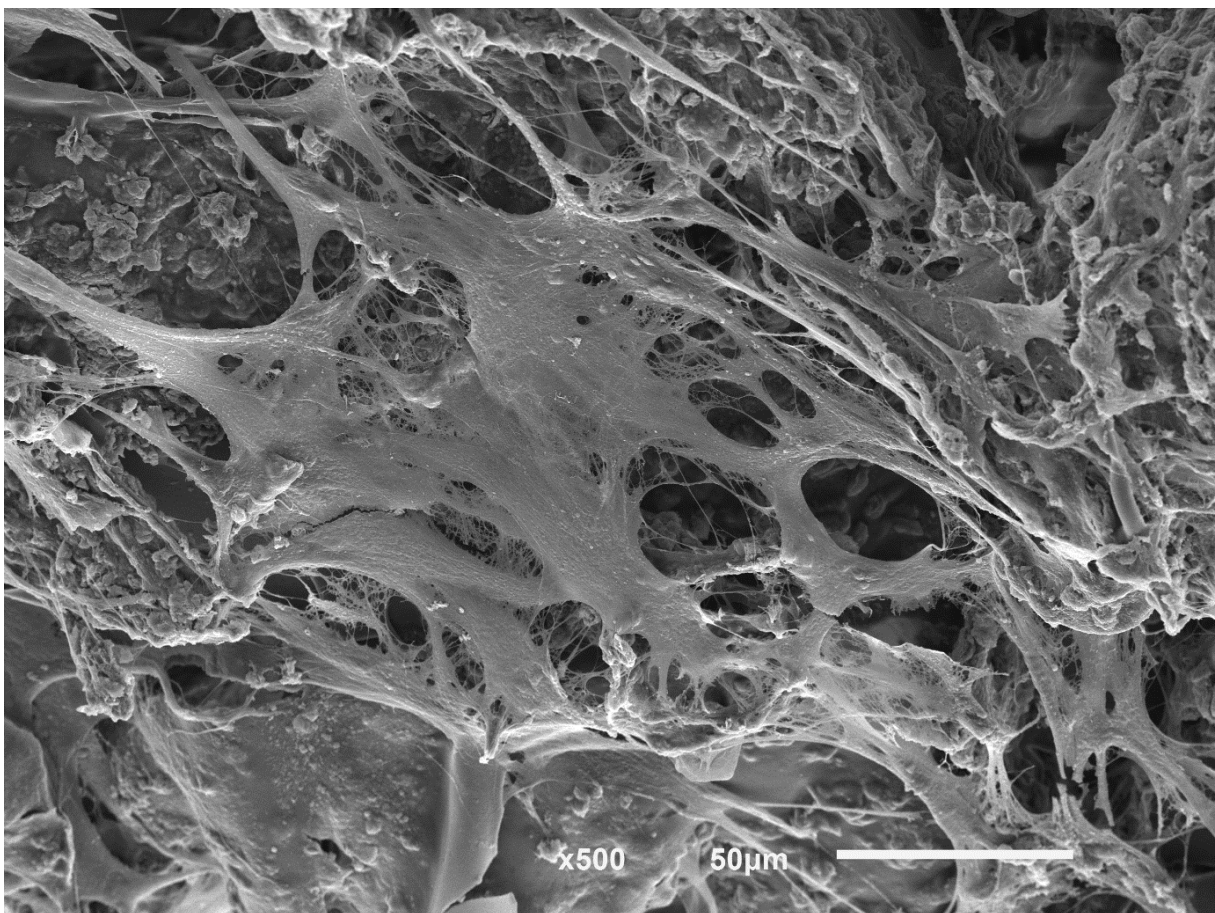


Figure 3: Representative SEM image of the scaffold after 3 weeks of cell cultivation. In the image, the pore part can be appreciated. Used magnification was 500x.

LDH concentration: Lactate dehydrogenase (LDH) is an intracellular enzyme that's released when cells are damaged. Thereby, the LDH concentration in the cell medium is a good indicator of material-related toxicity. The supernatant of the gels or scaffolds was collected after 1, 3, 7 and 14 days of cell culture and LDH was measured using

the Fluitest LDH- L Kit (Analyticon, Lichtenfels, Germany) as described in the manufacturer's instruction.

MTT test: The MTT assay [3-(4, 5-dimethylthiazol-2-yl)-2, 5-diphenyltetrazoliumbromide] is a test to evaluate cellular metabolic activity. It involves the ability of intracellular oxidoreductase enzymes to reduce the MTT reagent to formazan. This leads to a colour change, from yellow to purple, that can be photometrically quantified. The samples were incubated with the MTT solution for 3 h at 37°C. Subsequently, the gels were washed and the MTT precipitate was eluted using isopropanol. The supernatant was measured in triplicates at 570/690 nm.

Confocal microscopy: Cell distribution and viability were analysed on the scaffolds using fluorescent staining and confocal microscopy. Following 21 or 35 days of cell culture, the scaffolds were treated with 500 µl of a solution of 2 µM calcein-AM (Sigma Aldrich), 1.5 µM propidium iodide (Sigma Aldrich) and 1.5 µM 4',6-diamidino-2-phenylindole (DAPI, Invitrogen, Carlsbad, California, USA). Consequently, a green staining inside the cell membranes of vital cells, a blue marking of DNA in the nucleus and a red staining of damaged cells can be observed. All three layers of the cell-seeded scaffolds were evaluated by confocal microscopy (Olympus Fluoview FV10i, Tokyo, Japan).

DNA concentration: Cell proliferation was quantified by determining the amount of DNA on the constructs. For lysis of the cells seeded on the gel construct, the gels were first incubated in a collagenase type II solution (1 mg/ml, Biochrom GmbH) and intermittently mechanically crushed by pipetting the solution up and down. The scaffold samples as well as the pretreated gel samples were furthermore digested using a papain solution (500 µl, 0.1 mg/ml, Sigma Aldrich). Digestion was performed in a 37°C water bath for 3 h under regular shaking. All samples were stored at -80°C until measurement. DNA quantification was performed using the Quant-iT PicoGreen Kit (Invitrogen), a fluorescent staining that binds particularly to dsDNA. The measurement was performed according to the manufacturer's instructions. Briefly, one part of sample and one part of Quant-iT PicoGreen working solution were pipetted into a 96-well plate. Following incubation for 5 min at 37°C in the dark, the fluorescence was measured (emission: 520 nm, excitation: 485 nm, FLUOstar Omega photometer, BMG labtech, Ortenberg, Germany).

Evaluation of cell differentiation: ALP-activity, GAG-quantification, gene expression

Alkaline phosphatase activity: Alkaline phosphatase (ALP) is an enzyme marker for osteoblastic activity. To measure the activity in the samples, the scaffolds were washed with DPBS and incubated with the ALP substrate solution 4-nitrophenyl phosphate disodium salt hexahydrate (Sigma Aldrich). After 30 min, the supernatant was pipetted into a 96-well plate. Absorbance was determined at 405 nm and compared to a standard curve.

GAG quantification: Glycosaminoglycans (GAG) represent an important component of the ECM of native AC. Quantification of the GAG content in the samples was performed using the Blyscan Sulfated Glycosaminoglycan Assay (Biocolor, Carrickfergus, U.K.), according to the manufacturer's instructions. The samples were digested as previously described for the DNA quantification. In total, 50 µl sample and 50 µl aqua destillata were mixed and 1 ml of Blyscan reagent was added. Following 30 min of incubation at room temperature, centrifuging and dissolving in Blyscan dissociation reagent, the absorbance was determined at 656 nm. The GAG concentration was determined using a prepared standard curve. To achieve comparable results, the GAG concentration was reported normalised to the DNA concentration in the same sample.

Gene expression: To analyse the cell differentiation at the genetic level, samples were collected at days 1, 3, 7, 14, 21 or 35 after cell culture. The entire gel samples were used for all polymerase chain reaction (PCR) experiments. The entire scaffold samples were used for proliferation and apoptosis marker analysis as well as bisected at the interface of a cartilage and a bone region for specific differentiation markers. RNA isolation was performed using TRI reagent (Sigma Aldrich), frozen at -80°C , followed by chloroform extraction and isopropanol precipitation. The nucleic acid concentration and purity in the obtained solution was determined using the Hellma TrayCell Eppendorf BioPhotometer (Eppendorf AG, Hamburg, Germany). These steps were followed by the transcription of the mRNA to cDNA using the First Strand cDNA Synthesis Kit (Thermo Fisher, Waltham, MA, USA) and the Eppendorf MasterCycler (Eppendorf AG) according to the manufacturers' instructions. Quantitative real-time PCR was performed with SsoFast Eva Green Supermix (Bio-Rad Laboratories Inc., CA, USA) in the Bio-Rad CFX96 thermal cycler (Bio-Rad Laboratories Inc.). For all

experiments, beta-tubulin was selected as the housekeeping gene. Data is shown as fold-change expression in relation to the housekeeping gene. The samples of the gel experiments were analysed for the chondrogenesis markers SOX-9, collagen II and collagen III as well as for the hypertrophic cartilage markers matrix metalloproteinase-13 (MMP-13) and collagen X. Apoptosis and proliferation markers were tested with the complete samples of the scaffold experiments (bcl-2, Caspase 3, mcm-5, Cyclin D1). The bisected parts of the scaffold experiments were analysed for chondrogenesis markers (aggrecan, collagen II, collagen X and SOX-9), as well as for osteogenesis markers (collagen I, collagen III, osteocalcin, osteopontin, RUN-X2).

Histology

Cryohistology preparation: Gel samples were collected after 21 or 35 days of culture. Following washing with DPBS, 500 µl 3.7% paraformaldehyde was pipetted on the samples. The supernatant was removed after 10 min, and the samples were embedded in Tissue-Tek O.C.T. Compound (Sakura Finetek GmbH, Staufen, Germany). Following a brief immersion in liquid nitrogen, the specimens were kept frozen at -80°C . The samples were cut to 10 µm sections using a cryotome (Cryostat, Leica Biosystems, Wetzlar, Germany). Light microscopy of the stained sections was performed by light microscopy (Bioevo, BZ9000, Keyence). Scanning of the entire section was executed using the software BZ-II Viewer and BZ-II Analyzer (both Keyence).

Paraffin histology preparation: The scaffold samples were harvested after 3 or 5 weeks of culture. The samples were washed twice with DPBS and fixed in a 3.7% paraformaldehyde solution for 24 h. The dehydration process was performed by treating the samples in 40% and 70% EtOH solutions. Each step was performed twice for 24 h. Subsequently, the samples were embedded in a paraffin solution and cut to 7 µm sections.

Haematoxylin and eosin staining (H&E): H&E staining is widely used to obtain an overview of the cell distribution and tissue formation. Therefore, the samples were rehydrated and stained in a haemalaun solution for 10 min. Following a washing step with running tap water for 15 min, the next staining step was performed with eosin solution for 5 min. Subsequently, the samples were dehydrated in a series of EtOH

solutions of increasing concentration and finally Roti-Histol (Carl Roth GmbH, Karlsruhe, Germany).

Safranin-O/Fast Green: Safranin-O staining is commonly used to detect cartilage-specific ECM. Therefore, samples were stained with haematoxylin QS solution (Carl Roth GmbH) for 5 min, washed with tap water, destained with acid EtOH and counterstained with Fast Green solution (Carl Roth GmbH) for another 5 min. Subsequently, samples were rinsed with 1% acetic acid solution and stained in 0.1% safranin-O solution (Carl Roth GmbH) for 5 min. Following staining, dehydration with different concentrations of EtOH and finally Roti-Histol (Carl Roth GmbH) was performed.

Alcian blue: Alcian-blue staining is used to detect sulphated glycosaminoglycans, an important component of the ECM of AC. The fixated sections were incubated with Alcian blue (Carl Roth GmbH) for 30 min and counterstained with nuclear fast red (Sigma Aldrich) for 5 min. Following both these steps, stained sections were washed with tap water. Subsequent to staining, dehydration was performed following the steps described above.

Immunohistochemistry: Immunohistochemical staining of the cryohistology sections was performed for the cartilage markers Collagens I, II and X. Sections were incubated with 3% H₂O₂ solution for 5 min at room temperature. This was followed by thoroughly washing with 50 mM Tris-HCl (pH 7.4) and incubation with Proteinase K (Dako, Glostrup, Denmark) for 10 min at room temperature. Following this incubation, 2% bovine serum albumin (BSA) was pipetted onto the samples and incubated for another 60 min at room temperature. Subsequently, the diluted primary antibody solution was pipetted on the sections. The samples were incubated overnight in a humidified chamber at 4°C. The following dilutions of the antibodies were used (all diluted in 2% BSA): Collagen type 1 (Col 1, rabbit polyclonal antibody) 1:100, Collagen type 2 (Col 2, rabbit polyclonal antibody) 1:200, Collagen type 10 (Col10, mouse monoclonal antibody) 1:1000, non-specific rabbit antibodies 1:200, non-specific mouse antibodies (all Abcam, Cambridge, UK) 1:1000. Subsequently, the sections were washed with Tris-HCl and incubated with the secondary antibody (DAKO Envision Dual Link System-HRP, Dako) for 30 min at room temperature. Following another washing step with Tris-HCl, incubation with 3,3-Diaminobenzidine (DAB) solution (1:50, DAKO liquid

DAB + substrate Chromagen System, Dako) was performed. This was followed by washing with Tris-HCl and counterstaining with haematoxylin solution (Carl Roth GmbH). Dehydration was performed following the above-described protocol.

Biomechanics

For the biomechanical experiments, gel cultivation was achieved in specialised self-developed three-dimensional-printed gel holders. The wells were designed with a diameter of 7.5 mm and a depth of 5 mm. To provide suitable conditions for measurement, each well was filled to the upper rim. To supply the gels with culture media, the cultivation of the entire four-well-gel-holder was performed in six-well-plates. The production of the gel holders was performed using an Ultimaker 3D printer (Ultimaker B.V., Geldermalsen, The Netherlands). Copolyester was used as the material for the gel holder. Cultivation of the gels was performed as above described for 21 and 35 days. Measurement of gel micro-elasticity was performed using a novel nano-indentation instrument (Piuma Nanoindenter, Optics 11, Amsterdam, The Netherlands). The device combines fibre-optical Fabry-Perot interferometry with a monolithic cantilever-based probe. Therefore it is possible to analyse local micro-elasticity of low-modulus materials with high accuracy and precision. (Chavan et al. 2012) For all performed measurements, a probe with 0.088 N/m spring constant and a spherical indentation tip (25 μm) was used to determine load-indentation and load-time data. The measurement was performed as follows: The tip was brought into contact with the gel surface and automatically indented for 18.32 μm at a displacement velocity of 9.16 $\mu\text{m/s}$. The Hertz model was used to calculate the Young's Modulus from the load-indentation curves. To obtain reliable results, four gels of each condition were analysed as well as different points on each gel (distance of 100 μm). To evaluate the homogeneity of the surface, a Young's Modulus mapping was performed in a 100 μm squared grid, with 25 single measurements performed at a distance of 20 μm . The results were depicted in a colour-coded 3-dimensional area diagram.

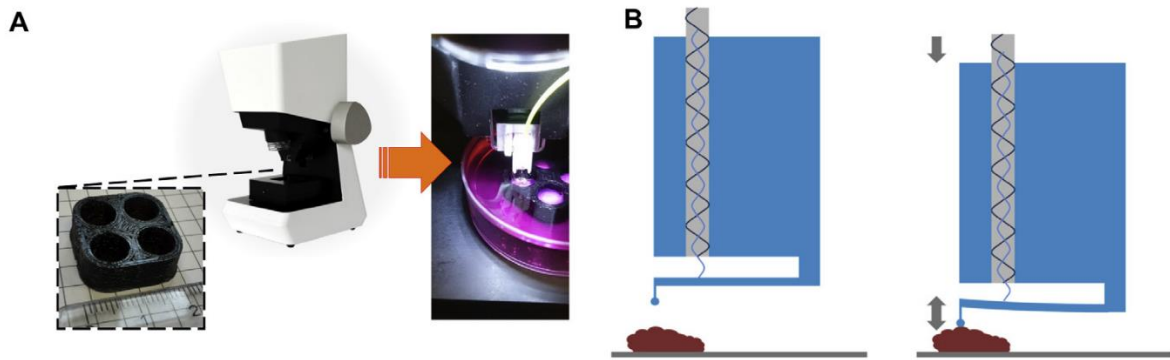


Figure 4: Biomechanical measurements of collagen gels. This figure was modified and reproduced from the publication included in this thesis (Amann et al. 2017) with permission from Elsevier.

Oxygen levels of cell-loaded gels

Dissolved oxygen levels were determined using a 50 μm diameter fibre-optical microsensor system (Microx TX3, PreSens, Regensburg, Germany). The measurement was performed after 21 and 35 days of culture in all different gel and co-culture compositions. Biological triplicates were used and a minimum of six measurements per gel were performed at a predetermined penetration depth in a 37°C incubator under 21% O_2 and 5% CO_2 .

Bioactivity assay of the scaffolds

Bioactivity is defined as the capacity of materials to form a bone-like apatite layer on their surface. The bioactivity potential of the scaffolds was analysed using simulated body fluid (SBF). SBF was prepared according to previously published protocol. (Oyane et al. 2003) The solution was produced by dissolving NaCl, NaHCO_3 , KCl, $\text{K}_2\text{HPO}_4 \cdot \text{H}_2\text{O}$, $\text{MgCl}_2 \cdot 6\text{H}_2\text{O}$, CaCl_2 , Na_2SO_4 and TRIS (all reagents: Merck KGaA, Darmstadt, Germany) in ion-exchanged and distilled water, and the pH adjusted to 7.40 at 36.5°C using 1.0 M-HCl. For the experimental set-ups, tubes containing 10 ml SBF solution, with or without (control group) adding a scaffold were prepared. The tubes were incubated in a water bath at 37°C under steady agitation for 1, 3 or 7 days. At the defined time, the scaffolds were removed from the solution, washed with ultra-pure water and dried in a desiccator. The remaining solutions were used for pH measurement and determination of the elemental concentrations of calcium and phosphorus by ICP-OES as described above. Each of the scaffold samples was

analysed for changes in morphology and chemical structure using XRD, SEM, EDS, FTIR-ATR and μ CT as described above. For μ CT, the samples were scanned without any iodine staining.

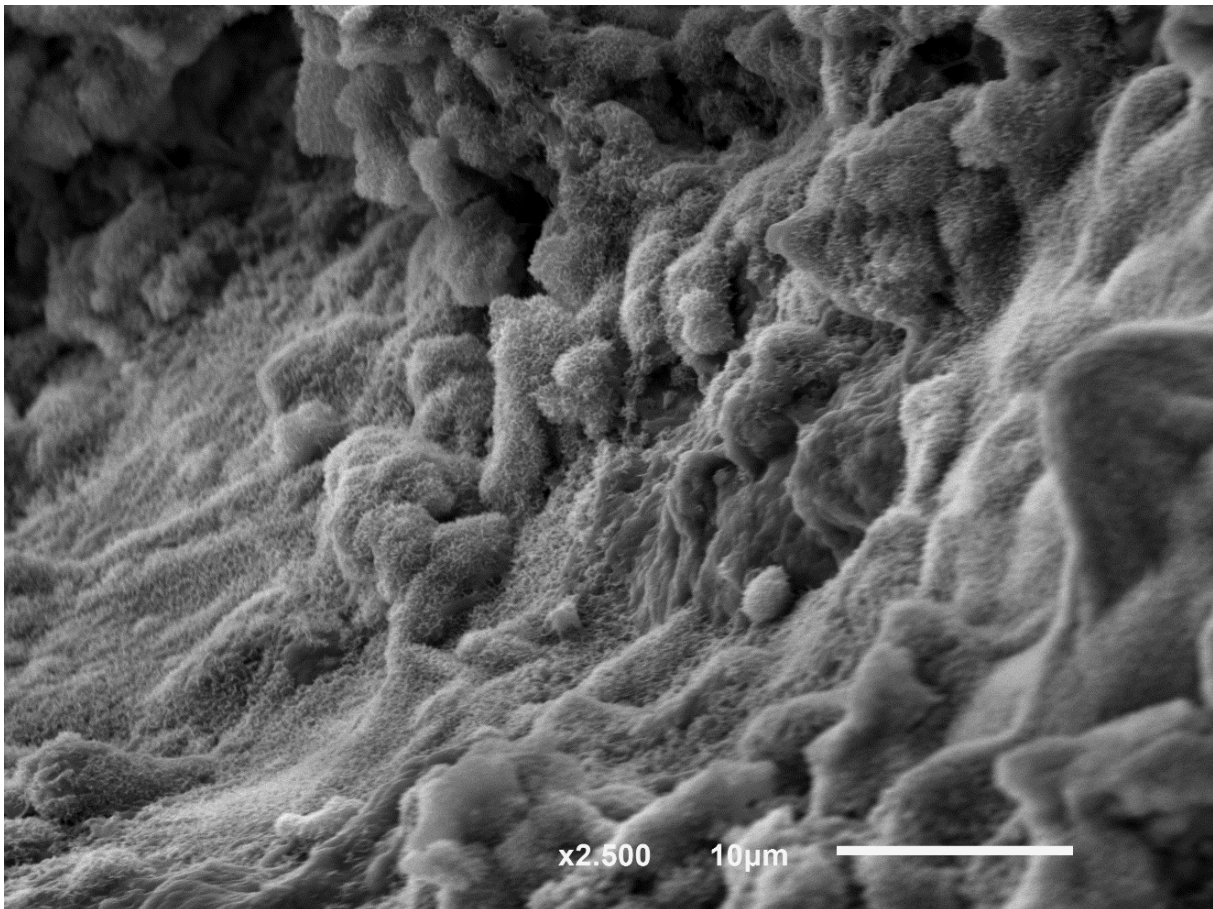


Figure 5: Representative SEM image showing bioactivity of the bone region of the scaffolds after 7 days of incubation in SBF. Magnification used was 2500x.

Statistical evaluation

All statistical evaluation was performed by GraphPad Prism version 6.00 (GraphPadSoftware, La Jolla, CA, USA). The data are presented as the mean value \pm standard error of the mean. All studies were performed out in two or more individual experiments with measurements at least in triplicates. For data that was normally distributed, the D'Agostino-Pearson test was used. Non-normally distributed data was analysed by the Kruskal-Wallis test with Dunn's correction for multiple comparisons. Comparisons of two groups were performed by t-test, and more than two groups by one-way analysis of variance followed by the Tukey's test. A probability of $p < 0.05$ was considered to be statistically significant.

Discussion

Tissue engineering is a complex and extensive field of research, particularly in terms of cartilage and bone regeneration. The ultimate aim of all research efforts is to achieve an optimal solution to treat patients with cartilage or osteochondral defects. The aim of our research was to increase the possibilities for a cell-based cartilage therapy by modifying different influencing factors.

From a surgeon's point of view, certain aspects have to be considered to achieve a satisfactory solution. The treatment should be easy to learn and apply. Moreover, it should be economical, widely available and customisable. To reduce the risks associated with multiple-stage procedures, future techniques should be minimally invasive and feasible as a single operation. In particular, the option of customising a scaffold exactly to the size and shape of the defect may improve the clinical outcome. In our study, we decided to use well known materials, including collagen, hyaluronic acid and chitosan, in the form of a gel or sponge that is readily adaptable to different defect sizes and shapes. Moreover, the selected materials have been extensively used for cartilage and bone engineering, (De Mori et al. 2018; Doulabi, Mequanint, and Mohammadi 2014) having been shown to be biocompatible and biodegradable. (Doulabi, Mequanint, and Mohammadi 2014; Liu et al. 2017)

In the recent decades, tissue engineering of cartilage has made enormous progress and several options are already available for clinical treatment. Nevertheless, the results, particularly in long-term-research, are very inhomogeneous and inconsistent. The currently most-used techniques in clinics are microfracture, OAT and cell-based therapies like MACI/MACT and ACI/ACT. They have been described in detail in previous chapters of this thesis.

Although microfracture is the easiest of all the described techniques, it also produces inferior results compared to ACI or MACI. In particular, in a long-term follow-up, microfracture groups had significantly higher re-operation rates. (Riboh et al. 2017) Salzman et al. published a large retrospective study in 2013 that showed a failure rate of > 25% in microfracture treatment, with a reoperation required after a mean of 1.6 years. (Salzman et al. 2013) Even when only small cartilage defects were treated, the failure rate was considerable. (Rosa et al. 2017) The group of Bentley et al. in 2012

evaluated the clinical outcome of ACI vs. microplasty (OAT) of symptomatic cartilage defects of the knee. A significantly higher failure rate of up to 55% was reported for the OAT group compared to ACI with a reported failure rate of 17%. (Bentley et al. 2012) Other studies support these findings. Ulstein et al. did not find any significant difference in the clinical outcome of microfracture versus the OAT technique. (Ulstein et al. 2014) Only for smaller lesions (<2 cm²) were satisfactory results achieved. (Richter et al. 2016) Similar procedures like sterilised and decellularized osteochondral allografts (SDOCA) displayed failure rates of nearly 75% and were excluded as possible options for clinical use. (Farr et al. 2016) There are only a few studies that examined the different existing techniques in a long-term follow-up. Behrens et al. evaluated the outcome of MACI/MACT at localised lesions in the knee after 5 years. (Behrens et al. 2006) Improvement in clinical scores was shown, but there remained a high failure rate. The authors reported of transplant detachment, a weak consistency of the transplant in re-arthroscopy and unsatisfactory results on histological examination. (Behrens et al. 2006) Kon et al. reported a 10-year follow-up after MACT at chondral lesions in the patellofemoral joint and found promising results. (Kon et al. 2016) This leads us to postulate that cell-based therapies are superior in their clinical outcome.

Earlier studies even showed a good clinical outcome of cartilage defects in weight-bearing areas of the knee without any specific cartilage repair treatment, and found comparable clinical results to the first generation of periosteum implantation or ACI as published by Homminga et al. and Brittberg et al. (Messner and Maletius 1996; Brittberg et al. 1994; Homminga et al. 1990) Recent studies frequently do not use control groups or just compare different techniques and use microfracture as a control group rather than a placebo treatment. (Kon et al. 2016; Bentley et al. 2012; Ulstein et al. 2014) This raises the question whether patients really benefit from the currently applied treatments with all the possible related risks. This brings us even more succinctly to the conclusion that established treatments should be improved.

As previously explained in the introduction section, tissue engineering is a triangle of biomaterials, cells and different bioactive agents. As bioactive agents, growth factors are frequently used.

In our study, we did not use the path of applying growth factors for cartilage engineering. Although there are many studies with promising results, there remain

numerous issues that have to be considered regarding the clinical translation. Current research shows Insulin-like growth factor 1 to be a well-studied growth factor in cartilage engineering. Although considerable safety has been reported, only a limited impact on arthritic cartilage was found. By contrast, TGF- β and bone morphogenetic protein 2 enhance proteoglycan production, particularly in arthritic chondrocytes, without noticeably influencing healthy cartilage. (van den Berg et al. 2001) However, it was shown that these growth factors lead to chondrophyte/osteophyte formation and cartilage formation in ligaments, and thereby joint stiffening. (van den Berg et al. 2001) Additionally, systemic side effects are detectable, including fibrotic diseases of the kidney, liver and skin. (van den Berg et al. 2001; Border and Ruoslahti 1992) To obtain approval for the use of these growth factors as a common clinical treatment, much research remains lacking, including the evaluation of the outcome in long-term studies and the analysis of the dosage per joint or patient, among others.

In the work that comprises this thesis, we focused on improving tissue engineering in terms of reducing the above discussed side effects and potential causes of failure.

One of the side effects we were aiming to resolve was donor-site morbidity. By using a co-culture of chondrocytes and AMSCs, we were able to show that it's possible to reduce the number of chondrocytes needed by 25% without lowering the tissue quality. Other studies, like Morrison et al., showed that a further reduction the chondrocytes is possible. (Morrison et al. 2018) This is quite important because Andrade et al. showed in a detailed review article that there is a relevant percentage of donor-site morbidity after knee-to-knee or knee-to-ankle osteochondral transfer. (Andrade et al. 2016) The mean donor-site morbidity was up to 17% of all patients. The authors described symptoms of persistent knee effusion and pain, particularly when climbing stairs and in a kneeling position, patellofemoral malfunction and postoperative crepitation of the knee. (Andrade et al. 2016; Matsuura et al. 2019; Quarch et al. 2014) Reducing the amount of cartilage harvested may also lower the risk for donor-site morbidity.

Using a co-culture system also improves another previously described issue: the tissue quality. We were able to show that replacing a certain percentage of chondrocytes by MSCs led to reduced hypertrophy and improved biomechanical properties of the tissue compared to a monoculture of MSCs or chondrocytes. (Zou, Bai, and Yao 2018) The co-culture reduced the rate of chondrocyte dedifferentiation and helped to regenerate

the bone and cartilage layer of osteochondral defects. (Zhang et al. 2018; Hubka et al. 2014) Furthermore, in-vitro and in-vivo studies demonstrated a satisfactory production of neo-cartilage in histological analysis. (Morrison et al. 2018; Waters et al. 2013) This is supported by the results of our study. The co-culture system displayed a good collagen I and II production while there was a reduced collagen X expression compared to the mono-cultures of MSCs or chondrocytes.

Furthermore, fixation and potential loosening of the implants are important issues of clinical translation. Studies showed that bioactive materials present a much more rapid bonding to the living bone compared to non-bioactive materials. (Pina et al. 2018) This does not only work by producing an apatite-like layer on the surface but also by stimulating osteogenesis of the surrounding osteoblasts. Such materials promote cell adhesion and proliferation, bond tightly to the collagen fibrils of the surrounding bone and improves biomechanical properties of the engineered tissue. (Moncada-Saucedo et al. 2019; Marionneaux et al. 2018) We demonstrated that the bony part of the multilayered osteochondral scaffold was capable of forming an apatite layer. This may be beneficial for scaffold fixation as well as healing of additional bone defects. Abdullah et al. published an extensive review of different bioactive implants in orthopaedic surgery. In conclusion, they found that bioactive materials lead to better osteointegration and mechanical strength of the implants. (Abdullah et al. 2015; Al Mugeiren and Baseer 2019) Studies show that bioactive materials can reduce the risk for implant loosening, using the example of dental implants. (Jiang et al. 2020) Therefore, the layered structure of our scaffolds with a bioactive bony segment can lead to improved integration into the osteochondral defect without any major influence of the cartilage segment.

Summary and Outlook

Our project demonstrates that it is possible to improve the quality of cartilage regeneration by influencing different variables. A smart scaffold design and combination of different cell types are promising approaches for enhanced cartilage tissue engineering.

As the next steps to clinical translation, animal experiments for an in-vivo examination should be performed. Additionally, a combination of the gel and scaffold project would be desirable. Using a co-culture of stem cells and chondrocytes on a multilayered scaffold may even increase the amount and quality of de-novo tissue formation. In summary, cartilage tissue engineering will be able to display good clinical results and less complications by modifying certain parameters.

Summaries of publications included in this thesis

Summary of publication #1 - Hyaluronic acid facilitates chondrogenesis and matrix deposition of human adipose derived mesenchymal stem cells and human chondrocytes co-cultures

The aim of this project was to evaluate chondrogenesis of a chondrocyte - stem cell co-culture in different compositions of COL-HA gels.

For all experiments, both different co-culture conditions and different gel-compositions were used and evaluated for cell viability, proliferation, gene expression, glycosaminoglycan production, tissue formation in histology and immunohistochemistry assays, biomechanical properties and oxygen distribution. Five different co-culture conditions were performed (I. 100% human AMSCs (hAMSCs), II. 75% hAMSCs + 25% hACs, III. 50% hAMSCs + 50% hACs, IV. 25% hAMSCs + 75% hACs and V. 100% hACs) and three different gel compositions (type I bovine collagen solution with 0%, 1% or 5% hyaluronic acid solution) were used.

Cell viability, evaluated by MTT and LDH-assay, displayed the best results in gel-compositions with a higher amount of hyaluronic acid. Cell proliferation was analysed by quantifying the dsDNA content. The highest proliferation rates were detected in the groups of only AMSCs, whereas ACs displayed the lowest proliferation rate. In all examined cell-compositions, the addition of HA led to significantly higher proliferation rates compared to the plain collagen gel.

The quality of chondrogenesis was evaluated by gene expression of cartilage and hypertrophy markers, assessment of GAG production, histology and immunohistochemistry evaluation as well as examination of the biomechanical properties. Supplementation of the gel with 1% HA displayed the best results in all experiments. It was also shown that replacing 25% of the ACs with AMSCs led to a similar tissue formation compared to the condition of 100% ACs. Furthermore, this addition of 25% AMSCs led to less hypertrophy and even better biomechanical properties.

To summarise, the research performed demonstrated that a co-culture of 75% ACs and 25% AMSCs displayed the best results in gene-expression and ECM production. Furthermore, a combination of type I collagen with 1% HA promoted an optimal environment for chondrogenesis of the aforementioned cell composition.

As first author of this publication, it was my task to perform the major part of the work including all material and cell experiments, data collection and treatment and statistical analysis as well as writing the first draft of the publication. The study design, planning and funding as well as manuscript correction and review were performed by Elizabeth R. Balmayor and Martijn van Griensven. The measurements of biomechanical properties were performed by me with the support of Ernst Breel, Optics 11, Amsterdam. The oxygen measurements were part of the project “Happihypo” funded by the Bayerische Forschungstiftung and performed by me with the support of Paul Wolff.

Summary of publication #2 - A graded, porous composite of natural biopolymers and octacalcium phosphate guides osteochondral differentiation of stem cells

The aim of the project was to develop a new graded scaffold for directed stem cell differentiation. Osteochondral lesions affect the hyaline cartilage as well as the subchondral bone. Bone and cartilage tissues are connected by an interface, termed the osteochondral interface, which is rich in calcified cartilage.

The scaffold was produced using a layer-by-layer freeze-drying process. The different layers consisted of collagen, chitosan and at the bony region OCP. A comprehensive characterization was performed to analyse the structure, biocompatibility and bioactivity of the scaffold.

μ CT analysis showed a fluent transition between all layers with a homogenous porous structure and wall thickness. Bioactivity was evaluated by incubating the scaffolds for up to 7 days in a SBF. By using various methods, it was shown that the scaffold was able to form an apatite-like layer first at the bony part and, following a longer incubation time, also on the rest of the scaffold.

To analyse the biocompatibility of the scaffolds, AMSCs were seeded on each scaffold and cultivated up to 35 days. In a first step, the optimal cell density was determined by analysing cell toxicity and viability of the different cell concentrations used. A total of 10^5 cells per scaffold displayed the best results and was, therefore, used for all further experiments.

Calcein-AM/PI/DAPI-staining showed an even distribution of the cells on the entire scaffold at each point of observation. Furthermore, SEM demonstrated the homogenous distribution of the cells and changes of morphology in the different layers. At the bony layer, mineral deposition was also visible and detectable by SEM-EDS. Gene expression was specifically evaluated by sectioning the scaffold in two parts – bone and cartilage parts. Osteogenic markers were upregulated in the bony part as well as chondrogenic markers in the cartilage part. The production of a cartilage-like matrix was also observable by a more intense Safranin-O staining after 35 days.

Our study demonstrated that it is possible to promote the differentiation of stem cells along different pathways on a single scaffold by using an intelligent scaffold design.

As first author of the described project, I performed all the experiments, data collection and analysis as well as writing the first draft of the publication. The scaffold design and production were performed by Amisel Amirall, Francisco J. Sola Dueñas and Gastón Fuentes Estévez of the Biomaterials Center, University of Havana, Cuba. This project was executed on the frame of a scientific collaboration of my thesis supervisor, Elizabeth R. Balmayor, and the Biomaterials Center in Cuba. The scaffold characterisation was performed during an internship at the 3B's Research Group, University of Minho, Portugal with the great support of Albina R. Franco, Isabel B. Leonor and Rui L. Reis. My research internship at the 3B's Research group in Portugal was funded by the TUM Graduate School. The study design, funding and planning as well as the correction and review of the manuscript were performed by Elizabeth R. Balmayor and Martijn van Griensven.

References

- Abdullah, M. R., A. Goharian, M. R. Abdul Kadir, and M. U. Wahit. 2015. 'Biomechanical and bioactivity concepts of polyetheretherketone composites for use in orthopedic implants-a review', *J Biomed Mater Res A*, 103: 3689-702.
- Ahmed, M. R., A. Mehmood, F. U. Bhatti, S. N. Khan, and S. Riazuddin. 2014. 'Combination of ADMSCs and chondrocytes reduces hypertrophy and improves the functional properties of osteoarthritic cartilage', *Osteoarthritis Cartilage*, 22: 1894-901.
- Al Mugeiren, O. M., and M. A. Baseer. 2019. 'Dental Implant Bioactive Surface Modifiers: An Update', *J Int Soc Prev Community Dent*, 9: 1-4.
- Albright, J. C., and A. K. Daoud. 2017. 'Microfracture and Microfracture Plus', *Clin Sports Med*, 36: 501-07.
- Aldrian, S., L. Zak, B. Wondrasch, C. Albrecht, B. Stelzeneder, H. Binder, F. Kovar, S. Trattnig, and S. Marlovits. 2014. 'Clinical and radiological long-term outcomes after matrix-induced autologous chondrocyte transplantation: a prospective follow-up at a minimum of 10 years', *Am J Sports Med*, 42: 2680-8.
- Amann, E., P. Wolff, E. Breeel, M. van Griensven, and E. R. Balmayor. 2017. 'Hyaluronic acid facilitates chondrogenesis and matrix deposition of human adipose derived mesenchymal stem cells and human chondrocytes co-cultures', *Acta Biomater*, 52: 130-44.
- Anderson, J. J., and D. T. Felson. 1988. 'Factors associated with osteoarthritis of the knee in the first national Health and Nutrition Examination Survey (HANES I). Evidence for an association with overweight, race, and physical demands of work', *Am J Epidemiol*, 128: 179-89.
- Andrade, R., S. Vasta, R. Pereira, H. Pereira, R. Papalia, M. Karahan, J. M. Oliveira, R. L. Reis, and J. Espregueira-Mendes. 2016. 'Knee donor-site morbidity after mosaicplasty - a systematic review', *J Exp Orthop*, 3: 31.
- Andriolo, L., D. Reale, A. Di Martino, S. Zaffagnini, F. Vannini, A. Ferruzzi, and G. Filardo. 2019. 'High Rate of Failure After Matrix-Assisted Autologous

- Chondrocyte Transplantation in Osteoarthritic Knees at 15 Years of Follow-up', *Am J Sports Med*: 363546519855029.
- Becerra, J., J. A. Andrades, E. Guerado, P. Zamora-Navas, J. M. Lopez-Puertas, and A. H. Reddi. 2010. 'Articular cartilage: structure and regeneration', *Tissue Eng Part B Rev*, 16: 617-27.
- Behrens, P., T. Bitter, B. Kurz, and M. Russlies. 2006. 'Matrix-associated autologous chondrocyte transplantation/implantation (MACT/MACI)--5-year follow-up', *Knee*, 13: 194-202.
- Bentley, G., L. C. Biant, S. Vijayan, S. Macmull, J. A. Skinner, and R. W. Carrington. 2012. 'Minimum ten-year results of a prospective randomised study of autologous chondrocyte implantation versus mosaicplasty for symptomatic articular cartilage lesions of the knee', *J Bone Joint Surg Br*, 94: 504-9.
- Berenbaum, F., I. J. Wallace, D. E. Lieberman, and D. T. Felson. 2018. 'Modern-day environmental factors in the pathogenesis of osteoarthritis', *Nat Rev Rheumatol*, 14: 674-81.
- Bert, J. M., and T. M. Bert. 2014. 'Nonoperative treatment of unicompartmental arthritis: from bracing to injection', *Clin Sports Med*, 33: 1-10.
- Blaney Davidson, E. N., P. M. van der Kraan, and W. B. van den Berg. 2007. 'TGF-beta and osteoarthritis', *Osteoarthritis Cartilage*, 15: 597-604.
- Border, W. A., and E. Ruoslahti. 1992. 'Transforming growth factor-beta in disease: the dark side of tissue repair', *J Clin Invest*, 90: 1-7.
- Brittberg, M., A. Lindahl, A. Nilsson, C. Ohlsson, O. Isaksson, and L. Peterson. 1994. 'Treatment of deep cartilage defects in the knee with autologous chondrocyte transplantation', *N Engl J Med*, 331: 889-95.
- Burr, D. B., and M. A. Gallant. 2012. 'Bone remodelling in osteoarthritis', *Nat Rev Rheumatol*, 8: 665-73.
- Chavan, D., T. C. van de Watering, G. Gruca, J. H. Rector, K. Heeck, M. Slaman, and D. Iannuzzi. 2012. 'Ferrule-top nanoindenter: an optomechanical fiber sensor for nanoindentation', *Rev Sci Instrum*, 83: 115110.
- Chen, S., P. Fu, H. Wu, and M. Pei. 2017. 'Meniscus, articular cartilage and nucleus pulposus: a comparative review of cartilage-like tissues in anatomy, development and function', *Cell Tissue Res*, 370: 53-70.

- Cicutтини, F., C. Ding, A. Wluka, S. Davis, P. R. Ebeling, and G. Jones. 2005. 'Association of cartilage defects with loss of knee cartilage in healthy, middle-age adults: a prospective study', *Arthritis Rheum*, 52: 2033-9.
- Croft, P., D. Coggon, M. Cruddas, and C. Cooper. 1992. 'Osteoarthritis of the hip: an occupational disease in farmers', *BMJ*, 304: 1269-72.
- Dall'Oca, C., M. Cengarle, A. Costanzo, N. Giannini, A. Vacchiano, and B. Magnan. 2017. 'Current concepts in treatment of early knee osteoarthritis and osteochondral lesions; the role of biological augmentations', *Acta Biomed*, 88: 5-10.
- De Mori, A., M. Pena Fernandez, G. Blunn, G. Tozzi, and M. Roldo. 2018. '3D Printing and Electrospinning of Composite Hydrogels for Cartilage and Bone Tissue Engineering', *Polymers (Basel)*, 10.
- Doulabi, A. H., K. Mequanint, and H. Mohammadi. 2014. 'Blends and Nanocomposite Biomaterials for Articular Cartilage Tissue Engineering', *Materials (Basel)*, 7: 5327-55.
- Driban, J. B., L. L. Price, J. Lynch, M. Nevitt, G. H. Lo, C. B. Eaton, and T. E. McAlindon. 2016. 'Defining and evaluating a novel outcome measure representing end-stage knee osteoarthritis: data from the Osteoarthritis Initiative', *Clin Rheumatol*, 35: 2523-30.
- Erol, M. F., and O. Karakoyun. 2016. 'A new point of view for mosaicplasty in the treatment of focal cartilage defects of knee joint: honeycomb pattern', *Springerplus*, 5: 1170.
- Eyre, D. R., D. M. Brickley-Parsons, and M. J. Glimcher. 1978. 'Predominance of type I collagen at the surface of avian articular cartilage', *FEBS Lett*, 85: 259-63.
- Farr, J., G. C. Gracitelli, N. Shah, E. Y. Chang, and A. H. Gomoll. 2016. 'High Failure Rate of a Decellularized Osteochondral Allograft for the Treatment of Cartilage Lesions', *Am J Sports Med*, 44: 2015-22.
- Felson, D. T. 2004. 'An update on the pathogenesis and epidemiology of osteoarthritis', *Radiol Clin North Am*, 42: 1-9, v.
- Felson, D. T., and Y. Zhang. 1998. 'An update on the epidemiology of knee and hip osteoarthritis with a view to prevention', *Arthritis Rheum*, 41: 1343-55.

- Felson, D. T., Y. Zhang, M. T. Hannan, A. Naimark, B. N. Weissman, P. Aliabadi, and D. Levy. 1995. 'The incidence and natural history of knee osteoarthritis in the elderly. The Framingham Osteoarthritis Study', *Arthritis Rheum*, 38: 1500-5.
- Frank, R. M., S. Lee, D. Levy, S. Poland, M. Smith, N. Scalise, G. L. Cvetanovich, and B. J. Cole. 2017. 'Osteochondral Allograft Transplantation of the Knee: Analysis of Failures at 5 Years', *Am J Sports Med*, 45: 864-74.
- Gimble, J. M., A. J. Katz, and B. A. Bunnell. 2007. 'Adipose-derived stem cells for regenerative medicine', *Circ Res*, 100: 1249-60.
- Heinegard, D., and A. Oldberg. 1989. 'Structure and biology of cartilage and bone matrix noncollagenous macromolecules', *FASEB J*, 3: 2042-51.
- Homminga, G. N., S. K. Bulstra, P. S. Bouwmeester, and A. J. van der Linden. 1990. 'Perichondral grafting for cartilage lesions of the knee', *J Bone Joint Surg Br*, 72: 1003-7.
- Huang, L., B. Guo, F. Xu, and J. Zhao. 2018. 'Effects of quadriceps functional exercise with isometric contraction in the treatment of knee osteoarthritis', *Int J Rheum Dis*, 21: 952-59.
- Hubka, K. M., R. L. Dahlin, V. V. Meretoja, F. K. Kasper, and A. G. Mikos. 2014. 'Enhancing chondrogenic phenotype for cartilage tissue engineering: monoculture and coculture of articular chondrocytes and mesenchymal stem cells', *Tissue Eng Part B Rev*, 20: 641-54.
- Hunziker, E. B. 2002. 'Articular cartilage repair: basic science and clinical progress. A review of the current status and prospects', *Osteoarthritis Cartilage*, 10: 432-63.
- Jiang, X., Y. Yao, W. Tang, D. Han, L. Zhang, K. Zhao, S. Wang, and Y. Meng. 2020. 'Design of Dental Implants at Materials Level: An Overview', *J Biomed Mater Res A*.
- Jones, K. J., and B. M. Cash. 2019. 'Matrix-Induced Autologous Chondrocyte Implantation With Autologous Bone Grafting for Osteochondral Lesions of the Femoral Trochlea', *Arthrosc Tech*, 8: e259-e66.
- Jordan, K. M., N. K. Arden, M. Doherty, B. Bannwarth, J. W. Bijlsma, P. Dieppe, K. Gunther, H. Hauselmann, G. Herrero-Beaumont, P. Kaklamanis, S. Lohmander, B. Leeb, M. Lequesne, B. Mazieres, E. Martin-Mola, K. Pavelka, A. Pendleton, L. Punzi, U. Serni, B. Swoboda, G. Verbruggen, I. Zimmerman-

- Gorska, M. Dougados, and Escisit Standing Committee for International Clinical Studies Including Therapeutic Trials. 2003. 'EULAR Recommendations 2003: an evidence based approach to the management of knee osteoarthritis: Report of a Task Force of the Standing Committee for International Clinical Studies Including Therapeutic Trials (ESCISIT)', *Ann Rheum Dis*, 62: 1145-55.
- Kon, E., G. Filardo, A. Gobbi, M. Berruto, L. Andriolo, P. Ferrua, I. Crespiatico, and M. Marcacci. 2016. 'Long-term Results After Hyaluronan-based MACT for the Treatment of Cartilage Lesions of the Patellofemoral Joint', *Am J Sports Med*, 44: 602-8.
- Liu, M., X. Zeng, C. Ma, H. Yi, Z. Ali, X. Mou, S. Li, Y. Deng, and N. He. 2017. 'Injectable hydrogels for cartilage and bone tissue engineering', *Bone Res*, 5: 17014.
- Lorenzo, P., M. T. Bayliss, and D. Heinegard. 1998. 'A novel cartilage protein (CILP) present in the mid-zone of human articular cartilage increases with age', *J Biol Chem*, 273: 23463-8.
- Marionneaux, A., J. Walters, H. Guo, and J. Mercuri. 2018. 'Tailoring the subchondral bone phase of a multi-layered osteochondral construct to support bone healing and a cartilage analog', *Acta Biomater*, 78: 351-64.
- Martel-Pelletier, J., A. J. Barr, F. M. Cicuttini, P. G. Conaghan, C. Cooper, M. B. Goldring, S. R. Goldring, G. Jones, A. J. Teichtahl, and J. P. Pelletier. 2016. 'Osteoarthritis', *Nat Rev Dis Primers*, 2: 16072.
- Matsuura, T., Y. Hashimoto, T. Kinoshita, K. Nishino, Y. Nishida, J. Takigami, H. Katsuda, and N. Shimada. 2019. 'Donor Site Evaluation After Osteochondral Autograft Transplantation for Capitellar Osteochondritis Dissecans', *Am J Sports Med*, 47: 2836-43.
- Medvedeva, E. V., E. A. Grebenik, S. N. Gornostaeva, V. I. Telpuhov, A. V. Lychagin, P. S. Timashev, and A. S. Chagin. 2018. 'Repair of Damaged Articular Cartilage: Current Approaches and Future Directions', *Int J Mol Sci*, 19.
- Meessen, Jmta, C. S. Leichtenberg, C. Tilbury, B. L. Kaptein, L. A. Koster, P. E. Slagboom, S. H. M. Verdegaal, R. Onstenk, H. M. J. van der Linden-van der Zwaag, H. Kaptijn, S. B. W. Vehmeijer, W. C. Marijnissen, P. J. Damen, Rghh Nelissen, and T. P. M. Vliet Vlieland. 2018. 'Frailty in end-stage hip or knee

- osteoarthritis: validation of the Groningen Frailty Indicator (GFI) questionnaire', *Rheumatol Int*, 38: 917-24.
- Meirer, F., B. Pemmer, G. Peponi, N. Zoeger, P. Wobrauschek, S. Sprio, A. Tampieri, J. Goettlicher, R. Steininger, S. Mangold, P. Roschger, A. Berzlanovich, J. G. Hofstaetter, and C. Strelt. 2011. 'Assessment of chemical species of lead accumulated in tidemarks of human articular cartilage by X-ray absorption near-edge structure analysis', *J Synchrotron Radiat*, 18: 238-44.
- Messner, K., and W. Maletius. 1996. 'The long-term prognosis for severe damage to weight-bearing cartilage in the knee: a 14-year clinical and radiographic follow-up in 28 young athletes', *Acta Orthop Scand*, 67: 165-8.
- Mithoefer, K., T. McAdams, R. J. Williams, P. C. Kreuz, and B. R. Mandelbaum. 2009. 'Clinical efficacy of the microfracture technique for articular cartilage repair in the knee: an evidence-based systematic analysis', *Am J Sports Med*, 37: 2053-63.
- Moncada-Saucedo, N. K., I. A. Marino-Martinez, J. Lara-Arias, V. J. Romero-Diaz, A. Camacho, J. A. Valdes-Franco, V. Perez-Silos, A. Garcia-Ruiz, H. Lin, R. S. Tuan, R. Ramos-Payan, M. Lara-Banda, R. Ortiz-Lopez, A. Rojas-Martinez, and L. Fuentes-Mera. 2019. 'A Bioactive Cartilage Graft of IGF1-Transduced Adipose Mesenchymal Stem Cells Embedded in an Alginate/Bovine Cartilage Matrix Tridimensional Scaffold', *Stem Cells Int*, 2019: 9792369.
- Morrison, R. J., H. B. Nasser, K. N. Kashlan, D. A. Zopf, D. J. Milner, C. L. Flanagan, M. B. Wheeler, G. E. Green, and S. J. Hollister. 2018. 'Co-culture of adipose-derived stem cells and chondrocytes on three-dimensionally printed bioscaffolds for craniofacial cartilage engineering', *Laryngoscope*, 128: E251-E57.
- Nagel-Heyer, S., C. Goepfert, P. Adamietz, N. M. Meenen, and R. Portner. 2006. 'Cultivation of three-dimensional cartilage-carrier-constructs under reduced oxygen tension', *J Biotechnol*, 121: 486-97.
- Nazempour, A., and B. J. Van Wie. 2016. 'Chondrocytes, Mesenchymal Stem Cells, and Their Combination in Articular Cartilage Regenerative Medicine', *Ann Biomed Eng*, 44: 1325-54.
- Ng, A., and K. Bernhard. 2017. 'Osteochondral Autograft and Allograft Transplantation in the Talus', *Clin Podiatr Med Surg*, 34: 461-69.

- Nguyen, P. D., T. D. Tran, H. T. Nguyen, H. T. Vu, P. T. Le, N. L. Phan, N. B. Vu, N. K. Phan, and P. Van Pham. 2017. 'Comparative Clinical Observation of Arthroscopic Microfracture in the Presence and Absence of a Stromal Vascular Fraction Injection for Osteoarthritis', *Stem Cells Transl Med*, 6: 187-95.
- Niemeyer, P., M. J. Feucht, J. Fritz, D. Albrecht, G. Spahn, and P. Angele. 2016. 'Cartilage repair surgery for full-thickness defects of the knee in Germany: indications and epidemiological data from the German Cartilage Registry (KnorpelRegister DGOU)', *Arch Orthop Trauma Surg*, 136: 891-7.
- Noyes, F. R., and C. L. Stabler. 1989. 'A system for grading articular cartilage lesions at arthroscopy', *Am J Sports Med*, 17: 505-13.
- Oyane, A., H. M. Kim, T. Furuya, T. Kokubo, T. Miyazaki, and T. Nakamura. 2003. 'Preparation and assessment of revised simulated body fluids', *J Biomed Mater Res A*, 65: 188-95.
- Pei, M., C. Yu, and M. Qu. 2000. 'Expression of collagen type I, II and III in loose body of osteoarthritis', *J Orthop Sci*, 5: 288-93.
- Pina, S., R. Rebelo, V. M. Correlo, J. M. Oliveira, and R. L. Reis. 2018. 'Bioceramics for Osteochondral Tissue Engineering and Regeneration', *Adv Exp Med Biol*, 1058: 53-75.
- Poole, C. A. 1997. 'Articular cartilage chondrons: form, function and failure', *J Anat*, 191 (Pt 1): 1-13.
- Quarch, V. M., E. Enderle, J. Lotz, and K. H. Frosch. 2014. 'Fate of large donor site defects in osteochondral transfer procedures in the knee joint with and without TruFit plugs', *Arch Orthop Trauma Surg*, 134: 657-66.
- Riboh, J. C., G. L. Cvetanovich, B. J. Cole, and A. B. Yanke. 2017. 'Comparative efficacy of cartilage repair procedures in the knee: a network meta-analysis', *Knee Surg Sports Traumatol Arthrosc*, 25: 3786-99.
- Richter, D. L., R. C. Schenck, Jr., D. C. Wascher, and G. Treme. 2016. 'Knee Articular Cartilage Repair and Restoration Techniques: A Review of the Literature', *Sports Health*, 8: 153-60.
- Rosa, D., S. L. Di Donato, G. Balato, A. D'Addona, F. Smeraglia, G. Correra, and G. Di Vico. 2017. 'How to Manage a Failed Cartilage Repair: A Systematic Literature Review', *Joints*, 5: 93-106.

- Salzmann, G. M., B. Sah, N. P. Sudkamp, and P. Niemeyer. 2013. 'Reoperative characteristics after microfracture of knee cartilage lesions in 454 patients', *Knee Surg Sports Traumatol Arthrosc*, 21: 365-71.
- Schinhan, M., M. Gruber, R. Dorotka, M. Pilz, D. Stelzeneder, C. Chiari, N. Rossler, R. Windhager, and S. Nehrer. 2013. 'Matrix-associated autologous chondrocyte transplantation in a compartmentalized early stage of osteoarthritis', *Osteoarthritis Cartilage*, 21: 217-25.
- Schneider, S., M. Unger, M. van Griensven, and E. R. Balmayor. 2017. 'Adipose-derived mesenchymal stem cells from liposuction and resected fat are feasible sources for regenerative medicine', *Eur J Med Res*, 22: 17.
- Schuetz, H. B., M. J. Kraeutler, and E. C. McCarty. 2017. 'Matrix-Assisted Autologous Chondrocyte Transplantation in the Knee: A Systematic Review of Mid- to Long-Term Clinical Outcomes', *Orthop J Sports Med*, 5: 2325967117709250.
- Schumacher, B. L., J. A. Block, T. M. Schmid, M. B. Aydelotte, and K. E. Kuettner. 1994. 'A novel proteoglycan synthesized and secreted by chondrocytes of the superficial zone of articular cartilage', *Arch Biochem Biophys*, 311: 144-52.
- Sherman, S. L., E. Thyssen, and C. W. Nuelle. 2017. 'Osteochondral Autologous Transplantation', *Clin Sports Med*, 36: 489-500.
- Ulstein, S., A. Aroen, J. H. Rotterud, S. Loken, L. Engebretsen, and S. Heir. 2014. 'Microfracture technique versus osteochondral autologous transplantation mosaicplasty in patients with articular chondral lesions of the knee: a prospective randomized trial with long-term follow-up', *Knee Surg Sports Traumatol Arthrosc*, 22: 1207-15.
- van den Berg, W. B., P. M. van der Kraan, A. Scharstuhl, and H. M. van Beuningen. 2001. 'Growth factors and cartilage repair', *Clin Orthop Relat Res*: S244-50.
- Vinatier, C., and J. Guicheux. 2016. 'Cartilage tissue engineering: From biomaterials and stem cells to osteoarthritis treatments', *Ann Phys Rehabil Med*, 59: 139-44.
- Waters, H. A., C. P. Geffre, D. A. Gonzales, W. A. Grana, and J. A. Szivek. 2013. 'Co-culture of adipose derived stem cells and chondrocytes with surface modifying proteins induces enhanced cartilage tissue formation', *J Invest Surg*, 26: 118-26.

- Xia, B., Chen Di, J. Zhang, S. Hu, H. Jin, and P. Tong. 2014. 'Osteoarthritis pathogenesis: a review of molecular mechanisms', *Calcif Tissue Int*, 95: 495-505.
- Yabumoto, H., Y. Nakagawa, S. Mukai, and T. Saji. 2017. 'Osteochondral autograft transplantation for isolated patellofemoral osteoarthritis', *Knee*, 24: 1498-503.
- Zhang, C., Y. Z. Cai, and X. J. Lin. 2016. 'Autologous chondrocyte implantation: Is it likely to become a saviour of large-sized and full-thickness cartilage defect in young adult knee?', *Knee Surg Sports Traumatol Arthrosc*, 24: 1643-50.
- Zhang, Y., W. Guo, M. Wang, C. Hao, L. Lu, S. Gao, X. Zhang, X. Li, M. Chen, P. Li, P. Jiang, S. Lu, S. Liu, and Q. Guo. 2018. 'Co-culture systems-based strategies for articular cartilage tissue engineering', *J Cell Physiol*, 233: 1940-51.
- Zou, J., B. Bai, and Y. Yao. 2018. 'Progress of co-culture systems in cartilage regeneration', *Expert Opin Biol Ther*, 18: 1151-58.

List of figures

Figure 1: Overview of methods used in the study	14
Figure 2: Digital microscope picture with full depth of field of 3-layered scaffold	16
Figure 3: Representative SEM image of the scaffold after 3 weeks of cell cultivation. In the image, the pore part can be appreciated. Used magnification was 500x.	19
Figure 4: Biomechanical measurements of collagen gels. This figure was modified and reproduced from the publication included in this thesis (Amann et al. 2017) with permission from Elsevier.	25
Figure 5: Representative SEM image showing bioactivity of the bone region of the scaffolds after 7 days of incubation in SBF. Magnification used was 2500x.	26

Acknowledgements

There are many people who accompanied me in my journey through university and this doctoral thesis. I would like to take a moment to thank them.

First, I would like to thank Elizabeth Rosado Balmayor, PhD and Professor Martijn van Griensven, PhD, as my mentor and supervisor, for enabling and supervising my projects, publications and this thesis. A big thank you, for being an inspiring and bright support. It was an honour to work with you.

I like to thank Professor Peter Biberthaler, MD, head of the Trauma Surgery, Klinikum rechts der Isar, for the opportunity to perform my research and thereby creating this thesis.

I like to thank my parents for their endless love, support and understanding. Their big effort and long-lasting help enabled me to become what I am today.

I also like to thank all my faithful companions, family, friends, teachers and acquaintances who helped me to never give up.

Finally, I would like to thank Anestes, my best friend and love of my life, for his patience, encouragement and support. This wouldn't have been possible without him.

Appendix

Full research article “Hyaluronic acid facilitates chondrogenesis and matrix deposition of human adipose derived mesenchymal stem cells and human chondrocytes co-cultures ”

Acta Biomaterialia 52 (2017) 130–144



Contents lists available at ScienceDirect

Acta Biomaterialia

journal homepage: www.elsevier.com/locate/actabiomat



Full length article

Hyaluronic acid facilitates chondrogenesis and matrix deposition of human adipose derived mesenchymal stem cells and human chondrocytes co-cultures [☆]



Elisabeth Amann ^a, Paul Wolff ^a, Ernst Breel ^b, Martijn van Griensven ^a, Elizabeth R. Balmayor ^{a,*}

^a Experimental Trauma Surgery, Klinikum rechts der Isar, Technical University of Munich, 81675 Munich, Germany

^b Optics11 BV, 1081 HV Amsterdam, The Netherlands

ARTICLE INFO

Article history:

Received 13 August 2016

Received in revised form 8 January 2017

Accepted 23 January 2017

Available online 25 January 2017

Keywords:

Co-culture

Human adipose-derived mesenchymal stem cells

Human chondrocytes

Hyaluronic acid

Chondrogenesis

ABSTRACT

Clinical success on cartilage regeneration could be achieved by using available biomaterials and cell-based approaches. In this study, we have developed a composite gel based on collagen/hyaluronic acid (Coll-HA) as ideal, physiologically representative 3D support for *in vitro* chondrogenesis of human adipose-derived mesenchymal stem cells (hAMSCs) co-cultured with human articular chondrocytes (hAC). The incorporation of hyaluronic acid (HA) attempted to provide an additional stimulus to the hAMSCs for chondrogenesis and extracellular matrix deposition. Coll-HA gels were fabricated by directly mixing different amounts of HA (0–5%) into collagen solution before gelation. hACs and hAMSCs were co-cultured at different ratios from 100% to 0% in steps of 25%. Thus, five different co-culture groups were tested in the various Coll-HA 3D matrices. HA greatly impacted the cell viability and proliferation as well as the mechanical properties of the Coll-HA gel. The effective Young's modulus changed from 5.8 to 9.0 kPa with increasing concentrations of HA in the gel. In addition, significantly higher amounts of glycosaminoglycan (GAG) were detected that seemed to be dependent on HA content. The highest HA concentration used (5%) resulted in the lowest Collagen type X (Col10) expression for most of the cell culture groups. Unexpectedly, culturing in these gels was also associated with decreased SOX9 and Collagen type II (Col2) expression, while Collagen type III (Col3) and metalloproteinase 13 notably increased. By using 1% HA, a positive effect on SOX9 expression was observed in the co-culture groups. In addition, a significant increase in GAGs production was also detected. Regarding co-culturing, the group with 25% hAMSCs + 75% hACs was the most chondrogenic one considering SOX9 and Col2 expression as well as GAGs production. This group showed negligible Col10 expression after 35 days of culture independently of the gel used. It also featured the highest effective Young's modulus (9.9 kPa) when cultivated in the 1% HA matrix. Concerning the level of dissolved oxygen *in situ*, the groups with a higher amount of hAMSCs showed lower oxygen levels (40–58% O₂) compared to hACs (63–74% O₂). This might be attributed to the higher cellular metabolism and proliferation rate of the hAMSCs. Interestingly, lower oxygen was detected in the HA-containing gels when compared to plain collagen. This may contribute to the better chondrogenesis observed in these groups. Altogether, our results indicated that HA may favor chondrogenesis, but its effect highly depends on the concentration used. Additionally, co-culture of hACs with hAMSCs also favors chondrogenesis and especially increases extracellular matrix production and decreases hypertrophy.

Statement of Significance

In the clinical situation, large cartilage defects can be treated with MACT. However, this is a two-stage procedure, which increases the risk for the patient. Moreover, culturing chondrocytes leads to dedifferentiation. The matrix used for MACT is a collagen-based scaffold. In this study, it was demonstrated that hyaluronic acid, a natural component of the extracellular matrix, supplementation to a collagen hydrogel stimulates chondrogenic differentiation in a dose dependent manner. 1% HA showed the best overall results. Furthermore, exchanging 25% of human articular chondrocytes with adipose-derived mesenchymal stem cells didn't change the chondrogenic potential, but reduced going in unwanted pathways and

[☆] Part of the Special Issue on Extracellular Matrix Proteins and Mimics, organized by Professor Katja Schenke-Layland.

* Corresponding author at: Experimental Trauma Surgery, Klinikum rechts der Isar, Technical University of Munich, Ismaninger Str. 22, 81675 Munich, Germany.

E-mail address: elizabeth.rosado-balmayor@tum.de (E.R. Balmayor).

improved biomechanical properties. This could translate to a one-step procedure and shows the potential of inducing differentiation by natural biomaterials.

© 2017 Acta Materialia Inc. Published by Elsevier Ltd. All rights reserved.

1. Introduction

Cartilage tissue features poor self-healing capacity and it is avascular by nature. Cartilage lesions occur mostly as a result of trauma, age related degeneration and also in conditions like osteoarthritis. Osteoarthritis has an incidence of approximately 10% in men and 13% in women aged over 60 [1]. These figures are likely to increase due to aging and obesity. Thus, cartilage regeneration represents a unique challenge and an eminent clinical need. Current treatments include the *in situ* induction of cartilage repair by microfracture and matrix-associated autologous chondrocytes transplantation (MACT) [2,3]. Although some satisfactory results may be achieved by the use of these methodologies, they are still unsatisfying for long-term regeneration. Microfracture is limited to smaller defects, while MACT is costly and needs several surgical interventions [4,5]. Thus, novel regeneration strategies for cartilage tissue are needed. Among recently investigated approaches, cell-based cartilage regeneration strategies represent a feasible and promising alternative. While advantages are clear, selecting the optimal cell type for treatment remains a major challenge. As expected, mainly chondrocytes have been reported for cartilage cell-based treatments. Their selection as first choice is evident, however, they also feature important limitations. Large numbers of chondrocytes are needed to generate a functional biological construct to implant into the defect area [6,7]. Therefore, *in vitro* expansion is always needed. *In vitro* culture of chondrocytes has been reported to result in dedifferentiation resulting in fibrous and mechanically inferior newly formed cartilage tissue [8].

Currently, mesenchymal stem cells (MSCs) from various sources have been used as an attractive cell alternative. These cells can be isolated in greater number than chondrocytes. They can be expanded *in vitro* without losing their chondrogenic potential. Furthermore, they can be isolated from tissues like bone marrow and adipose tissue with minimal manipulation even at the operation theatre. Adipose-derived MSCs (AMSCs) feature additional advantages like the usage of “waste tissue material” with an abundant cell number per cm^3 of tissue [9]. Unfortunately, the use of pure MSCs for cartilage repair results in unstable and hypertrophic cartilage tissue with a high tendency to ossification [10,11]. Recent ideas support the use of a combination of MSCs and chondrocytes for cell-based approaches in cartilage regeneration [12,13]. Numerous advantages have been described. Among them are the possibly reduced number of chondrocytes needed and the stimulation of MSCs' chondrogenesis by the chondrocyte population based on a “teacher-student” approach [13]. Indeed, reduced hypertrophy and mineralization *in vitro* have been reported for MSCs/chondrocytes co-cultures when compared to pure MSCs [14]. Reducing the number of chondrocytes may be relevant for clinical translation. Furthermore, the need for *in vitro* expansion of chondrocytes may be overcome using freshly isolated cells.

Besides the cellular composition, the application of an adequate 3D matrix is of major importance in order to ensure sufficient nutrient supply to and extracellular matrix production by the cells. The materials used to compose the matrix may include important chondrogenic cues for a greater differentiation outcome. In addition, biomimetic materials mimicking the composition of native cartilage extracellular matrix composition and featuring similar mechanical properties are desired. Native articular cartilage is a composite material composed primarily of proteoglycans and collagen [15].

Proteoglycans bind to a hyaluronic acid (HA) backbone to form macromolecules. Thus, HA is a key component in the extracellular matrix of cartilage. Moreover, it is a major constituent of synovial fluid [16]. As a biomaterial, HA can be described as a biodegradable and highly biocompatible polysaccharide [16]. In addition, HA may interact with cells through surface receptors such as CD44, enabling modulation of cell activities such as migration, proliferation and differentiation, as well as matrix secretion [16,17].

The mechanical properties of the cartilage tissue are determined by the amounts and interaction of its main components, i.e. collagen, proteoglycan and water. Hence, the biomechanical properties of the cell-loaded matrices are critical for cell fate and extracellular matrix deposition. On the other hand, the levels of dissolved oxygen within the tissue seem to be essential for cell differentiation. It has been reported that lower oxygen levels are associated with better chondrogenesis [18,19]. This may be an expected result given the low oxygen environmental characteristic of native articular cartilage tissue [20].

In this study, we aimed to develop a functional 3D biological construct for cartilage regeneration based on natural extracellular matrix proteins and co-cultures of human AMSCs and human adult chondrocytes. On the one hand, we designed 3D collagen gels to which HA was added in different concentrations. This attempted to recreate a natural environment of lower oxygen levels and adequate biomechanics to support cartilage formation in the 3D matrix. The *in vitro* chondrogenesis was assessed by means of gene expression and extracellular matrix production as main evaluation criteria. On the other hand, we investigated co-cultures of AMSCs and chondrocytes as possible cell sources. Both cell types were isolated from human tissue, namely AMSCs from abdominal fat and articular chondrocytes from femur head cartilage. Thus, there is no species mismatch. In addition, the donor's age was in the range of 39–74 years old. Thereby, the age of the cells used better reflects the patient situation. Using chondrocytes from animal origin are almost always from pre-adolescent animals. They have a high intrinsic regeneration potential not reflecting the clinical situation. The main goal was to determine the best composition of the collagen-HA hydrogels and the optimal ratio of cell types in the co-culture.

2. Materials and methods

2.1. Isolation and culture of human adipose-derived mesenchymal stem cells (hAMSCs)

This study was approved by the local ethical committee of the University Hospital “Klinikum recht der Isar” at the Technical University of Munich, Germany. Human adipose tissue was obtained from the abdomen during gynecological surgeries with written informed patient's consent prior tissue collection. N = 3 donors (average age (\pm SD) 71 \pm 3.6 years) were used for tissue harvest.

Collected fat tissue was cut into small pieces and poured into 50 ml falcon tubes filled up with sterile Dulbecco's Phosphate-Buffered Saline without calcium and magnesium (DPBS). The mixture was centrifuged at room temperature for 10 min at 450g without breaks. Next, the upper fat layer was transferred into fresh falcon tubes and washed several times with DPBS. Next, the tissue was digested using a collagenase solution (0.8 mg/ml DPBS, colla-

genase type II, Biochrom GmbH, Berlin, Germany) at 37 °C for 30 min. After this incubation time, the collagenase reaction was stopped with pre-warmed complete cell culture media (Dulbecco's Modified Eagle's Medium (high glucose DMEM, Sigma-Aldrich, St. Louis, MO, USA) supplemented with 10% Fetal Calf Serum (FCS, Sigma-Aldrich) and 1% Penicillin/Streptomycin (P/S, Sigma-Aldrich)). The mixture was centrifuged at 600g for 10 min. The resulting cell pellet was resuspended with complete cell culture media and subsequently filtered through a 40 µm cell strainer (BD Falcon, NJ, USA). The cells were seeded at a density of 3000 cells/cm². A medium change was performed on the next day to remove non-adherent cells. hAMSCs were expanded until passage 2 using complete cell culture media as described above. Medium changes were performed twice a week.

2.2. Isolation and culture of human articular chondrocytes (hACs)

Human femur heads were collected from patients (N = 3, average age (±SD) 59 ± 19.2 years) with hip replacement procedures after written informed consent. The tissue harvested for isolation was healthy cartilage. Patients with previous diagnosis of osteoarthritis, arthrosis, osteosarcoma and bone metastases were excluded from our study as tissue donors. Similar to adipose tissue, the tissue collection and further use in this study was approved by the local ethical committee of the University Hospital "Klinikum recht der Isar" at the Technical University of Munich, Germany.

The articular cartilage was peeled off with scalpels and cut into small pieces of approximately 1 × 1 mm. The cartilage pieces were washed twice with DPBS. Next, the tissue was digested to obtain the cells (digestion solution: high glucose DMEM, 1% P/S, 0.15% collagenase type II (Biochrom GmbH)). The cartilage was digested overnight at 37 °C in 5% CO₂ under constant stirring (52 rpm) using 10 ml digestion solution per each gram of tissue. Subsequently, the mixture was filtered through a 100 µm cell strainer (BD Falcon) and the collected solution was centrifuged (500g) at room temper-

ature for 10 min. The resulting cell pellet was resuspended in chondrocyte expansion media (i.e. low glucose DMEM, 10% FCS, 1% P/S) and seeded at a density of 7500 cells/cm². The medium was changed 24 h after isolation and thereafter twice a week. hAC expansion was carried out until passage 2. At that moment, the cells still showed a chondrogenic phenotype.

2.3. Collagen-hyaluronic acid gels (Coll-HA)

100 mg of hyaluronic acid sodium salt from *Streptococcus equi* (molecular weight 1.5–1.8 MDA, Sigma-Aldrich) was dissolved in 10 ml DPBS under steady stirring at 4 °C overnight. The resulting viscous solution was sterilized by autoclaving for 15 min at 121 °C. The sterile HA solution was stored at 4 °C for subsequent use.

In order to form the collagen gels, a mixture consisting of 8 parts PureCol type I bovine collagen solution (Advanced BioMatrix, Carlsbad, CA, USA), 1 part 10× DMEM (Sigma-Aldrich) and 1 part 20 mM L-Glutamine (Sigma-Aldrich) was used. A volume of 500 µl of this mixture was pipetted into 48-well plates and incubated at 37 °C for 2 h to ensure gelation. In addition, in order to obtain the Coll-HA gels, HA was added to the collagen mixture just prior gelation. The final HA concentrations in the Coll-HA gels were 1% and 5% (w/v).

2.4. hAMSCs/hACs co-culture in Coll-HA gels

Both cell types were detached with trypsin/EDTA (Sigma-Aldrich), counted and each pooled from 3 different donors (i.e. for each cell type). Next, hAMSC and hACs were mixed to create five different co-culture conditions used in our study (Fig. 1) i.e. 75% hAMSCs/25%hACs (hereafter referred to as group II), 50% hAMSCs/50%hACs (group III) and 25%hAMSCs/75%hACs (group IV). In addition, two control groups were used, namely, 100% hAMSCs (group I) and 100% hACs (group V).

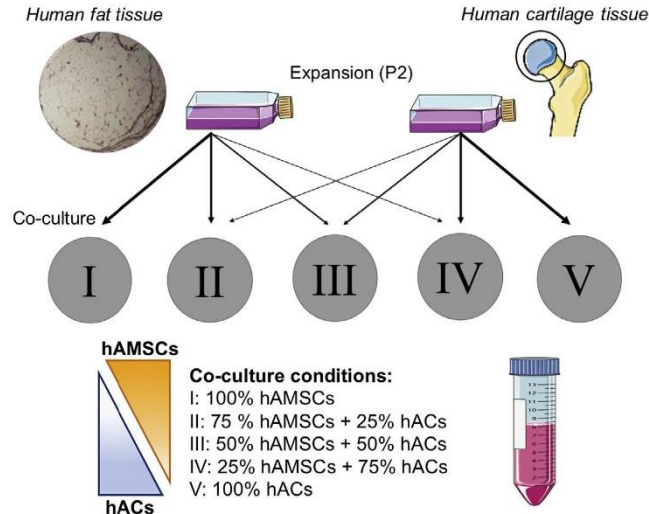


Fig. 1. Experimental set-up. Cell isolation from human fat tissue and human articular cartilage derived from femur heads obtained from patients needing total hip replacement after fracture. Culture and expansion was performed until passage 2. The human adipose-derived mesenchymal stem cells (hAMSC) were co-cultured with human articular chondrocytes (hAC) in steps of 25%. Thus, five different co-culture conditions I–V were established, whereas group I and group V were control groups with the single cell type alone each.

The cell mixtures were added to the gels using the L-Glutamine solution (being one part of the gel composition). The cell density used was 1×10^5 cells/500 μ l. Cell-laden hydrogels were cultured in 500 μ l culture medium (low glucose DMEM, 10% FCS, 1% P/S). Medium changes were performed twice a week and constructs were cultured up to 35 days.

2.5. Cell viability

For the evaluation of cell viability and possible material-related toxicity, the cell-seeded gels were cultured for 1, 3 and 7 days under standard culture conditions as described above. As indication of cell destruction, the presence of lactate dehydrogenase (LDH) was evaluated in the collected supernatant using a Fluitest LDH-L Kit (Analyticon, Lichtenfels, Germany).

To evaluate cell viability, an MTT [3-(4,5-Dimethylthiazol-2-yl)-2,5-diphenyltetrazoliumbromide] assay was performed following a previously described protocol [21] slightly modified for the cell-seeded 3D gels. In brief, DPBS washed gels were incubated in MTT solution containing 1.2 mM thiazolyl blue for 3 h at 37 °C and 5% CO₂. Next, gels were washed twice with DPBS and the MTT precipitate was dissolved with isopropanol for 18 h, protected from evaporation and light. 100 μ l of the supernatant was then transferred in triplicates to a 96-well plate and measured at 570/690 nm.

2.6. Cell proliferation

Cell-seeded Coll and Coll-HA gels were washed and subsequently digested in a two-step protocol. The samples were first treated with collagenase type II solution (1 mg/ml, Biochrom GmbH) for 20 min at 37 °C. During this incubation time, gels were mechanically detached and mixed by vigorously pipetting up and down. Subsequently, a papain digestion solution (0.1 mg/ml, Sigma-Aldrich) was added to the samples and the digestion was continued for another 3 h at 37 °C under gentle shaking. Finally, samples were collected and stored at –80 °C until further DNA and GAGs determinations.

DNA was quantified using the Quant-iT PicoGreen dsDNA assay kit (Invitrogen, Carlsbad, CA, USA). The measurement was performed after 7, 21 and 35 days of culture following the instructions manual. Shortly, equal volumes of cell lysate and Quant-iT PicoGreen working solution were pipetted into a 96-well plate. Five minutes after light-protected incubation at 37 °C, fluorescence was measured (emission: 520 nm and excitation: 485 nm) in a FLUOstar Omega photometer (BMG labtech).

2.7. RNA isolation and cDNA transcription

For RNA isolation, cell-seeded Coll and Coll-HA gels were collected at 7, 21 and 35 days by means of TRI Reagent (Sigma-Aldrich). Samples were stored at –80 °C until further processing using chloroform and isopropanol. Measurements of total RNA concentrations and RNA purity were performed spectrophotometrically using the Hellma Tray Cell Eppendorf BioPhotometer (Eppendorf AG, Hamburg, Germany). cDNA transcription was performed from total RNA by using the First Strand cDNA Synthesis Kit (Thermo Fischer, Waltham, MA, USA) according to the manufacturer's instructions.

2.8. Quantitative real-time PCR

The expression of Collagen type II (Col2), Collagen type III (Col3), Collagen type X (Col10), SOX9 and metalloproteinase 13 (MMP-13) was determined by means of real-time quantitative reverse transcription polymerase chain reaction (RT-PCR). SsoFast

Eva Green Supermix (Bio-Rad Laboratories Inc., CA, USA) was used and real time PCR was carried out on a Bio-Rad CFX96 thermal cycler (Bio-Rad Laboratories Inc., CA, USA). Human β -tubulin was selected as a housekeeping gene. Data were expressed as fold change in expression related to the housekeeping gene.

2.9. Glycosaminoglycans (GAGs) quantification

In order to quantify the glycosaminoglycan content, the Blyscan Sulfated Glycosaminoglycan Assay (Biocolor, Carrickfergus, U.K.) was used following the manufacturer's instruction. Briefly, the samples were diluted to 1:1 ratio with deionized water in a total volume of 100 μ l. Next, 1 ml of Blyscan reagent was added and samples were incubated for 30 min under gentle shaking. Further, the samples were centrifuged at 13,500g for 10 min and the pellet was dissolved with 500 μ l Blyscan dissociation reagent. For the measurements, 200 μ l were transferred to a 96-well plate and absorbance was determined at 656 nm. GAGs concentration was calculated from a standard curve.

2.10. Histology and immunohistochemistry

Samples were collected at 21 days after culture, washed twice with DPBS and fixed in 3.7% paraformaldehyde at room temperature for 10 min. Subsequently, samples were embedded in Tissue-Tek O.C.T Compound (Sakura Finetek GmbH, Staufen, Germany) and frozen at –80 °C. Frozen gels were horizontally sliced with 10 μ m thickness using a cryotome. The samples were stained with Safranin-O/Fast green for detection of cartilage-specific ECM. Stained slides were imaged with a light microscope (Biorevo BZ9000, Keyence, Osaka, Japan) at 20 \times magnification. Scans of the entire histological sections were performed using the software BZ-II Viewer and BZ-II Analyzer (Keyence).

For immunohistochemistry, slides were incubated with 3% hydrogen peroxide for 5 min at room temperature to block endogenous peroxidase activity. Next, slides were thoroughly washed with Tris-HCl buffer (50 mM, pH 7.4) and incubated in proteinase K (Dako, Glostrup, Denmark) for 10 min at room temperature. The slides were then incubated with 2% bovine serum albumin (BSA) for 60 min at room temperature. Subsequently, the slides were incubated with the respective primary antibody (using previously optimized concentrations) in a humidified chamber overnight at 4 °C. Collagen type I (Col1, rabbit polyclonal, Abcam, Cambridge, UK) was used at 1:100 dilution in 2% BSA. Col2 (rabbit polyclonal, Abcam) was used at 1:200 dilution in 2% BSA. Col10 (mouse monoclonal, Abcam) was used at 1:1000 dilution in 2% BSA. Non-specific rabbit and mouse IgG antibodies (Abcam) were used as isotype controls diluted at 1:200 and 1:1000 in 2% BSA, respectively. After washing the slides with Tris-HCl, the slides were incubated with the corresponding secondary antibody (DAKO Envision Dual Link System-HRP, Dako) for 30 min at room temperature. The slides were carefully washed with Tris-HCl and subsequently incubated with 3,3'-Diaminobenzidine (DAB) solution (1:50, DAKO liquid DAB + substrate Chromagen System, Dako) for color development. Finally, the slides were washed with Tris-HCl and counterstained with Haematoxylin. Slides were photographed with a light microscope (Biorevo BZ9000, Keyence) and scans of the entire sections were performed as previously described.

2.11. Biomechanics

For biomechanical determinations, the culture of the cell-seeded gels was carried out using self-developed 3D printed gel holders made out of CPE using a Ultimaker 3D printer (Ultimaker B.V., Geldermalsen, The Netherlands). The dimension of each well

on the gel holders was 7.5 mm in diameter and 5 mm in depth (Fig. 9A). Biomechanical evaluation was performed at 21 days.

The micro-elasticity of the samples was determined using a novel nanoindentation instrument (Piuma Nanoindenter, Optics11, Amsterdam, The Netherlands). By combining fiber-optical Fabry-Perot interferometry with a monolithic cantilever-based probe, local micro-elasticity of low-modulus materials can be examined with high accuracy and precision [22].

A probe with a 0.088 N/m spring constant and a 25 μm spherical indentation tip was used. During indentation the spherical tip was brought in contact with the sample surface and load-indentation and load-time data was recorded. Probe displacement was set at 18.32 μm and the probe displacement velocity was 9.16 $\mu\text{m/s}$. The Young's Modulus was derived from the load-indentation curves using the Hertz model [23], which was applied to the loading dataset that corresponds to 0–30% of the maximum load point. Per sample, four unique points in a 2 \times 2 point grid were measured using a lateral pitch of 100 μm . In order to determine the homogeneity of the gel surfaces, surface scans were reconstructed out of 25 single measurements in a square of 100 \times 100 μm . Each measuring spot had a distance of 20 μm .

2.12. Measurement of dissolved oxygen levels

The level of dissolved oxygen within the cell-seeded Coll and Coll-HA gel constructs was measured using a fiber-optical oxygen microsensor set-up (Microx TX3, PreSens, Regensburg, Germany). The experimental setup consisted of a retractable oxygen microsensor of 50 μm in diameter. This microsensor was embedded in a syringe needle. The connection occurred via an optical fiber to an oxygen meter (Microx TX3). For the analysis, the fiber-optical sensor was mounted on a custom self-developed platform that enabled accurate positioning of the sensor tip within the gels. The microsensor was placed into the gel construct at a designated penetration depth. Oxygenation analysis was performed at three different localizations in the constructs having the same depth. The oxygen concentration was measured in sequential intervals of 10 s under stable signal output. For each measurement point, a minimum of 6 single values was recorded. All different Coll and Coll-HA gel compositions were analyzed in triplicate, under 21% O_2 conditions in a humidified atmosphere supplemented with 5% CO_2 at 37 $^\circ\text{C}$.

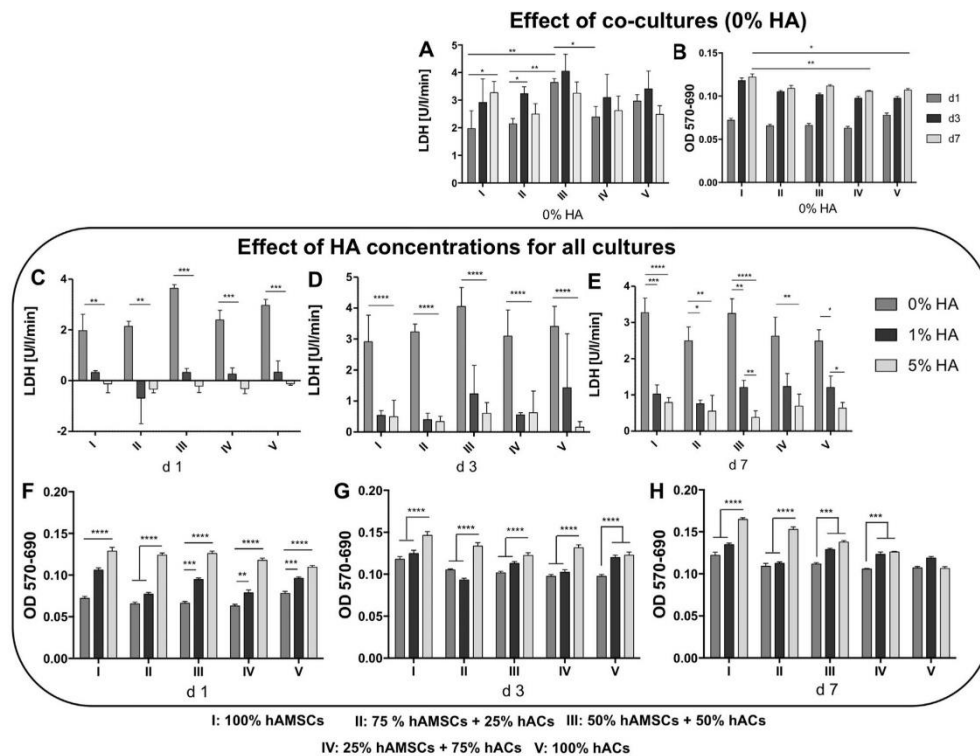


Fig. 2. Cell viability and toxicity. Toxicity was evaluated using lactate-dehydrogenase (LDH) measurements in the supernatant. Cell viability was determined by MTT assay. To show the effect of co-culturing human adipose-derived mesenchymal stem cells with human articular chondrocytes, the values of LDH and MTT are shown in the collagen hydrogels only (0% hyaluronic acid (HA)). The kinetics from day 1, 3, and 7 are shown (A and B). To be able to evaluate the effect of the addition of HA (1% and 5%), the values of LDH (C–E) and MTT (F–H) are plotted together in one graphic for each separate day. OD 570–690 = optical density measured at $\lambda = 570 \text{ nm}$ – the optical density measured at $\lambda = 690 \text{ nm}$. Group I = 100% hAMSC, group II = 75%hAMSC/25%hAC, group III = 50%hAMSC/50%hAC, group IV = 25%hAMSC/75%hAC, group V = 100% hAC. * $p < 0.05$, ** $p < 0.01$, *** $p < 0.001$, **** $p < 0.0001$.

2.13. Statistical analysis

Data is presented as mean value \pm standard error of the mean (SEM). For all the assays and measurements performed in this study, samples were evaluated at least in triplicates and in two or more individual experiments. Statistical analysis was carried out with GraphPad Prism version 6.00 (GraphPad Software, La Jolla, CA, USA). Normal distribution of the data was analyzed by D'Agostino-Pearson test. *T*-test was used for comparisons of two groups. One-way ANOVA followed by Tukey's test for multiple comparisons was used for comparison between three or more different groups. To analyze the oxygen data, two-way ANOVA corrected by Bonferroni test for multiple comparisons was used. In case the data were not normally distributed, a Kruskal-Wallis test with Dunn's correction for multiple comparisons was applied. A probability of $p < 0.05$ was considered as significant.

3. Results

3.1. Cell viability and toxicity

3.1.1. Effect of co-culture

The effect of co-culturing the two different cell types on cell viability (mitochondrial activity) and toxicity (LDH) was evaluated in Coll hydrogels (Fig. 2A and B). LDH concentrations showed no significant difference between the different co-culture conditions up to 7 days of *in vitro* culture. Interestingly, 100% hAMSC (group I) showed a continuous non-significant rise in LDH. All other groups, containing different amounts of hACs, showed trendwise consistently less LDH at day 7 compared to day 3. These LDH results were confirmed by the MTT assay. Similarly, no significant differences in cell viability were detected between the groups containing different amounts of hACs (Fig. 2B). At 7 days after culture, however, the group with 100% hAMSCs (I) showed significantly higher cell viability in comparison to all other groups (Fig. 2B).

3.1.2. Effect of HA concentration

A positive effect of HA regarding cell viability was observed for all groups. LDH values significantly decreased for all groups when comparing Coll to Coll-HA gels (Fig. 2C–E). Increasing HA concentrations up to 5% showed significant improvements on cell toxicity (Fig. 2E pronounced effect after 7 days of culture). MTT results also supported this observation (Fig. 2F–H), however in a less clear manner. Indeed, MTT was reciprocal to the LDH in most conditions. Thus, the more HA in the gels, the higher MTT values were generally obtained. Having two different cell types mixed in the co-cultures, the clearness of the results is somewhat impaired. It seems that hAMSC (group I) have per se a higher metabolic activity than hAC (group V). This is consequently reflected in the co-culture groups with increasing numbers of hAMSC, where higher metabolic activity is observed.

3.2. Proliferation

As shown above, MTT is a problematic parameter in co-cultures with different cell types having different intrinsic mitochondrial activities. Thus, to have a better idea about proliferation and amount of cells, DNA quantification was performed for longer culture times, i.e. up to 35 days (Fig. 3).

3.2.1. Effect of co-culture

The effect of the co-culture on cell proliferation can be best appreciated in Fig. 3A. In the 100% hAMSC group I, a significant increase of cell number was observed in the Coll gels over time. No proliferation occurred during the observation time, when only hAC (group V) were present. In the co-culture groups II–IV, significantly higher cell numbers were determined at day 35. The highest proliferation was observed in group III with 50%hAMSC/50% hAC at day 35. In all the co-culture groups, the increase from day 21 to 35 was more pronounced than from day 7 to 21.

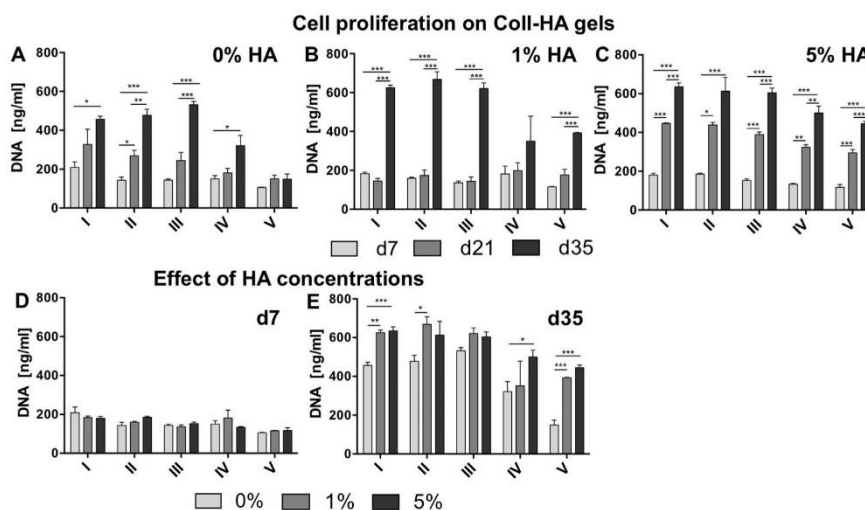


Fig. 3. DNA-quantification via Quant-IT PicoGreen assay. Kinetic DNA values during the observation time in the collagen only hydrogel (0% HA, A), 1% hyaluronic acid (B) and 5% hyaluronic acid (C) are shown for the different groups. The different bars in each graphic represent the different times of measurement, namely 7, 21 and 35 days after seeding. In order to compare the effect of the hyaluronic acid at the early (d7, D) and late (d35, E) time point, the values in the different gel compositions are plotted for each culture group. Group I = 100% hAMSC, group II = 75%hAMSC/25%hAC, group III = 50%hAMSC/50%hAC, group IV = 25%hAMSC/75%hAC, group V = 100% hAC. * $p < 0.05$, ** $p < 0.01$, *** $p < 0.001$.

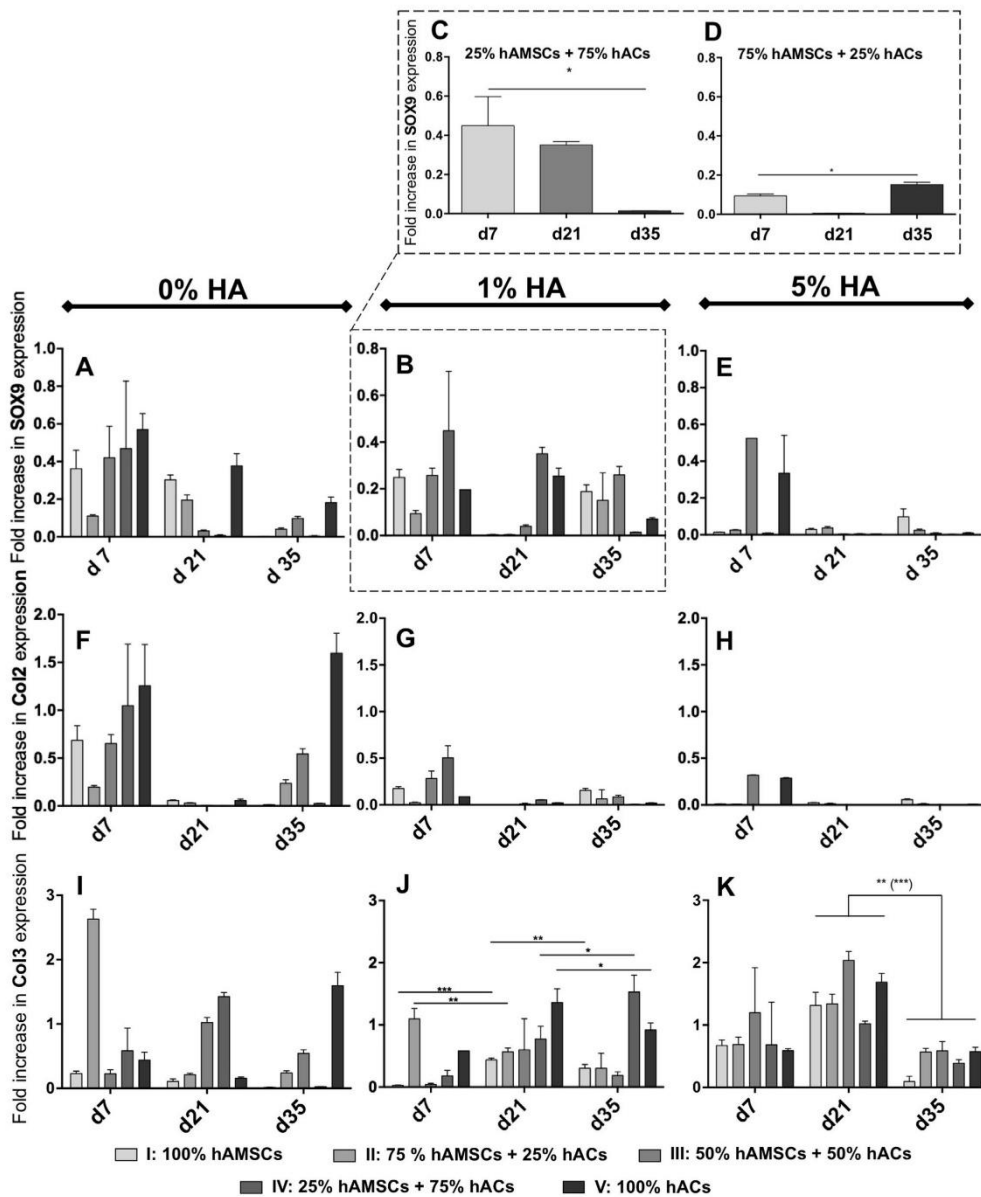


Fig. 4. Expression of chondrogenesis related genes SOX9 (A–E), Collagen type II (Col2, F–H) and Collagen type III (Col3, I–K) up to 35 days of culture. From left to right, the different gel compositions are indicated (A, F and I correspond to 0% HA. B–D, G and J show results for 1% HA. E, H and K depict the results for 5% HA). The inserts C and D show the co-cultures with predominant hAC (C) and predominant hAMSC (D) in 1% HA gels over time. All figures show the expression of the respective genes as fold increase compared to the house keeping gene β -Tubulin. Group I = 100% hAMSC, group II = 75%hAMSC/25%hAC, group III = 50%hAMSC/50%hAC, group IV = 25%hAMSC/75%hAC, group V = 100% hAC. * $p < 0.05$, ** $p < 0.01$, *** $p < 0.001$, **** $p < 0.0001$.

3.2.2. Effect of HA concentration

When HA was added to the gels (Fig. 3B and C), there was a significant increase of proliferation of the 100% hACs group during the observation period. This effect appears to be more pronounced at higher HA concentrations (Fig. 3C). Moreover, the proliferation was now faster at the earlier times of culture. The DNA content showed an increase of 2.5-fold from day 7 to 21 and of 1.5-fold from day 21 to 35 ($p < 0.001$ for all co-culture groups). There was no effect of adding HA on the proliferation of the co-cultures after 7 days of culture (Fig. 3D). However, at 35 days after culture, the gels containing HA significantly stimulated cell proliferation irrespective of the HA concentration (Fig. 3E).

3.3. Gene expression

3.3.1. Effect of co-culture

In the Coll hydrogels, the cartilage markers SOX9 and Col2 showed highest expression in group V with only hAC (Fig. 4A and F). However, Col3 (Fig. 4I) and MMP-13 (Fig. 5A) were hardly expressed in this group. SOX9 expression in this group V decreased over time until day 35, whereas Col2 was higher at day 35 compared to day 7. Most effects concerning the co-cultures can be seen at day 7. Here, the expression of SOX9 and Col2 decrease with decreasing percentage of hAC. However, group IV (25%hAMSC/75%hAC) doesn't show a significant difference with group V (100% hAC). Interestingly, for this co-culture group (IV) the expression of Col10 significantly decreased from d7 to d35 of cul-

ture (Fig. 5, $p < 0.03$ for all gels). This effect was present in all Coll-HA matrices used.

3.3.2. Effect of HA concentration

The addition of HA to the Coll hydrogel caused an overall prolonged expression of SOX9 up to day 35. This effect seems to be dependent on the predominant cell type in the co-culture system. Fig. 4C and D shows the effect of 1% HA on co-cultures with more hACs (75%, group IV) and more hAMSCs (75%, group II) respectively. For the co-culture group with predominant chondrocytes (group IV, Fig. 4C), SOX9 expression was highly upregulated at day 7 and 21, but significantly decreased at day 35 post-culture in 1% Coll-HA gels ($p = 0.027$). The groups with predominant hAMSCs (group II, Fig. 4D) showed an upregulation of SOX9 at day 7. The expression was, however, 4.8-fold higher in group IV compared to group II. It decreased to almost no SOX9 expression at day 21, with a significant rise in 1% Coll-HA at day 35 ($p = 0.0212$). Interestingly, increasing the HA content from 1 to 5% showed a detrimental effect on SOX9 expression for all investigated groups.

In that same 5% Coll-HA group, Col3 expression was the highest compared to Coll and 1% Coll-HA (Fig. 4I–K). This observation was similar in all studied groups. In the 5% Coll-HA group, Col3 expression was significantly downregulated in all culture groups from day 21 to day 35 of culture ($p \leq 0.0011$).

In addition, MMP-13 expression was not detectable or very low in Coll and 1% Coll-HA matrices for all groups studied (Fig. 5A and B). When gels containing 5% HA were used, a signifi-

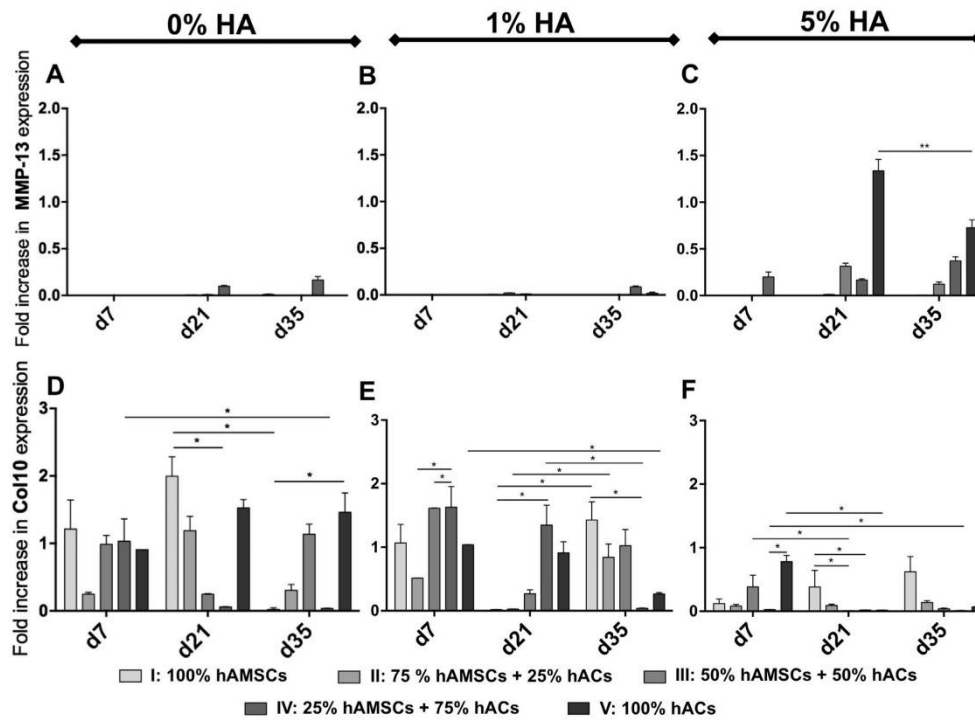


Fig. 5. Gene expression of metalloproteinase 13 (MMP-13) and Collagen type X (Col10) as markers of hypertrophy during chondrogenesis. The figures display the expression of MMP-13 (A–C) and Col10 (D–F) as fold increase compared to the house keeping gene β -Tubulin. From left to right, the different gel compositions are indicated (A and D 0% HA, B and E 1% HA and C and F 5% HA). Group I = 100% hAMSC, group II = 75%hAMSC/25%hAC, group III = 50%hAMSC/50%hAC, group IV = 25%hAMSC/75%hAC, group V = 100% hAC. * $p < 0.05$, ** $p < 0.01$.

cant upregulation of MMP-13 expression was observed from day 21 to day 35 (Fig. 5C, $p = 0.0015$). Remarkably, the 5% HA gels resulted in low to undetectable Col10 expression in all groups studied (Fig. 5F). This effect was more pronounced from day 21 onwards in the cultures containing hAC (either as co-cultures or 100% hAC).

3.4. Glycosaminoglycan (GAGs) production

HA supplementation to the Coll gels induced significantly increased GAG production in all groups (Fig. 6A, $p < 0.001$). This was independent of the HA concentration (1% vs 5% Coll-HA). Group IV (25%hAMSC/75%hAC) and group V (100% hAC) showed highest GAG content. Therefore, these groups are highlighted concerning the kinetics in Fig. 6B–G. In the gels made out of plain Coll, GAG content remained constant up to 21 days after culture

(Fig. 6B). In the 1% Coll-HA gels, however, there is a significant steady increase over culture time (Fig. 6C). Although the GAG content increases in the 5% Coll-HA gels, the absolute GAG concentration is lower than for the 1% Coll-HA (Fig. 6D).

A similar behavior was observed for the 100% hACs group V (Fig. 6E–G). The 1% Coll-HA gels resulted in higher GAG production. This was steadily increasing with culture time. As a matter of fact, the concentrations in this group were similar to the co-culture group IV. The GAGs content at 21 days after culture was 31% lower in the 5% Coll-HA gels when compared to the 1% Coll-HA gels. Yet, it was 2.5 times higher than in the plain Coll gels ($p = 0.0002$).

3.5. Histology and immunohistochemistry

Safranin-O staining revealed more positive cells in the single culture groups (Figs. 7, S4). For 100% hAMSC, a more pronounced

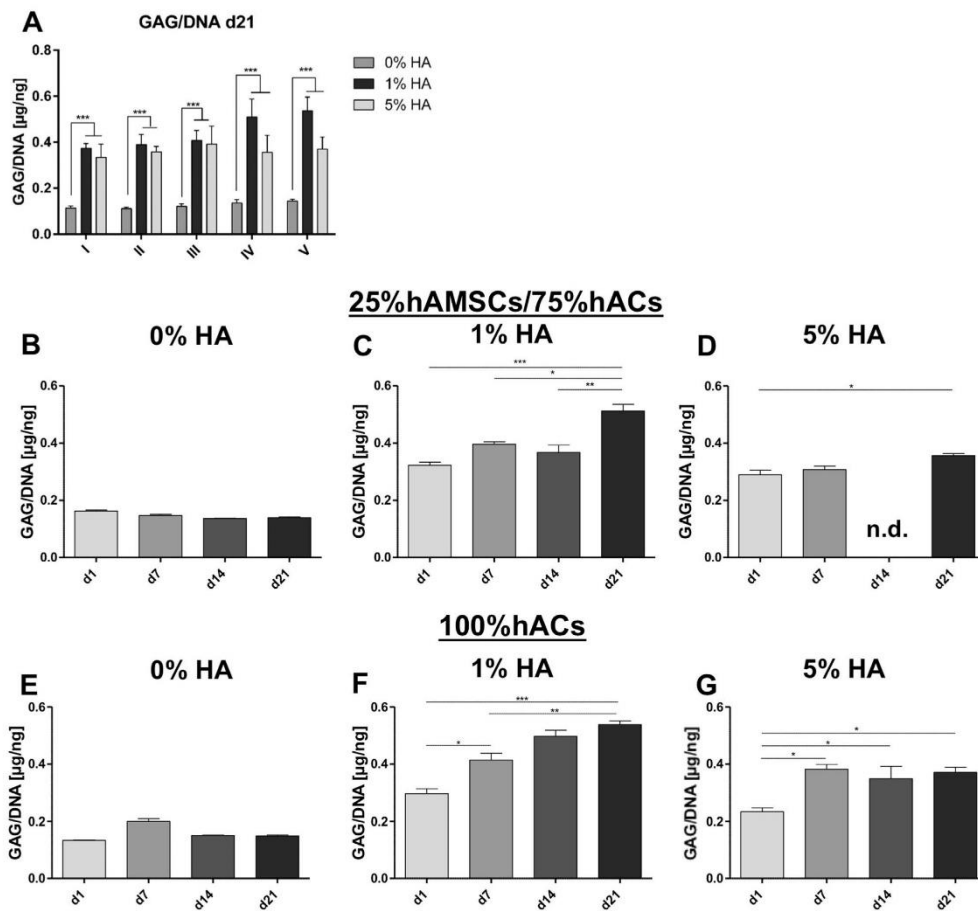


Fig. 6. Glycosaminoglycan (GAG) quantification. Representative figure showing GAG content at day 21 depicting the various gel compositions used for each culture group (A). Each individual figure shows the GAG content in a kinetic way from day 1 up to day 21 for group IV being the best co-culture group concerning GAG production (B–D). As a control, each individual figure shows the GAG content in a kinetic way from day 1 up to day 21 for group V with only hAC (E–G). GAG values were normalized against DNA content. Group I = 100% hAMSC, group II = 75%hAMSC/25%hAC, group III = 50%hAMSC/50%hAC, group IV = 25%hAMSC/75%hAC, group V = 100% hAC. * $p < 0.05$, ** $p < 0.01$, *** $p < 0.001$.

staining was obtained in the Coll gels (Fig. 7A), while for the 100% hAC, more positive cells can be observed in HA containing gels (Figs. 7I, S4F and S4I). Col1 (Fig. S1) and Col2 (Figs. 8A–I, S2) staining was positive for both single cultures as well as for the co-culture 25%hAMSC/75%hAC. Interestingly, this co-culture group shows a discreet Col10 staining when compared to both single cultures (Figs. 8J–R, S3). The intensity of the Col10 staining in both, 100% hAMSC and 100% hAC was diminished with increase of HA in the composition of the gels (Fig. 8J, M and P, Figs. 8L, O and R, S3).

3.6. Biomechanical properties

In general, an increase of effective Young's modulus was observed in gels containing HA when compared to Coll gels. All evaluated co-culture groups showed approximately the same level of effective Young's modulus when plain Coll gels were used as matrix. The effect of HA on the Young's modulus seemed to be dependent on the cell type or co-culture ratio (Fig. 9C). The co-culture group including 25%hAMSCs/75%hACs (group IV) showed the highest value of effective Young's modulus of 9.9 kPa (Fig. 9C). There is a significant difference to the single hAMSCs culture (group I) with 5.1 kPa ($p = 0.001$) and also to the 50%hAMSCs/50% hACs co-culture group (group III) with 3.9 kPa ($p = 0.0079$).

Representative images of a surface scan are shown in Fig. 9D and E. The color range represents the different values of effective Young's modulus. The gels showed a heterogeneous surface that was in the range of approximately 5 kPa independently of the co-culture condition used.

3.7. Oxygen measurements

The *in situ* dissolved oxygen concentration in the cell-seeded gels was analyzed after 21 and 35 days (Fig. 10). For the samples

at 21 days (Fig. 10A), levels of dissolved oxygen increased significantly with increasing hACs percentage in the co-cultures ($p < 0.05$). Single cultures of hACs featured a level of dissolved oxygen concentration up to 5.5% higher when compared to single hAMSCs cultures. Interestingly, adding HA to the gels resulted in a significant decrease in oxygen concentration. The effect of HA on the oxygenation was more pronounced in the presence of hAMSCs and lost significance in co-cultures with increasing hACs. The lowest mean values of dissolved oxygen *in situ* were observed for the 1% Coll-HA gels in co-cultures with predominant hAMSCs.

At day 35, similar levels of dissolved oxygen were obtained for co-cultures with 100% hAMSCs (14.7% O_2) and 100% hACs (14.7% O_2) in Coll gels. Remarkably, the levels of dissolved oxygen in Coll-HA gels showed similar or even higher values as the Coll gels. Indeed, the gel compositions with the highest level of dissolved oxygen at this time of observation were the gels supplemented with 5% HA.

There was a clear increase in levels of dissolved oxygen with increasing culture time for almost all samples analyzed (Fig. 10C–G). An exception was observed for the co-cultures with predominant hACs in Coll gels (group III–V, 0% HA, Fig. 10E–G). On the contrary, the co-cultures with high amount of hAMSCs showed a significant increase in dissolved oxygen over time. This effect was more pronounced in gels containing HA.

4. Discussion

In the clinical situation, large cartilage defects can be treated with MACT. However, this is a two-stage procedure, which increases the risk for the patient [24]. Moreover, culturing chondrocytes over longer time leads to dedifferentiation. The matrix used for MACT is a collagen-based scaffold. In this study, it was demonstrated that hyaluronic acid supplementation to a collagen

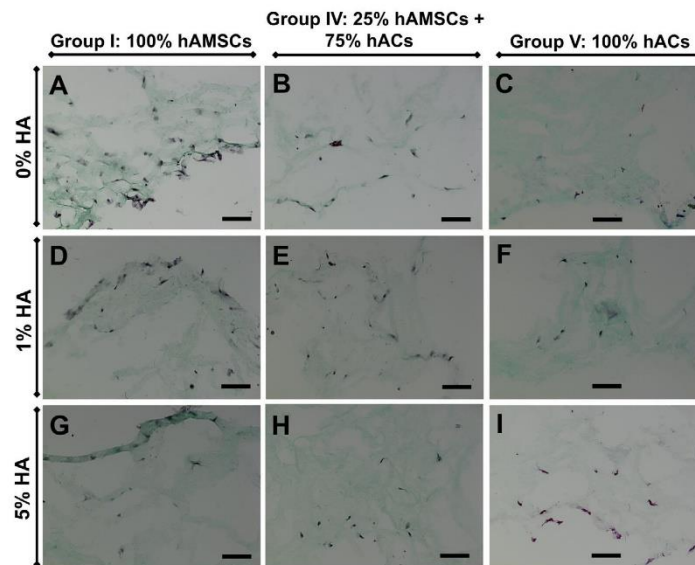


Fig. 7. Safranin-O staining after 21 days of culture. From top to bottom, increasing concentrations of hyaluronic acid (HA; A–C 0%, D–F 1% and G–I 5%) are depicted. From left to right, the different culture conditions are shown i.e. A, D and G corresponds to 100% hAMSCs (group I), B, E and H corresponds to the co-culture group IV 25% hAMSCs + 75% hACs. C, F and I resemble the 100% hACs (group V). Scale bar = 100 μ m.

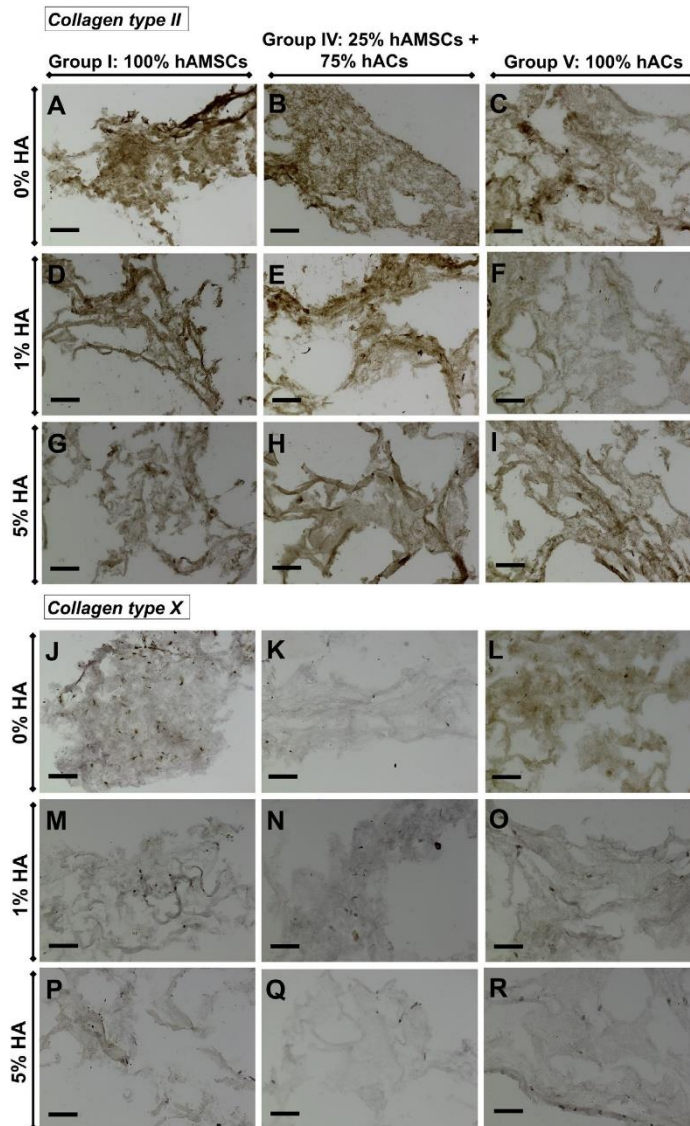


Fig. 8. Collagen type II (Col2) and Collagen type X (Col10) immunohistochemistry staining (brown) after 21 days of culture. Two panels depict the images for the different collagen: Col2 (A–I) and Col10 (J–R). From top to bottom, increasing concentrations of hyaluronic acid (HA) for each collagen are represented i.e. A–C and J–L 0% HA, D–F and M–O 1% HA, G–I and P–R 5% HA). From left to right, the selected cell compositions are shown (A, D and G as well as J, M and P correspond to 100% hAMSCs. B, E and H as well as K, N and Q correspond to 25% hAMSCs + 75% hACs. C, F and I along with L, O and R resemble the 100% hACs group). Scale bar = 100 μ m.

hydrogel stimulates chondrogenic differentiation in a dose dependent manner. 1% HA showed the best overall results. Furthermore, exchanging 25% of human articular chondrocytes with adipose-derived mesenchymal stem cells didn't change the chondrogenic potential, but reduced going in unwanted pathways, hypertrophy and improved biomechanical properties. Although it may seem not a huge leap in chondrocyte reduction, it still is 25% less.

Solchaga et al. showed that sponges based on HA can be successfully used to regenerate osteochondral defects. HA may attract mesenchymal progenitor cells and promote their differentiation into a chondrogenic phenotype [25]. Wu et al. observed that hyaluronic acid increases chondrogenesis and cartilaginous matrix formation. This was shown by significantly increased expressions of SOX9, collagen type II and aggrecan [26]. Furthermore, CD44 is

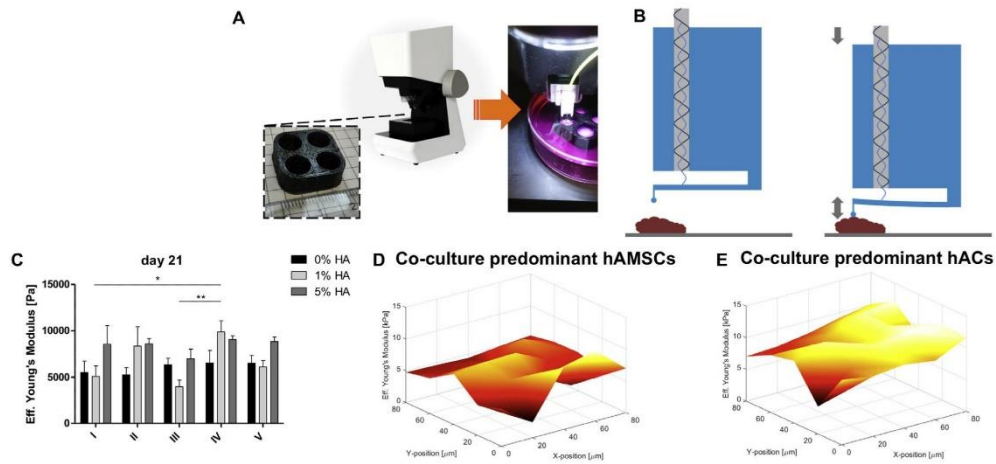


Fig. 9. Biomechanical measurements with a Piuma Nanoindenter. 3D-printed holder with 4 wells used for presenting the sample to the cantilever-based probe (A). Schematic representation of the indentation principle using a fiber-optical probe (B). Effective Young's Modulus obtained after 21 days of culture for the different gel compositions per culture group (C). Surface scans after 21 days in gels consisting of 5% hyaluronic acid in collagen for group II (D) and for group IV (E). Group I = 100% hAMSC, group II = 75% hAMSC/25%hAC, group III = 50%hAMSC/50%hAC, group IV = 25%hAMSC/75%hAC, group V = 100% hAC. * $p < 0.05$, ** $p < 0.01$.

the responsible receptor for hyaluronic acid interaction with MSCs and influences matrix formation [27,28]. CD44 is also upregulated in chondrocytes as a reaction of monolayer cultivation [29]. The interaction between CD44 and hyaluronan was shown to result in an upregulation of BMP-2 expression in adipose-derived stem cells. CD44 as a part of the cartilage link protein superfamily is able to bind several ligands at the same time [30]. Link proteins are shown to build complexes with cartilage proteoglycans and hyaluronic acid [31]. This production of macro-complexes leads to a better connection of ECM components.

Previous studies confirmed our observation that supplementation with hyaluronic acid or even culturing in a HA-scaffold leads to a lower expression of collagen type II [32], but an upregulation of GAG expression [28]. Especially, low HA supplementation leads to higher GAG deposition [17,33]. Lower concentrations of HA (0.1 mg/ml) induce cartilage tissue production whereas higher amounts do not lead to a higher stimulation of chondrogenesis [34]. Based on this previous evidence, we chose to supplement Coll gels with HA instead of using plain HA gels as chondrogenic matrix. Our hypothesis was that the combination of these two relevant materials could result in a chondrogenic matrix with improved mechanical properties. In order to achieve the right composite, we studied a range of HA concentrations (up to 5%) to supplement the Coll gels. Several studies on HA supplementation reported ranges from 0.1% to 65% [33–37]. HA concentrations of 5% have been reported as suboptimal in terms of chondrogenesis and adequate mechanical properties [35,36]. Thus we selected this concentration as maximum supplementation in our study. The groups supplemented with HA had higher values of effective Young's Modulus compared to the groups without. Depending on the culture condition used, the Coll gel supplemented with 1% HA resulted in better mechanical properties. This observation is in line with previous reports [35,36]. It's already shown that the microenvironment stiffness and elasticity is important for stem cell differentiation [38] and the form of tissue shaped by the cells [39,40].

Besides the influence of HA on GAG production, co-culturing has also been identified as a positive stimulus. Chondrocyte/AMSC co-cultures resulted in higher GAG production than AMSCs cul-

tured with chondrocyte-conditioned media [41]. This implies that direct cell-cell contact is more important than soluble factors. This could, however, not be investigated in our setting. Improved chondrogenic potential of different direct and indirect cultures of MSCs/chondrocytes was shown by addition of different cocktails of growth factors like TGF- β 3 and BMP-6 [42–44]. Moreover, MMP-13 and Col10 expression, markers for hypertrophy of cartilage tissue, are significantly downregulated in co-cultures with MSCs [45,46]. This was also seen in our study, where hAC alone displayed higher MMP-13 and Col10 expression than group IV with 25%hAMSC/75%hAC. Overall, it seems that addition of hAMSC prevents hAC hypertrophy. Yet, in the case of Col10 expression, the supplementation with HA appeared to have a more dramatic influence.

Our study also indicated that HA had an influence on oxygen levels within the hydrogels and thereby on chondrogenic differentiation and matrix production. Significant differences in the oxygen levels were given in-between the single gel compositions in the culture constellations (I–V) tested. We observed that addition of HA resulted in decreased of oxygen levels within the hydrogel. HA composite gels were also characterized by higher Young's modulus. We conjecture that the low levels of oxygen in the Coll-HA gels might be the result of poor oxygen diffusion due to higher stiffness of those gels. Abaci et al. reported that dissolved oxygen levels drop dramatically in 3D hydrogel systems compared to 2D cultures [47,48]. The same group recently described that the availability of dissolved oxygen in 3D hydrogel systems is dependent on oxygen diffusion and oxygen consumption of the encapsulated cells [49]. In this report, the authors described lower dissolved oxygen levels and upregulation of angiogenic factors in stiff HA gels (higher elastic modulus) when compared to medium stiff and soft gels. Other parameters like cell density, survival and migration seem to play a more critical role on dissolved oxygen levels in 3D gels at longer culture times [49]. This might explain the unexpected increase in oxygen levels for the 5% HA matrix at 35 days of culture. Recently, Leijten et al. reported a triggering effect of the prevailing oxygen concentration on cell fate of exposed MSCs *in vitro* [50]. Cells cultured in gels with the supplementation of

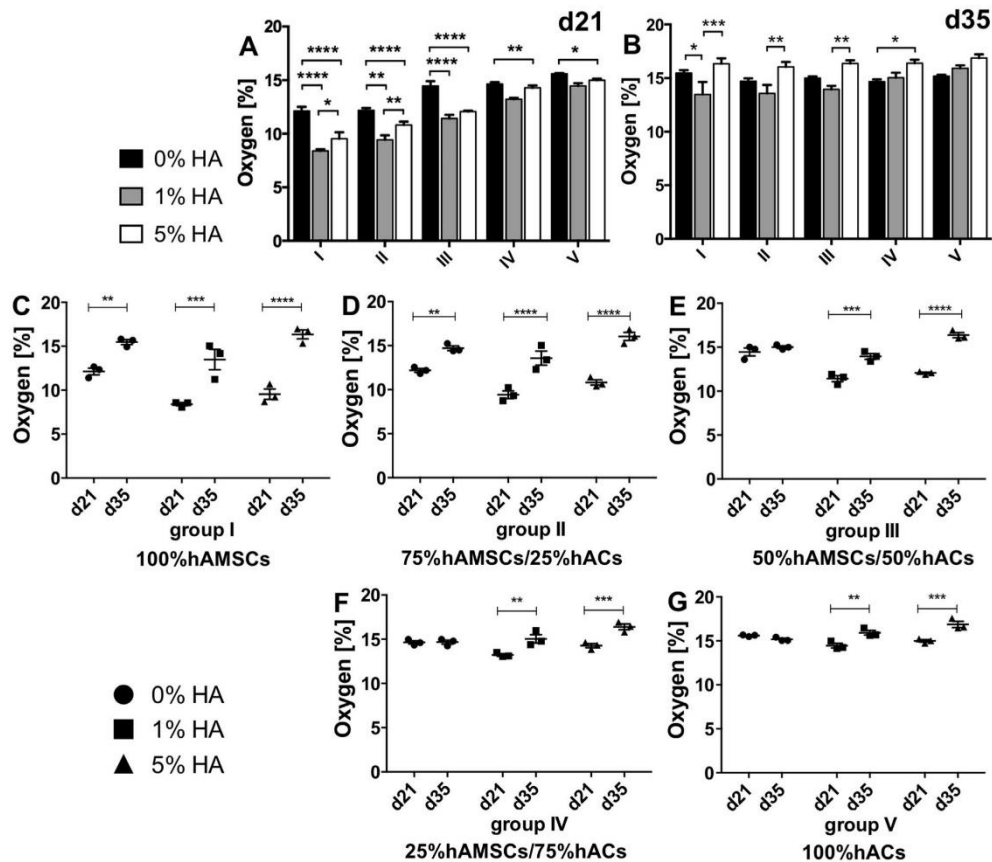


Fig. 10. Local oxygen measurements using a microsensor. Comparison of the different gel compositions after 21 days (A) and 35 days (B) of culture for all culture conditions studied. In order to show the effects within a culture group, oxygen levels are displayed per each hydrogel composition at d21 and d35 (C–G). Group I = 100% hAMSC, group II = 75%hAMSC/25%hAC, group III = 50%hAMSC/50%hAC, group IV = 25%hAMSC/75%hAC, group V = 100% hAC. * $p < 0.05$, ** $p < 0.01$, *** $p < 0.001$, **** $p < 0.0001$.

1% HA showed lowest levels of oxygen and highest values of GAG deposition. This coincided also with our MTT data. The higher oxygen levels were measured, the lower the MTT values. MTT is associated with mitochondrial activity and thus with oxygen consumption. Li et al. reported in a combined *in silico* and *in vitro* study of so-called threshold levels of oxygen affecting the extracellular matrix synthesis by hACs in a scaffold free environment [51]. Thus, the synthesis of distinct ECM components such as collagen and proteoglycans need adequate levels of oxygen *in situ*. Therefore, we assume these parameters in sum reflected the amount of matrix-producing cells of chondrogenic type, as these typically show a lower oxygen consumption rate *in vitro* [52].

An important feature of our study is the cell source. Most published studies investigating co-culture systems were performed with cells of animal origin or cell lines [43,53]. In contrast, our study used primary human cells from adipose tissue and articular cartilage. This is important, as tissue from animals is mostly harvested from young organisms with a high intrinsic regeneration potential [43,53,54]. In our study, chondrocyte donors were on

average 59 ± 19.2 years and fat tissue donors 71 ± 3.6 years. Thus, the age of the cells with their intrinsic regeneration potential reflects the patient situation. Furthermore, there is also no species mismatch. Interestingly, co-culturing freshly isolated osteoarthritic articular chondrocytes with MSCs lead to enhanced chondrogenic differentiation of the MSCs [45]. Given that different human donors were used to isolate both cell types used in the co-cultures, one concern that may arise is the occurrence of immune reactions. Stem cells have been widely described as hypoimmunogenic or “immune privileged” with no definitive advantages of autologous over allogenic MSCs applications clinical demonstrated to date [55]. Several studies have been published that report the inhibition of pro-inflammatory cytokines and the increase in expression of suppressive cytokines in human MSCs co-culture with various other cell populations (multiple donor effect included; e.g. [56,57]). These existing reports collectively support the notion that the MSCs fraction is likely to modulate any immune response that occurs during co-culture with other human cells. Hence, we don't foresee the occurrence of such

immune reaction between the two cell populations used in our study. However, this is a highly controversial topic that should be investigated further.

Of note, our study cannot discern which cells are the main effector cells. We have tried to label the different cell types with cell tracker dyes. Unfortunately, the stained cell populations could not be distinguished from each other due to (auto-)fluorescence issue of the gels. Thus, it was not possible to count the number of cells derived from the different cell types. This is subject to further research in order to elucidate the contribution of each cell type in the co-culture system.

A 500 times higher number of MSCs can be harvested from the same amount of adipose tissue compared to bone marrow [58]. That leads to the fact that AMSCs can also be used directly in the operating theatre without many expansion steps. This reduces costs and problems associated aging due to passaging [59]. But also a small amount of fat can be harvested and expanded up to P10, what reduces donor-site morbidity of tissue harvest. These are more passages in comparison to BMSCs that lose their potential to differentiate into chondrocytes after P5 [60].

In summary, adding 1% HA to collagen hydrogels leads to lower oxygen levels, higher GAG content, increased SOX9 expression, and higher Young's modulus. The co-culture of 25% hAMSC with 75% hAC shows best chondrogenic potential with highest SOX9 expression, lowest Col10 and highest GAG content (besides the effects of the HA). Thus, a construct consisting of 1% HA and 25% hAMSC may allow for optimized cartilage regeneration.

Disclosures

EA, PW, MvG and ERB have no conflict of interest to disclose. EB is employee of Optics 11, a company that develops optomechanical measurement systems.

Acknowledgments

The oxygen measurements performed in this study are part of the project "Happihypo" (Nr. 1163-15) funded by the Bayerische Forschungsstiftung.

Appendix A. Supplementary data

Supplementary data associated with this article can be found, in the online version, at <http://dx.doi.org/10.1016/j.actbio.2017.01.064>.

References

- [1] Y. Zhang, J.M. Jordan, Epidemiology of osteoarthritis, *Clin. Geriatr. Med.* 26 (3) (2010) 355–369.
- [2] C.L. Camp, M.J. Stuart, A.J. Krych, Current concepts of articular cartilage restoration techniques in the knee, *Sports Health* 6 (3) (2014) 265–273.
- [3] E. Kon, G. Filardo, B. Di Matteo, F. Perdisa, M. Marcacci, Matrix assisted autologous chondrocyte transplantation for cartilage treatment: a systematic review, *Bone Joint Res.* 2 (2) (2013) 18–25.
- [4] C. Erggelet, P. Vavken, Microfracture for the treatment of cartilage defects in the knee joint - A golden standard?, *Journal of clinical orthopaedics and trauma* 7 (3) (2016) 145–152.
- [5] E. Kon, G. Filardo, A. Roffi, L. Andriolo, M. Marcacci, New trends for knee cartilage regeneration: from cell-free scaffolds to mesenchymal stem cells, *Curr. Rev. Musculoskelet. Med.* 5 (3) (2012) 236–243.
- [6] G.J. van Osch, M. Brittberg, J.E. Dennis, Y.M. Bastiaansen-Jenniskens, R.G. Erben, Y.T. Kontinen, F.P. Luyten, Cartilage repair: past and future—lessons for regenerative medicine, *J. Cell Mol. Med.* 13 (5) (2009) 792–810.
- [7] K. von der Mark, V. Gauss, H. von der Mark, P. Muller, Relationship between cell shape and type of collagen synthesised as chondrocytes lose their cartilage phenotype in culture, *Nature* 267 (5611) (1977) 531–532.
- [8] S. Chen, P. Fu, R. Cong, H. Wu, M. Pei, Strategies to minimize hypertrophy in cartilage engineering and regeneration, *Genes Dis.* 2 (1) (2015) 76–95.
- [9] J.M. Gimble, A.J. Katz, B.A. Bunnell, Adipose-derived stem cells for regenerative medicine, *Circ. Res.* 100 (9) (2007) 1249–1260.
- [10] M.J. Farrell, M.B. Fisher, A.H. Huang, J.I. Shin, K.M. Farrell, R.L. Mauck, Functional properties of bone marrow-derived MSC-based engineered cartilage are unstable with very long-term in vitro culture, *J. Biomech.* 47 (9) (2014) 2173–2182.
- [11] K. Peltari, A. Winter, E. Steck, K. Goetzke, T. Hennig, B.G. Ochs, T. Aigner, W. Richter, Premature induction of hypertrophy during in vitro chondrogenesis of human mesenchymal stem cells correlates with calcification and vascular invasion after ectopic transplantation in SCID mice, *Arthritis Rheum.* 54 (10) (2006) 3254–3266.
- [12] M.R. Ahmed, A. Mehmood, F.U. Bhatti, S.N. Khan, S. Riazuddin, Combination of ADMSCs and chondrocytes reduces hypertrophy and improves the functional properties of osteoarthritic cartilage, *Osteoarthritis Cartilage* 22 (11) (2014) 1894–1901.
- [13] A. Nazempour, B.J. Van Wie, Chondrocytes, mesenchymal stem cells, and their combination in articular cartilage regenerative medicine, *Ann. Biomed. Eng.* 44 (5) (2016) 1325–1354.
- [14] V.V. Meretoja, R.L. Dahlin, S. Wright, F.K. Kasper, A.G. Mikos, The effect of hypoxia on the chondrogenic differentiation of co-cultured articular chondrocytes and mesenchymal stem cells in scaffolds, *Biomaterials* 34 (17) (2013) 4266–4273.
- [15] J.M. Mansour, Biomechanics of cartilage, in: C.A. Oatis (Ed.), *Kinesiology: the Mechanics and Pathomechanics of Human Movement*, Lippincott Williams and Wilkins, Philadelphia, 2003, pp. 66–79.
- [16] R. Jin, L.S. Moreira Teixeira, A. Krouwels, P.J. Dijkstra, C.A. van Blitterswijk, M. Karperien, J. Feijen, Synthesis and characterization of hyaluronic acid-poly (ethylene glycol) hydrogels via Michael addition: an injectable biomaterial for cartilage repair, *Acta Biomater.* 6 (6) (2010) 1968–1977.
- [17] M. Akmal, A. Singh, A. Anand, A. Kesani, N. Aslam, A. Goodship, G. Bentley, The effects of hyaluronic acid on articular chondrocytes, *J. Bone Joint. Surg. Am. British* 87 (8) (2005) 1143–1149.
- [18] C.T. Buckley, T. Vinardell, D.J. Kelly, Oxygen tension differentially regulates the functional properties of cartilaginous tissues engineered from infrapatellar fat pad derived MSCs and articular chondrocytes, *Osteoarthritis Cartilage* 18 (10) (2010) 1345–1354.
- [19] H.H. Lee, C.C. Chang, M.J. Shieh, J.P. Wang, Y.T. Chen, T.H. Young, S.C. Hung, Hypoxia enhances chondrogenesis and prevents terminal differentiation through PI3K/Akt/FoxO dependent anti-apoptotic effect, *Sci. Rep.* 3 (2013) 2683.
- [20] J.E. Lafont, Lack of oxygen in articular cartilage: consequences for chondrocyte biology, *Int. J. Exp. Pathol.* 91 (2010) 99–106.
- [21] M. Prause, C. Seeliger, M. Unger, M. van Griensven, A.T. Haug, Pantoprazole increases cell viability and function of primary human osteoblasts in vitro, *Injury* 45 (8) (2014) 1156–1164.
- [22] D. Chavan, T.C. van de Watering, G. Gruca, J.H. Rector, K. Heeck, M. Slaman, D. Iannuzzi, Ferrule-top nanoindenter: an optomechanical fiber sensor for nanoindentation, *Rev. Sci. Instrum.* 83 (11) (2012) 115110.
- [23] H.R. Hertz, Ueber die Beruehrung fester elastischer Koerper (On Contact between hard Elastic Bodies), *J. Reine Angew. Math.* 92 (1881) 156–171.
- [24] T. Welch, B. Mandelbaum, M. Tom, Autologous chondrocyte implantation: past, present, and future, *Sports Med. Arthrosc.* 24 (2) (2016) 85–91.
- [25] L.A. Solchaga, J. Gao, J.E. Dennis, A. Awadallah, M. Lundberg, A.I. Caplan, V.M. Goldberg, Treatment of osteochondral defects with autologous bone marrow in a hyaluronan-based delivery vehicle, *Tissue Eng.* 8 (2) (2002) 333–347.
- [26] S.C. Wu, J.K. Chang, C.K. Wang, G.J. Wang, M.L. Ho, Enhancement of chondrogenesis of human adipose derived stem cells in a hyaluronan-enriched microenvironment, *Biomaterials* 31 (4) (2010) 631–640.
- [27] C.B. Knudson, Hyaluronan and CD44: strategic players for cell-matrix interactions during chondrogenesis and matrix assembly, *Birth Defects Res. C. Embryo Today* 69 (2) (2003) 174–196.
- [28] S.C. Wu, C.H. Chen, J.K. Chang, Y.C. Fu, C.K. Wang, R. Eswaramoorthy, Y.S. Lin, Y. H. Wang, S.Y. Lin, G.J. Wang, M.L. Ho, Hyaluronan initiates chondrogenesis mainly via CD44 in human adipose-derived stem cells, *J. Appl. Physiol.* 114 (11) (2013) 1610–1618.
- [29] J. Diaz-Romero, J.P. Gaillard, S.P. Grogan, D. Nestic, T. Trub, P. Maimil-Varlet, Immunophenotypic analysis of human articular chondrocytes: changes in surface markers associated with cell expansion in monolayer culture, *J. Cell. Physiol.* 202 (3) (2005) 731–742.
- [30] M. Culty, K. Miyake, P.W. Kincade, E. Sikorski, E.C. Butcher, C. Underhill, The hyaluronate receptor is a member of the CD44 (H-CAM) family of cell surface glycoproteins, *J. Cell Biol.* 111 (6 Pt 1) (1990) 2765–2774.
- [31] S. Chandrasekhar, H.K. Kleinman, J.R. Hassell, Interaction of link protein with collagen, *J. Biol. Chem.* 258 (10) (1983) 6226–6231.
- [32] R.B. Jakobsen, A. Shahdadfar, F.P. Reinholt, J.E. Brinckmann, Chondrogenesis in a hyaluronic acid scaffold: comparison between chondrocytes and MSC from bone marrow and adipose tissue, *Knee Surg. Sports Traumatol. Arthrosc.* 18 (10) (2010) 1407–1416.
- [33] S.P. Frean, L.A. Abraham, P. Lees, In vitro stimulation of equine articular cartilage proteoglycan synthesis by hyaluronan and carprofen, *Res. Vet. Sci.* 67 (2) (1999) 183–190.
- [34] K. Yoshikawa, N. Kitamura, T. Kurokawa, J.P. Gong, Y. Nohara, K. Yasuda, Hyaluronic acid affects the in vitro induction effects of synthetic PAMPs and PDMAAm hydrogels on chondrogenic differentiation of ATDC5 cells, depending on the level of concentration, *BMC Musculoskelet. Disord.* 14 (2013) 56.
- [35] L.E. Erickson, A.H. Huang, S. Sengupta, S. Kestle, J.A. Burdick, R.L. Mauck, Macromer density influences mesenchymal stem cell chondrogenesis and

- maturation in photocrosslinked hyaluronic acid hydrogels, *Osteoarthritis Cartilage* 17 (12) (2009) 1639–1648.
- [36] I.E. Erickson, S.R. Kestle, K.H. Zellars, M.J. Farrell, M. Kim, J.A. Burdick, R.L. Mauck, High mesenchymal stem cell seeding densities in hyaluronic acid hydrogels produce engineered cartilage with native tissue properties, *Acta Biomater.* 8 (8) (2012) 3027–3034.
- [37] S. Tang, M. Spector, Incorporation of hyaluronic acid into collagen scaffolds for the control of chondrocyte-mediated contraction and chondrogenesis, *Biomed. Mater.* (Bristol, England) 2 (3) (2007) S135–S141.
- [38] A.J. Engler, S. Sen, H.L. Sweeney, D.E. Discher, Matrix elasticity directs stem cell lineage specification, *Cell* 126 (4) (2006) 677–689.
- [39] D.E. Discher, P. Janmey, Y.L. Wang, Tissue cells feel and respond to the stiffness of their substrate, *Science* 310 (5751) (2005) 1139–1143.
- [40] V. Vogel, M. Sheetz, Local force and geometry sensing regulate cell functions, *Nat. Rev. Mol. Cell Biol.* 7 (4) (2006) 265–275.
- [41] J.S. Lee, G.I. Im, Influence of chondrocytes on the chondrogenic differentiation of adipose stem cells, *Tissue Eng. Part A* 16 (12) (2010) 3569–3577.
- [42] N. Indrawattana, G. Chen, M. Tadokoro, L.H. Shann, H. Ohgushi, T. Tateishi, J. Tanaka, A. Bunyaratvej, Growth factor combination for chondrogenic induction from human mesenchymal stem cell, *Biochem. Biophys. Res. Commun.* 320 (3) (2004) 914–919.
- [43] H.A. Waters, C.P. Geffre, D.A. Gonzales, W.A. Grana, J.A. Szivek, Co-culture of adipose derived stem cells and chondrocytes with surface modifying proteins induces enhanced cartilage tissue formation, *J. Invest. Surg.* 26 (3) (2013) 118–126.
- [44] N.S. Hwang, S.G. Im, P.B. Wu, D.A. Bichara, X. Zhao, M.A. Randolph, R. Langer, D. G. Anderson, Chondrogenic priming adipose-mesenchymal stem cells for cartilage tissue regeneration, *Pharm. Res.* 28 (6) (2011) 1395–1405.
- [45] H.J. Diao, C.W. Yeung, C.H. Yan, G.C. Chan, B.P. Chan, Bidirectional and mutually beneficial interactions between human mesenchymal stem cells and osteoarthritic chondrocytes in micromass co-cultures, *Regen. Med.* 8 (3) (2013) 257–269.
- [46] M. Maumus, C. Manferdini, K. Toupet, J.A. Peyrafitte, R. Ferreira, A. Facchini, E. Gabusi, P. Bourin, C. Jorgensen, G. Lisignoli, D. Noel, Adipose mesenchymal stem cells protect chondrocytes from degeneration associated with osteoarthritis, *Stem Cell Res.* 11 (2) (2013) 834–844.
- [47] H.E. Abaci, R. Truitt, E. Luong, G. Drazer, S. Gerecht, Adaptation to oxygen deprivation in cultures of human pluripotent stem cells, endothelial progenitor cells, and umbilical vein endothelial cells, *Am. J. Physiol. Cell Physiol.* 298 (6) (2010) C1527–C1537.
- [48] H.E. Abaci, R. Truitt, S. Tan, S. Gerecht, Unforeseen decreases in dissolved oxygen levels affect tube formation kinetics in collagen gels, *Am. J. Physiol. Cell Physiol.* 301 (2) (2011) C431–C440.
- [49] Y.I. Shen, H.E. Abaci, Y. Krupsi, L.C. Weng, J.A. Burdick, S. Gerecht, Hyaluronic acid hydrogel stiffness and oxygen tension affect cancer cell fate and endothelial sprouting, *Biomater. Sci.* 2 (5) (2014) 655–665.
- [50] J. Leijten, N. Georgi, L. Moreira Teixeira, C.A. van Blitterswijk, J.N. Post, M. Karperien, Metabolic programming of mesenchymal stromal cells by oxygen tension directs chondrogenic cell fate, *Proc. Natl. Acad. Sci. U.S.A.* 111 (38) (2014) 13954–13959.
- [51] S. Li, R.O. Oreffo, B.G. Sengers, R.S. Tare, The effect of oxygen tension on human articular chondrocyte matrix synthesis: integration of experimental and computational approaches, *Biotechnol. Bioeng.* 111 (9) (2014) 1876–1885.
- [52] J. Malda, J. Rouwkema, D.E. Martens, E.P. Le Comte, F.K. Kooy, J. Tramper, C.A. van Blitterswijk, J. Riesle, Oxygen gradients in tissue-engineered PEGT/PBT cartilaginous constructs: measurement and modeling, *Biotechnol. Bioeng.* 86 (1) (2004) 9–18.
- [53] R.L. Dahlin, L.A. Kinard, J. Lam, C.J. Needham, S. Lu, F.K. Kasper, A.G. Mikos, Articular chondrocytes and mesenchymal stem cells seeded on biodegradable scaffolds for the repair of cartilage in a rat osteochondral defect model, *Biomaterials* 35 (26) (2014) 7460–7469.
- [54] T. Fukui, N. Kitamura, T. Kurokawa, M. Yokota, E. Kondo, J.P. Gong, K. Yasuda, Intra-articular administration of hyaluronic acid increases the volume of the hyaline cartilage regenerated in a large osteochondral defect by implantation of a double-network gel, *J. Mater. Sci. - Mater. Med.* 25 (4) (2014) 1173–1182.
- [55] J.A. Ankrum, J.F. Ong, J.M. Karp, Mesenchymal stem cells: immune evasive, not immune privileged, *Nat. Biotechnol.* 32 (3) (2014) 252–260.
- [56] S. Aggarwal, M.F. Pittenger, Human mesenchymal stem cells modulate allogeneic immune cell responses, *Blood* 105 (4) (2005) 1815–1822.
- [57] M.M. Zanone, E. Favaro, I. Miceli, G. Grassi, E. Camussi, C. Caorsi, A. Amoroso, M. Giovarelli, P.C. Perin, G. Camussi, Human mesenchymal stem cells modulate cellular immune response to islet antigen glutamic acid decarboxylase in type 1 diabetes, *J. Clin. Endocrinol. Metab.* 95 (8) (2010) 3788–3797.
- [58] J.K. Fraser, I. Wulur, Z. Alfonso, M.H. Hedrick, Fat tissue: an underappreciated source of stem cells for biotechnology, *Trends Biotechnol.* 24 (4) (2006) 150–154.
- [59] A. Noer, L.C. Lindeman, P. Collas, Histone H3 modifications associated with differentiation and long-term culture of mesenchymal adipose stem cells, *Stem Cells Dev.* 18 (5) (2009) 725–736.
- [60] R. Izadpanah, C. Trygg, B. Patel, C. Kriedt, J. Dufour, J.M. Gimble, B.A. Bunnell, Biologic properties of mesenchymal stem cells derived from bone marrow and adipose tissue, *J. Cell. Biochem.* 99 (5) (2006) 1285–1297.

Elsevier permit for reuse



RightsLink®

[Home](#)
[Help](#)
[Email Support](#)
[Sign in](#)
[Create Account](#)



Hyaluronic acid facilitates chondrogenesis and matrix deposition of human adipose derived mesenchymal stem cells and human chondrocytes co-cultures

Author: Elisabeth Amann, Paul Wolff, Ernst Bree, Martijn van Griensven, Elizabeth R. Balmayor

Publication: Acta Biomaterialia

Publisher: Elsevier

Date: 1 April 2017

© 2017 Acta Materialia Inc. Published by Elsevier Ltd. All rights reserved.

Please note that, as the author of this Elsevier article, you retain the right to include it in a thesis or dissertation, provided it is not published commercially. Permission is not required, but please ensure that you reference the journal as the original source. For more information on this and on your other retained rights, please visit: <https://www.elsevier.com/about/our-business/policies/copyright#Author-rights>

BACK
CLOSE WINDOW

© 2020 Copyright - All Rights Reserved | Copyright Clearance Center, Inc. | [Privacy statement](#) | [Terms and Conditions](#)
 Comments? We would like to hear from you. E-mail us at customer@copyright.com

Journal author rights

In order for Elsevier to publish and disseminate research articles, we need publishing rights. This is determined by a publishing agreement between the author and Elsevier. This agreement deals with the transfer or license of the copyright to Elsevier and authors retain significant rights to use and share their own published articles. Elsevier supports the need for authors to share, disseminate and maximize the impact of their research and these rights, in Elsevier proprietary journals* are defined below:

For subscription articles	For open access articles
<p>Authors transfer copyright to the publisher as part of a journal publishing agreement, but have the right to:</p> <ul style="list-style-type: none"> • Share their article for Personal Use, Internal Institutional Use and Scholarly Sharing purposes, with a DOI link to the version of record on ScienceDirect (and with the Creative Commons CC-BY-NC-ND license for author manuscript versions) • Retain patent, trademark and other intellectual property rights (including research data). • Proper attribution and credit for the published work. 	<p>Authors sign an exclusive license agreement, where authors have copyright but license exclusive rights in their article to the publisher**. In this case authors have the right to:</p> <ul style="list-style-type: none"> • Share their article in the same ways permitted to third parties under the relevant user license (together with Personal Use rights) so long as it contains a CrossMark logo, the end user license, and a DOI link to the version of record on ScienceDirect. • Retain patent, trademark and other intellectual property rights (including research data). • Proper attribution and credit for the published work.

A Graded, Porous Composite of Natural Biopolymers and Octacalcium Phosphate Guides Osteochondral Differentiation of Stem Cells

Elisabeth Amann, Amisel Amirall, Albina R. Franco, Patrina S. P. Poh, Francisco J. Sola Dueñas, Gastón Fuentes Estévez, Isabel B. Leonor, Rui L. Reis, Martijn van Griensven, and Elizabeth R. Balmayor*

Lesions involving the osteochondral unit are difficult to treat. Biomimetic scaffolds are previously shown as promising alternative. Such devices often lack multiple functional layers that mimic bone, cartilage, and the interface. In this study, multilayered scaffolds are developed based on the use of natural extracellular matrix (ECM)-like biopolymers. Particular attention is paid to obtain a complex matrix that mimics the native osteochondral transition. Porous, sponge-like chitosan-collagen-octacalcium phosphate (OCP) scaffolds are obtained. Collagen content increases while the amount of OCP particles decreases toward the cartilage layer. The scaffolds are bioactive as a mineral layer is deposited containing hydroxyapatite at the bony side. The scaffolds stimulate proliferation of human adipose-derived mesenchymal stem cells, but the degree of proliferation depends on the cell seeding density. The scaffolds give rise to a zone-specific gene expression. RUNX2, COL1A1, BGLAP, and SPP1 are upregulated in the bony layer of the scaffold. SOX9 is upregulated concomitant with COL2A1 expression in the cartilage zone. Mineralization in presence of the cells is prominent in the bone area with Ca and P steadily increasing over time. These results are encouraging for the fabrication of biomimetic scaffolds using ECM-like materials and featuring gradients that mimic native tissues and their interface.

1. Introduction

Osteochondral defects may result from primary osteoarthritis (OA) or as a consequence of fractures with joint involvement. Studies on incidence revealed that 10–15% of persons aged over 60 years suffer from clinical OA,^[1] with an increasing incidence due to obesity and lack of physical activity.^[1–2] Patients with osteochondral lesions suffer from pain and loss of function that may result in disability. Current clinical approaches to heal osteochondral defects remain highly challenging. Moreover, healing mostly occurs unsatisfactorily. Advanced OA therapy often results in joint replacement with known associated risks and side effects.^[3] Other treatments, like microfracture and matrix-associated autologous chondrocytes transplantation, still produce unsatisfactory results in long-term cartilage regeneration.^[4]

Scaffold-based regeneration models have been reported as a highly promising approach for osteochondral lesions.^[5] Indeed,

E. Amann, Dr. P. S. P. Poh, Prof. M. van Griensven, Dr. E. R. Balmayor
Experimental Trauma Surgery
Klinikum rechts der Isar
Technical University of Munich
Munich 81675, Germany
E-mail: e.rosadobalmayor@maastrichtuniversity.nl
Dr. A. Amirall, F. J. Sola Dueñas, Dr. G. Fuentes Estévez
Biomaterials Center
University of Havana
Havana 10 400, Cuba

Dr. A. R. Franco, Dr. I. B. Leonor, Prof. R. L. Reis
3B's Research Group
13Bs-Research Institute on Biomaterials
Biodegradables and Biomimetics
University of Minho
Headquarters of the European Institute of Excellence on Tissue
Engineering and Regenerative Medicine
Avepark, Barco, Guimarães 4805-017, Portugal
Dr. A. R. Franco, Dr. I. B. Leonor, Prof. R. L. Reis
ICVS/3B's—PT Government Associate Laboratory
Braga, Guimarães, Portugal
Dr. P. S. P. Poh
Julius Wolff Institute
Charité—Universitätsmedizin Berlin
13353 Berlin, Germany
Prof. R. L. Reis
The Discoveries Centre for Regenerative and Precision Medicine
Headquarters at University of Minho
Avepark, Barco, Guimarães 4805-017, Portugal

The ORCID identification number(s) for the author(s) of this article can be found under <https://doi.org/10.1002/adhm.202001692>

© 2021 The Authors. *Advanced Healthcare Materials* published by Wiley-VCH GmbH. This is an open access article under the terms of the Creative Commons Attribution-NonCommercial-NoDerivs License, which permits use and distribution in any medium, provided the original work is properly cited, the use is non-commercial and no modifications or adaptations are made.

DOI: 10.1002/adhm.202001692

this type of approach may be particularly useful for the regeneration of two distinct tissues and a stable interface.^[6] The clinical application of such therapeutic scaffolds may be achieved in a one-step procedure with clear advantages. Ideally, these scaffolding materials should be able to promote attachment of the cells, mimic the natural environment, and integrate into the surrounding tissue. In addition, cell differentiation should be supported. This is crucial to promote tissue regeneration.^[5b,7] Scaffolds for osteochondral regeneration should feature multiple layers to mimic bone, cartilage, and their interface. Several strategies have been reported to develop scaffolds for osteochondral regeneration that can be summarized as i) two single scaffolds combined at the defect site, ii) scaffold for bone and scaffold-free approach for the cartilage layer, iii) single, homogeneous scaffold for both tissues and the interface, and iv) single, heterogeneous composite scaffold (elegantly reviewed in Noeaid et al.^[5b]). As materials of choice, several natural- and synthetic-origin polymers are being investigated. Examples of natural materials include collagen, hyaluronan, and chitosan.^[8] Bioactive ceramics, including hydroxyapatite (HA) and calcium phosphates, are mostly used for the bony layer. These ceramics are frequently entrapped in a matrix of synthetic polymers widely used for bone engineering, including polycaprolactone and poly(lactic acid).^[9]

In our study, we developed a chitosan-collagen composite scaffold that contains octacalcium phosphate (OCP) at the top of the bony layer. The aim was to develop a novel multilayered scaffold for osteochondral regeneration based on natural extracellular matrix (ECM)-like materials. Gradients of chitosan and collagen were used that mimic the distinct tissues and the interface. Such a material gradient may promote desired stem cell differentiation that is specific for each tissue zone. In addition, a mineral component was incorporated in the bony layer. The scaffolds were designed as a continuous, single but heterogeneous material to avoid a predetermined breaking point between the bone and the cartilage layers. Chitosan and collagen were selected as biopolymers to generate the composite used in the present study. Chitosan is a natural, non-toxic biopolymer, which is highly biocompatible, biodegradable, and bioactive. It is structurally similar to glycosaminoglycan and offers an appropriate stimulus for stem cell differentiation.^[10] Collagen is the main ECM component in both native cartilage and bone tissue.^[11] The bony layer in our scaffold includes OCP as the mineral component. Calcium phosphates are widely used in bone tissue engineering and have been reported to promote bone regeneration.^[12] The developed scaffolds were carefully characterized for their morphology, porosity, and pore size as well as their composition, crystallinity, and mechanical properties. The bioactivity of the scaffolds was

evaluated in simulated body fluid (SBF) and their biocompatibility with human adipose-derived mesenchymal stem cells (hAMSCs). Considerable effort was made in evaluating the differentiation of hAMSCs on each of the different layers of the scaffold.

Our hypothesis is that by using a single composite scaffold that contains gradients of natural ECM-like materials and adequate porosity, we could guide stem cells toward zone-specific differentiation.

2. Experimental Section

2.1. Scaffold production

2.1.1. Materials

OCP was synthesized by dripping a solution of 0.04 mol L⁻¹ calcium acetate (Ca(CH₃COO)₂, VWR BDH Chemicals Ltd., Radnor, PA, USA) into a solution of 0.04 mol L⁻¹ sodium acid phosphate (Na₂HPO₄, Panreac Quimica SA, Barcelona, Spain) and following a reported methodology.^[13] The synthesis was performed at 60 °C for 3 h. During precipitation of the OCP, the solution was maintained under stirring. Subsequently, the precipitate was filtered and washed several times with distilled water. Finally, the product obtained was dried at room temperature. Chitosan from shrimp shells, ~75% deacetylated was obtained from Sigma Aldrich (St. Louis, MO, USA). Fibers of collagen type I were used as collagen source (bovine origin, commercial grade, Novaprom, Lins, Brazil). Both biopolymers were used as received by the manufacturers. Solutions of chitosan and collagen were prepared at a concentration of 2%, with constant stirring maintained for 24 h. Subsequently, 1% acetic acid was added and the stirring was continued for another 24 h. All raw materials used in the study were characterized by FTIR following the procedure described earlier in Section 2.2.3.

2.1.2. Production of Graded, Composite Multilayered Scaffold

Figure 1 presents a scheme illustrating the sequential layer-by-layer fabrication methodology to produce the scaffolds. First, the solutions corresponding to the different layers were independently produced (Figure 1A). For the bony layer and the interface, chitosan-collagen (1:1) was used. Two percent OCP was additionally added to the solution for the bony layer. For the cartilage layer, the collagen content was increased to obtain a ratio of chitosan-collagen of 1:3. Under stirring, 1 M NaOH was added to each layer to neutralize the acetic acid. For the fabrication of the multilayer composite scaffolds, each solution was stirred to obtain a foam and poured into a mold followed by a freezing step. Following freezing of the first layer, the polymeric solution corresponding to the next layer was deposited on top and the next freezing cycle was performed. All freezing cycles were performed at -20 °C. Subsequently, molds containing the three layers were frozen and lyophilized (Figure 1B). Finally, the scaffolds were cut out into cylinders of 5 mm diameter using a biopsy punch (Figure S2, Supporting Information) and sterilized using ethylene oxide (inpac Medizintechnik GmbH, Birkenfeld, Germany).

Prof. M. van Griensven
Department of Cell Biology-Inspired Tissue Engineering
MERLN Institute for Technology-Inspired Regenerative Medicine
Maastricht University
Maastricht 6229 ER, The Netherlands
Dr. E. R. Balmayor
Department of Instructive Biomaterials Engineering
MERLN Institute for Technology-Inspired Regenerative Medicine
Maastricht University
Maastricht 6229 ER, The Netherlands

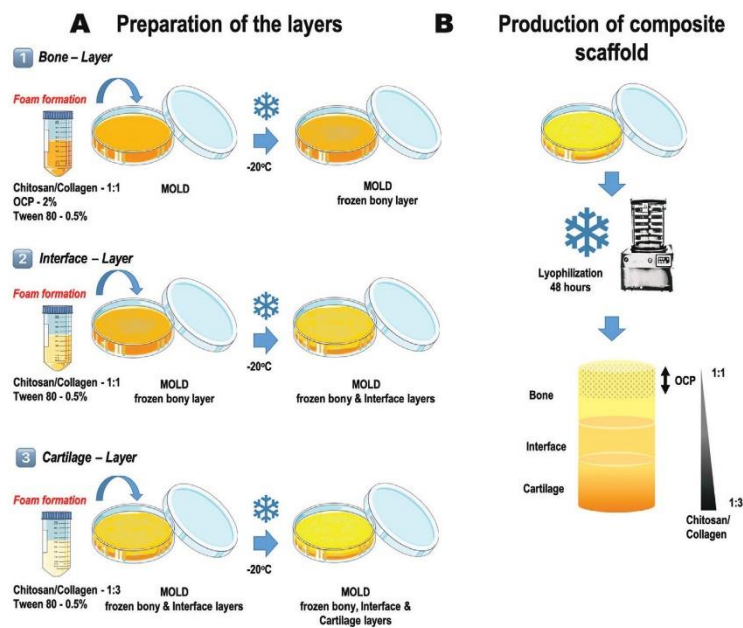


Figure 1. Schematic representation of the fabrication strategy followed to produce the multiphasic chitosan-collagen-octacalcium phosphate scaffolds. A) Material combinations used to obtain each independent layer. Consecutive freezing of the layers was performed; starting with the bony layer (1), then the interface (2), and finally the cartilage zone (3). B) Lyophilization of the material composite solutions previously deposited and frozen layer by layer into a mold. Illustration of the resulting scaffold. Different zones and material composition are identified.

2.2. Scaffold characterization

2.2.1. Morphology and Elemental Composition: Light Microscopy and Scanning Electron Microscopy—Energy Dispersive Spectroscopy

The structure and morphology (i.e., general and of the surface) of the composite scaffolds were characterized by observational light microscopy (VHX-900F, Keyence, Osaka, Japan) and SEM (JSM-6010LV, JEOL, Tokyo, Japan). By means of light microscopy, image depth of field and surface topography analysis were performed. For this analysis, scaffolds were bisected to obtain a plane surface. SEM was performed to analyze general morphological properties. In addition, an initial insight on porosity and pores shapes was obtained by this technique. To detect the presence of elements (i.e., Ca, P, C, and O) of different regions of interest (ROI) on the scaffolds, EDS (INCA-X-Act, PentaFET Precision, Oxford Instruments, Abingdon, UK) was performed. In addition, an element mapping of the entire scaffold was also obtained by EDS. Prior to SEM observation, the scaffolds were coated with platinum by ion sputtering. Backscattered electron imaging was used for overview images and secondary electron imaging for all detailed images (i.e., higher magnifications). For EDS analysis, scaffolds were used without coating.

2.2.2. Pore Size and Wall Thickness Analysis: Micro-Computed Tomography

Scaffolds were characterized using μ CT (SkyScan 1176, Bruker, Kontich, Belgium) for porosity, pore size, and wall thickness distribution. $N = 4$ scaffolds were used for the analysis. Briefly, scaffolds were stained with iodine vapor for 12 h and scanned at 40 kV and 600 μ A with 9 μ m resolution. The tomography was reconstructed using NRecon software (Version 1.6.9.18, Bruker). For the characterization of scaffold properties, three ROI representing the cartilage (ROI 1), interface (ROI 2), and bone (ROI 3) regions were selected and analyzed using CTAnalyser software (Version 1.17.7.2, Bruker) with adaptive thresholding between 40 and 200 (greyscale) for the collagen structure and global thresholding between 220 and 255 (greyscale) for the OCP particles. Finally, volume rendering of the scaffold was performed using CTVoxel (Version 3.3, Bruker).

2.2.3. Chemical and Crystallographic Properties: FTIR and X-Ray Diffraction

FTIR (IR Prestige-21 spectrometer Shimadzu, Kyoto, Japan) with attenuated total reflectance was used to analyze the chemical

structure of the raw materials and scaffolds. The spectra were received in a transmittance mode of over 100 scans in a spectral range of 400–4000 cm^{-1} . For each raw material, a standard sample preparation was followed. For each scaffold, the bone and cartilage layers were independently analyzed. The crystalline phases on the scaffolds were detected using thin-film XRD (D8 Advance, Bruker, XRD Division, Karlsruhe, Germany). The data collection was performed by the 2θ scan method, with 1° as the incident beam angle using a $\text{Cu K}\alpha$ X-ray line and a scan speed of $0.05^\circ \text{min}^{-1}$ over 9 h.

2.2.4. Mechanical Properties: Oscillatory Shear Measurements

Rheological measurements were performed using an AR-2000ex rheometer (TA Instruments, New Castle, DE, USA) with the samples immersed in distilled water. In brief, swollen samples were placed between parallel plates (non-porous, stainless steel, diameter 12 mm) and the gap was adjusted using a normal force of 0.2 N. Once the samples reached an equilibrium stage, a gap was adjusted to 1000 μm . The specimen temperature was set at 37°C and controlled by a Peltier heating stage. Initial measurements were performed in a shear deformation mode. To start, a range of strain amplitudes was determined in which the samples exhibited a linear viscoelasticity. Dynamic strain/frequency sweep tests were performed. For the strain test, amplitudes from 0.1% to 20% at a frequency of 1 Hz were used. Thereby, the dynamic shear modulus was determined as function of strain. For the frequency test, frequencies in the range 0.01–70 Hz were used. The strain corresponding to the sample linear region was used as a fixed value. Here, the dependency of the dynamic shear modulus and loss factor on frequency was obtained. Values of the G' , G'' , G^* , and $\tan \delta$ were obtained. Standard equations reported elsewhere were used for G^* ($\sqrt{(G')^2 + (G'')^2}$) and $\tan \delta$ (G''/G').^[14]

2.3. Scaffold Bioactivity in Simulated Body Fluid

The ability of apatite to form on the scaffold surface was evaluated by *in vitro* bioactivity. For this test, the materials were immersed in SBF with ion concentrations nearly equal to those of human blood plasma. The test was performed by incubating the scaffolds in SBF for 1, 3, or 7 days at 37°C with steady agitation. SBF solution was prepared according to the published protocol of Kokubo et al.^[15] Briefly, NaCl , NaHCO_3 , KCl , $\text{KPO}_4 \cdot 3\text{H}_2\text{O}$, $\text{MgCl}_2 \cdot 6\text{H}_2\text{O}$, HCl , CaCl_2 , Na_2SO_4 , and TRIS were dissolved in ion-exchanged, distilled water. The final pH was adjusted to 7.40 using HCl (1 N). The solution was prepared always fresh and immediately before use. Scaffolds were immersed into 10 mL SBF solution, ensuring that all the material was fully covered. Plain SBF solution (i.e., without scaffolds) was used as a control for each observation time. After 1, 3, and 7 days, both the SBF solutions and scaffolds were collected and analyzed.

2.3.1. Analysis of SBF Solutions Recovered after Scaffolds Incubation: pH and Inductively Coupled Plasma Optical Emission Spectroscopy

pH measurements were performed on all solutions recovered. Furthermore, Ca and P concentrations were determined using in-

ductively coupled plasma optical emission spectroscopy (JY2000-2, HORIBA Jobin Yvon, Kyoto, Japan). The solutions were filtered using a 0.22 μm filter and diluted (1:10) in 1% nitric acid. All the treated solutions were stored at -20°C until further use. Plain SBF solution was used as a control.

2.3.2. Analysis of the Scaffolds Harvested after SBF Incubation: XRD, SEM-EDS, FTIR, and μCT

Scaffolds collected from the SBF solution were rinsed thoroughly with ultra-pure water and allowed to dry overnight in a desiccator. Subsequently, the scaffolds were analyzed by thin-film XRD, SEM-EDS, FTIR, and μCT to evaluate chemical changes and the mineral deposits on the scaffold surface, among other relevant features. XRD, SEM-EDS, and FTIR were used as described above. For μCT , no iodine staining was performed on the scaffolds recovered from SBF. Instead, scaffolds were scanned without any previous treatment. NRecon (Version 1.6.9.18, Bruker) software was used for reconstruction of the tomography data. The different phases were distinguished using a CTAnalyzer (Version 1.17.7.2, Bruker). Briefly, a multi-level Otsu method was used to separate the greyscale value on the entire dataset into six distinct phases. The grey scale value 25–85 was shown in white (chitosan-collagen structure), the value 100–160 was shown in yellow (calcium phosphate deposit), and the value 200–220 was shown in red (HA deposit).

2.4. Cell Isolation and Seeding on the Scaffolds

The ethical committee of the University Hospital “Klinikum rechts der Isar” at the Technical University of Munich, Germany approved the described study. All procedures were performed in accordance with the declaration of Helsinki in its latest amendment. For all cellular experiments described hereafter, hAMSCs were isolated and used. Fresh human fat tissue harvested from abdominal fat of $N = 3$ patients was used. Patients provided informed consent.

Cells were isolated following the previously described protocol.^[16] Briefly, harvested fat tissue was cut into small pieces, placed into 50 mL falcon tubes to which sterile Dulbecco's phosphate-buffered saline without calcium or magnesium (DPBS, Sigma Aldrich) was added. The mixture was centrifuged at room temperature for 10 min without brakes (450 g). The resulting fat layer was collected into a new 50 mL falcon tube and washed 2–3 times with DPBS. Collagenase solution (0.8 mg mL^{-1} DPBS, collagenase type II, Biochrom GmbH, Berlin, Germany) was added and digestion was performed for 30 min in a 37°C water bath. The digestion reaction was stopped by filling the tubes with pre-warmed cell culture medium (Dulbecco's Modified Eagle's Medium—DMEM, high glucose, Sigma Aldrich) that had been supplemented with 10% fetal calf serum (Sigma Aldrich) and 1% penicillin/streptomycin (Sigma Aldrich). The solution was centrifuged for 10 min at 600 g and subsequently the pellet was resuspended in supplemented cell culture medium and filtered through a 40 μm cell strainer (BD Falcon, Franklin Lakes, NJ, USA). The resulting cell suspension was transferred into cell culture flasks. The cell seeding density was 3000 cells cm^{-2} . Cells isolated from each individual donor

were cultured independently. The cell culture medium was changed on the first day after isolation and subsequently twice weekly. For the cellular studies described in this paper, hAMSCs were used in passages 2 and 3.^[16]

For cell seeding on the scaffolds, hAMSCs from 3 different donors were pooled immediately before seeding. Four different concentrations of cells were used (i.e., 10^4 , 10^5 , 5×10^5 , and 10^6 cells per scaffold). The cell suspension containing the different cell concentrations were prepared in 50 μ L supplemented DMEM. Sterile scaffolds were carefully placed into 48-well plates and the 50 μ L cell suspension was pipetted onto the scaffold. Care was taken to distribute the cell suspension homogeneously throughout the entire scaffold. Cell-seeded scaffolds were placed into an incubator for 1 h at 37 °C under 5% CO₂. Thereafter, 500 μ L supplemented DMEM was carefully added. The constructs were cultivated for up to 35 days and media change was performed twice weekly.

2.5. Evaluation of cell attachment, toxicity, and proliferation

2.5.1. Cell Attachment, Distribution, and Morphology: SEM-EDS

After 14, 21, and 35 days of hAMSCs culture on the scaffolds, specimens were removed from the culture media, washed twice with DPBS and fixed for SEM. Briefly, the constructs were fixed for 30 min with 2.5% glutaraldehyde in a 0.1 M sodium cacodylate buffer (pH 7.4, 2% sucrose). The fixed scaffolds were washed with sodium cacodylate buffer and dehydrated in a series of ethanol of a concentration from 30% up to 100%. Critical point drying was achieved by immersion of the samples in hexamethyldisilazane (HMDS) for 10 min. Treatment with HMDS was repeated three times. Scaffolds were used uncoated for EDS analysis and sputter coated for SEM following the same procedure as previously described in the present study.

2.5.2. Cell Viability and Potential Toxicity of the Scaffolds: Lactate Dehydrogenase and Calcein-AM/PI Staining

To evaluate the biocompatibility of the developed scaffolds, cell viability was evaluated at 3, 7, and 14 days after seeding. In addition, the effect of the different cell concentrations used was considered. For the assay, the concentration of LDH, a marker for cell death, was evaluated in the supernatants collected after each observation time. Fluitest LDH-L Kit (Analyticon Biotechnologies AG, Lichtenfels, Germany) was used following the manufacturer's instructions. All experiments were performed in triplicate and were normalized to a standard curve. Furthermore, live-dead staining was performed after 21 and 35 days of cell culture on the scaffolds. Here, harvested scaffolds were washed carefully with DPBS and subsequently incubated in 500 μ L staining solution (2 μ M calcein-AM (Sigma Aldrich) and 1.5 μ M propidium iodide (Sigma Aldrich)). Following incubation at 37 °C for 20 min, the cell morphology and distribution were evaluated in each layer by confocal microscopy using an Fluoview FV10i microscope (Olympus, Tokyo, Japan). Moreover, cell infiltration through the entire scaffold was evaluated after 35 days of cell culture. For this, cell-seeded scaffolds were horizontally sectioned, from top to

bottom, to obtain 5 individual pieces. Each piece was stained with Calcein-AM/PI and imaged using the confocal microscope. In an attempt to quantify cell morphology, ImageJ v1.53f (National Institutes of Health, MD, USA) was used. Confocal microscopy images corresponding to each zone of the scaffold after 21 days of cell culture were converted to grey-scale, 8 bits images. Next, a fixed threshold (min. 70 and max. 255) was introduced and a binary image was created. The particle analysis tool from ImageJ was used. Events smaller than 20 μ m as well as cell clusters were excluded from the analyzed population. Over 200 cells were analyzed for each scaffold zone. Shape descriptor parameters such as circularity, roundness, and aspect ratio (A/R) were considered. Cells featuring values of circularity and roundness between 0.7 and 1 were considered as round. Three independent scientists performed the analysis and results were averaged.

2.5.3. Cell Proliferation: DNA Quantification

The ability of hAMSCs to proliferate on the scaffolds was assayed by quantifying the DNA content after different observation times. Therefore, cell seeded scaffolds were cultured for 3, 7, and 14 days. At each observation time, the samples were washed using DPBS and digested using 500 μ L papain solution (0.1 mg mL⁻¹, Sigma Aldrich) per scaffold. Digestion was performed overnight at 65 °C. Subsequently, the solution was stored at -80 °C. Quantification of DNA content was performed using the Quant-iT PicoGreen dsDNA Assay Kit (Invitrogen) following the manufacturer's instructions. Briefly, 70 μ L digested cell solution and 70 μ L Quant-iT PicoGreen dsDNA working solution were pipetted into a 96-well plate. The plate was incubated for 5 min at 37 °C in the dark. The fluorescence was quantified at an emission wavelength of 520 nm and an excitation wavelength of 485 nm using a FLUOstar Omega photometer (BMG labtech, Ortenberg, Germany). All experiments were performed in triplicate. DNA concentrations were calculated using a standard curve.

2.6. Evaluation of gene expression and cell differentiation

2.6.1. Alkaline Phosphatase Activity

Alkaline phosphatase (ALP) activity was determined after 3, 14, and 21 days of culture. ALP substrate solution was prepared with 4-nitrophenyl phosphate (pNPP, Sigma Aldrich). In the presence of ALP, pNPP substrate will be converted to an equal amount of yellow-colored 4-nitrophenol (pNP). For the assay, the scaffolds were washed twice with DPBS and incubated with ALP substrate solution for 30 min at 37 °C. Following incubation, 100 μ L of the solution was transferred to a 96-well plate and the absorption was determined at 405 nm in the FLUOstar Omega photometer. All experiments were performed in triplicate. pNP concentrations were calculated from a standard curve. ALP activity was reported as a function of the pNP concentration found in each sample.

2.6.2. Expression of Apoptosis, Proliferation, Osteogenic, and Chondrogenic Genes: Quantitative Real-Time PCR

Cell-seeded scaffolds were used to evaluate the expression of apoptosis, proliferation, osteogenic, and chondrogenic markers.

For apoptosis, the apoptosis regulator BCL2 and CASP3 were evaluated. For proliferation, MCM5 and CCND1 were analyzed. In the case of osteogenic differentiation, the expression of COL1A1, COL3A1, BGLAP (osteocalcin), SPP1 (osteopontin), and RUNX2 were evaluated. While for chondrogenesis, SOX9, COL2A1, COL10A1, and ACAN markers were analyzed. In the case of differentiation markers, the scaffolds were carefully sectioned to analyze the gene expression in the bone and cartilage layers independently. Thereby, only the upper (OCP-rich, bone zone) or lower (cartilage zone) layer of the scaffold was used for RNA isolation and further processing. Gene expression was performed by quantitative real-time PCR. In brief, cell-seeded constructs were harvested using Tri Reagent (Sigma Aldrich) at 1, 3, 7, 14, and 21 days after culture. Subsequently, 100 μL chloroform was added and the samples were incubated on ice for 10 min. Following centrifugation (14 000 g for 10 min at 4 °C), the clear phase was transferred into tubes containing 250 μL isopropanol. Following another incubation step on ice, a pellet was obtained by centrifugation (14 000 g for 10 min at 4 °C). Washing was performed with 70% ethanol and the final pellet was resuspended in 30 μL ultra-pure, DNase- and RNase-free, PCR grade water. Measurement of the total RNA content was performed using a Hellma TrayCell Eppendorf BioPhotometer (Eppendorf AG, Hamburg, Germany). The cDNA transcription was performed using the First Strand cDNA Synthesis Kit (Thermo Fisher, Waltham, MA, USA) following the manufacturer's instructions. A Mastercycler nexus (Eppendorf AG) was used for the synthesis of cDNA. Following transcription, all samples were diluted with PCR grade water to a concentration of 10 ng μL^{-1} . Quantitative real-time PCR was performed using Sso Fast EvaGreen Super Mix (Bio-Rad Laboratories Inc., Hercules, CA, USA) in a Bio-Rad CFX96 thermal cycler (Bio-Rad Laboratories Inc.). cDNA (30 ng) was used in a total reaction volume of 20 μL . Results were reported as fold expression normalized to the used housekeeper (i.e., tubulin beta class I: TUBB). Therefore, the ΔC_T method using a reference gene was used.

2.6.3. Matrix Deposition on the Scaffolds: Histology

Histology examination was performed at 21 and 35 days after cell culture on the scaffolds. The cell-seeded constructs were washed twice with DPBS and fixed with 3.7% paraformaldehyde. Dehydration was performed using gradually increasing concentrations of ethanol. Thereafter, specimens were embedded in paraffin and sectioned in 7 μm slices. The rehydration process was performed using Roti-Histol (Carl Roth GmbH, Karlsruhe, Germany) and immersion in 100%, 95%, and 70% ethanol. Hematoxylin and eosin (H&E) staining was used to obtain an overview of the cells populating the scaffolds. Briefly, specimens were stained by 10 min immersion in hemalaun followed by a rinsing step in running tap water. The sections were immersed for 5 min in eosin solution and dehydrated using 70%, 95%, and 100% ethanol and Roti-Histol. Safo staining was used to detect cartilage-specific ECM. For Safo, sections were treated with hematoxylin QS solution for 5 min, washed in running tap water, and subsequently rinsed rapidly with acid ethanol. Counterstaining was performed by immersing the sections for 5 min in 0.05% fast green solution. Subsequently, the sections were rinsed with

a 1% acetic acid solution and stained in 0.1% Safo solution by immersion for 5 min. The dehydration process was performed following the same procedure already described for H&E. Dried specimens were mounted and imaged with a light microscope (BZ9000 Biorevo, Keyence, Osaka, Japan). A general scan of the entire sections was obtained using the software packages BZ-II Viewer and BZ-II Analyzer (Keyence, Osaka, Japan). All images were taken under the same exposure time and white balance was regularly applied.

2.7. Statistical Analysis

Statistical analysis was performed using GraphPad prism version 5.00 (GraphPad Software, San Diego, CA, USA). Data are shown as mean value \pm standard deviation. For multiple group comparison, either one-way or two-way analysis of variance (ANOVA) followed by Tukey's test was applied. Multiple *t*-test corrected by Holm-Sidak was used to analyze the pH data as well as the Ca and P concentrations. All experiments were performed at least in triplicate (technical replicates = 3). *p* values are reported following the GraphPad style (i.e., four digits after the decimal point). A probability of $p \leq 0.05$ was considered to be significant.

3. Results

3.1. Composite, Multilayered Scaffold with Smooth Bone-to-Cartilage Interface Mimics the Osteochondral Structure with Relevant Elements Present at the Bone Layer

Single unit scaffolds were obtained made of a chitosan-collagen-OCP composite (Figure 2A,B). Throughout the entire length, the chitosan-collagen composition as well as the presence of OCP varied. Thereby, a graded scaffold was obtained. The scaffolds were fabricated in such fashion that all present zones appeared subsequently after each other in the same single 3D. Thus, the specific tissue layers were not glued, stitched, or assembled to one another post-fabrication. Macroscopic images (Figure 2A) illustrate the fabricated scaffolds. A porous structure was observed throughout the entire scaffold length. The scaffolds consisted of three layers, that is, a bone layer, an interface, and a cartilage layer (Figure 2A). Macro- and microscopically, a distinction between the two main layers present in the scaffold was possible. Analysis of the scaffold surface topography (Figure 2A) showed a slightly rougher surface at the bone and interface regions compared to the cartilage region. This observation was supported by morphology analysis using scanning electron microscopy (SEM, Figure 2C). An SEM image obtained at lower magnification allowed the observation of the entire scaffold structure (Figure 2C, centered image). In this image, the transition between the different areas of the scaffold could be observed. Moreover, the gradient in mineral content, from the bony toward the cartilage layer, was also evidenced by the presence of shiny OCP particles. The OCP-rich region was characterized by an irregular pore distribution, whereas the interface and cartilage layer were dominated by aligned pores with a smoother surface (Figure 2C, left and right images). The incorporation of OCP showed an even distribution in the entire bony layer. The incorporation of OCP crystals, solely into the bony layer, was confirmed by energy dispersive spectroscopy (EDS, Figure 2D). In the image, the presence

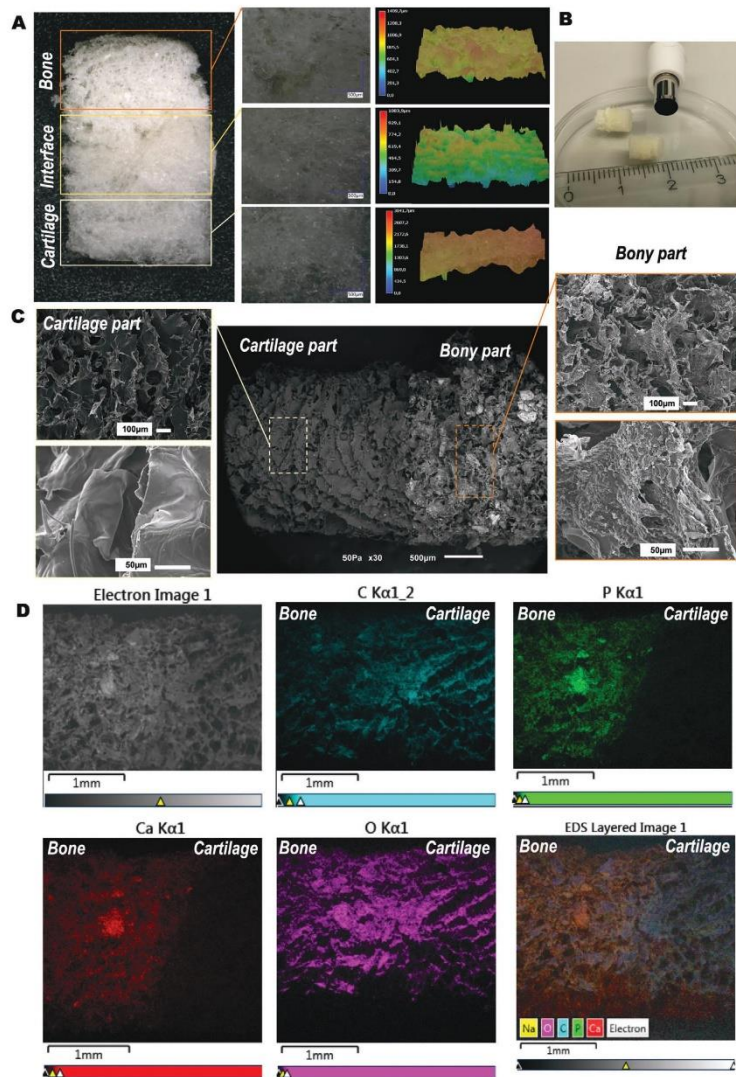


Figure 2. Morphological and elemental characterization of obtained chitosan-collagen-octacalcium phosphate scaffolds. A) Digital light microscopy images showing the different zones in the multilayered scaffold. The layers of the scaffold corresponding to the bone, interface, and cartilage regions are indicated by colored boxes added to the images. Higher magnifications of the different zones are shown. The left panel shows the surface roughness of each zone of the scaffolds. B) Macroscopic image showing the general appearance of the scaffolds. C) Scanning electron microscopy images illustrating the microstructure and morphological features of the obtained scaffolds. The central panel shows the entire scaffold. Detailed, higher magnifications images are depicted in the right and left panels for the cartilage and bone zones, respectively. D) Element mapping at the scaffolds' surface by means of energy dispersive spectroscopy. Starting at the left upper image, images shown correspond to: SEM, C (turquoise), P (green), Ca (red), O (pink), and superposition of all elements.

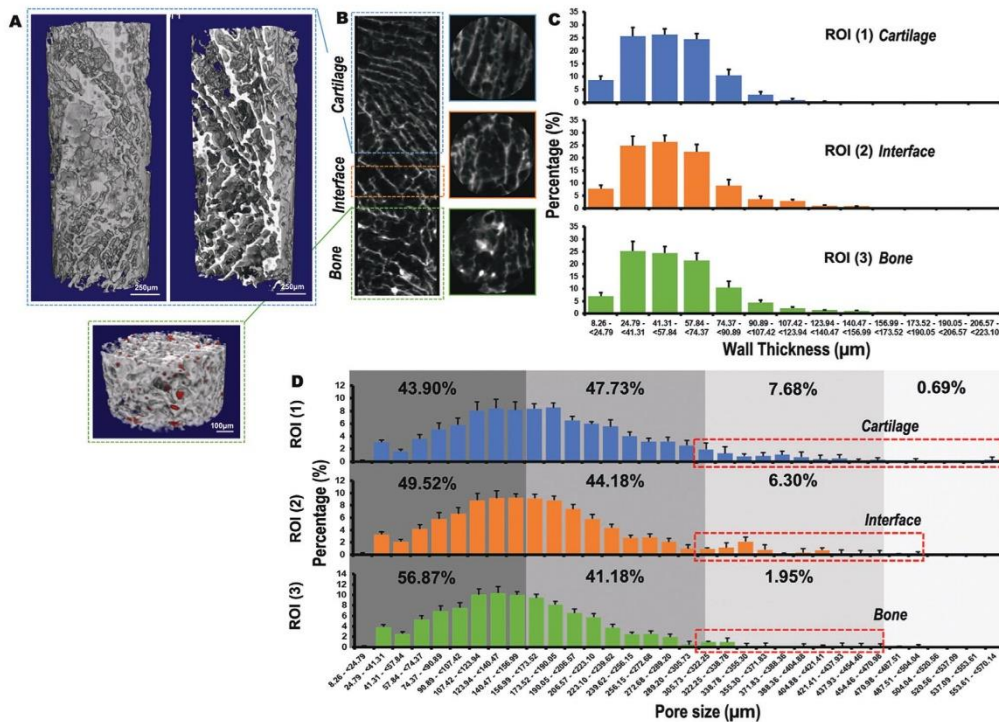


Figure 3. Microstructure, pore size, and wall thickness of obtained chitosan-collagen-octacalcium phosphate (OCP) scaffolds. A) 3D μ CT reconstruction showing the cartilage (Scale bar = 250 μ m) and bony layers (OCP particles in red, Scale bar = 100 μ m) and B) μ CT image of the different zones of the scaffold. The layers of the scaffold corresponding to the bone (green), interface (orange), and cartilage (blue) regions are indicated by colored boxes added to the images. The colors match the graphical representations for wall thickness and pore size distribution in each zone of the scaffold. C) Wall thickness and D) pore size distribution for each area of the scaffold. The pore size distribution range (μ m) was divided in quarters that represent four different pore size thresholds. The quarters are indicated with different grey color shadows. Provided values indicate the % of pores that falls inside each size distribution threshold. Additionally, larger pores (i.e., >300 μ m) are indicated inside a red box for each scaffold zone. For determination of both wall thickness and pore size distribution, three independent regions of interest (ROI) representing each zone were selected (i.e., ROI (1) = cartilage, ROI (2) = interface, and ROI (3) = bone). $N = 4$ scaffolds were used for analysis. Data are shown as mean value \pm standard deviation.

of the elements C (turquoise), P (green), Ca (red), and O (pink) could be clearly observed for the entire scaffold. P and Ca were only detected in the zone corresponding to the bone, whereas C and O displayed a homogenous distribution throughout the entire scaffold length.

Micro-computed tomography (μ CT) 3D reconstruction revealed detailed information of the scaffold's microstructure (Figure 3A). A highly porous structure was confirmed for the entire scaffold. Open and interconnected porosity characterized the scaffolds in all zones. Sagittal and axial slices generated by the μ CT reconstruction (Figure 3B) indicated a rather unidirectional porosity, with a fibril-like structure in the cartilage layer. An irregular porosity, featuring round pores, was observed in the bony layer. The incorporation of OCP into the bony layer was also corroborated in the μ CT analysis (Figure 3A, lower image, OCP particles in red). The OCP particles, characterized by a high

attenuation in the μ CT, were displayed as having a high density with a bright appearance and were thus highly visible in the μ CT scans. This clearly contrasted with the low density collagen-chitosan composite material that constituted the overall scaffolds.

Despite the varying pore morphology in the different scaffold layers, wall thickness (Figure 3C) and pore size distribution (Figure 3D) remained similar throughout the scaffold structure. Wall thickness was generally found to be <124 μ m, with most of the measurements in the range of 25–50 μ m. Interestingly, wall thickness increased toward the bony zone. In this region of the scaffold, 4.59% of the measurements returned values between 124 and 223 μ m. By contrast, only 0.30% of the measurements in the cartilage layer showed wall thickness values <190 μ m. Regarding pore size distribution, >90% of pores present in the entire scaffold had a diameter <300 μ m. Most of the pores were between 75 and 240 μ m, with a peak of \approx 150 μ m. Larger pores

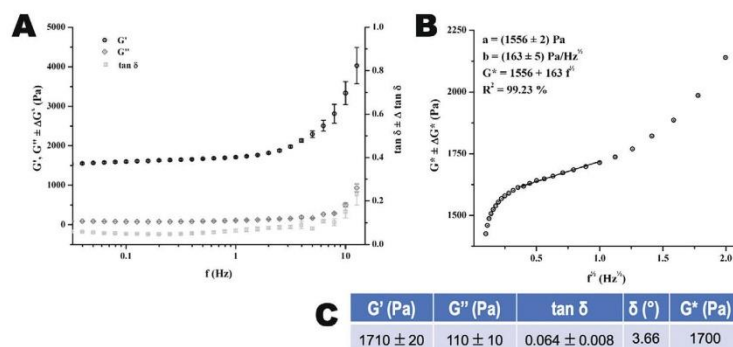


Figure 4. Mechanical properties of obtained chitosan-collagen-octacalcium phosphate (OCP) scaffolds. A) Evolution of the storage modulus (G'), loss modulus (G''), and loss factor ($\tan \delta$) with increasing frequency. Measurements were performed at 37 °C. Each curve corresponds to an average of three different samples analyzed. B) Dependence of the dynamic (complex) shear modulus (G^*) on $f^{1/2}$ at 37 °C. Fitted line corresponds to the least-square linear regression of the linear region. C) Average values for storage modulus (G'), loss modulus (G''), loss factor ($\tan \delta$), loss angle (δ), and dynamic (complex) shear modulus (G^*) obtained at 1 Hz, with the corresponding standard deviation.

were found in the cartilage zone, where >8% of the pores were >300 μm in contrast to only 1.95% of such dimensions in the bony layer.

3.2. Multilayered Scaffolds Showed a Viscoelastic Behavior, with Dynamic (Complex) Shear Modulus (G^*) Markedly Influenced by the Storage (Elastic) Modulus (G')

The chitosan-collagen-OCP scaffolds showed a viscoelastic behavior characterized by storage modulus (G') > loss modulus (G'') for viscoelastic solids. G' , G'' , and loss factor ($\tan \delta$) increased with frequency as shown in Figure 4A. This increase was at first minimal and showed a steep increase for high frequencies that are near to 10 Hz. G' values were higher than G'' for the studied frequency range of 0.1–10 Hz. The value of G' was in the range of 1500–4000 Pa while G'' was found to be <1000 Pa for the mentioned frequency interval. Figure 4C shows values obtained for G' and G'' at a fixed frequency of 1 Hz. For that frequency, G' was found to be 1710 ± 20 Pa while G'' was equal to 110 ± 10 Pa. This indicates that the storage (elastic) modulus G' is the major contributor to the dynamic (complex) shear modulus (G^*). This also reveals that our scaffolds displayed a high degree of elasticity. The loss factor $\tan \delta$ was found to be equal to 0.064 (3.66°) for the chitosan-collagen-OCP scaffolds. This value matches well with reported ones for collagen-based materials. G^* characterizes the overall stiffness of materials, and it is considered one of the most appropriate representations of their mechanical properties. G^* values are dependent on the frequency. Thus, they were determined by a frequency sweep test. Obtained results are depicted in Figure 4B, in which non-linear as well as linear behaviors could be identified. A non-linear relationship of G^* with $f^{1/2}$ is found at low frequencies (i.e., <0.3 Hz), followed by a linear behavior that was lost at frequencies higher than 1 Hz. An equation that describes the dependency of G^* with frequency was obtained for the chitosan-collagen-OCP scaffolds (Figure 4B, $G^* = 1556 + 163 f^{1/2}$).

3.3. Multilayered Scaffolds were Bioactive with Surface Deposits Rich in Calcium and Phosphorus

Fourier-transformed infrared spectroscopy (FTIR) spectra obtained for the raw materials and the chitosan-collagen-OCP composite can be found in the Figure S1, Supporting Information. The main bands on the spectra were assigned (Figure S1D, Supporting Information) and the presence of the single materials was confirmed in the composition of the blend.

Bioactive materials are expected to form an apatite-like layer on their surface as a result of their incubation in SBF solution. FTIR and X-Ray Diffraction (XRD) were performed to characterize the chemical and crystalline structures of the scaffold surface deposits after SBF incubation. FTIR spectra obtained for the different scaffold layers are presented in Figure 5 (A: bone and B: cartilage). The bands located at ≈ 1500 – 1650 cm^{-1} could be assigned to the amide I (vibration of valence of C=O) and amide II (dubbing of N–H) bands. Those chemical groups are present in the peptide bonds of collagen and in the acetyl groups of chitosan. The band located at 1057 cm^{-1} was attributed to the symmetric stretching vibration of the PO_4^{3-} group of OCP and HA, while the band at $\approx 600 \text{ cm}^{-1}$ corresponded to P–O bending vibrations in PO_4^{3-} . A well-defined peak, corresponding to the phosphate group, was clearly identified in the bony section of the scaffolds. With increasing incubation time in SBF, the intensity of this band notably increased. This was generally not observed in the cartilage layer of the scaffolds independently of the incubation time assayed. Noteworthy is the high intensity band at day 1, which was more likely related to a possible interference from the bony layer. XRD patterns are presented in Figure 5C. The peaks with the highest intensities have been identified with an asterisk (*) and can be observed in 2θ at 26°, 32°, and 40° and a broad peak around 50°. Several of the shown diffraction peaks could be assigned to an apatite-like phase according to the Joint Committee on Power Diffraction Standards ASTM JCPDS 9-432. By increasing the incubation time in SBF, the intensities of the apatite peaks increased and the single peaks became better defined.

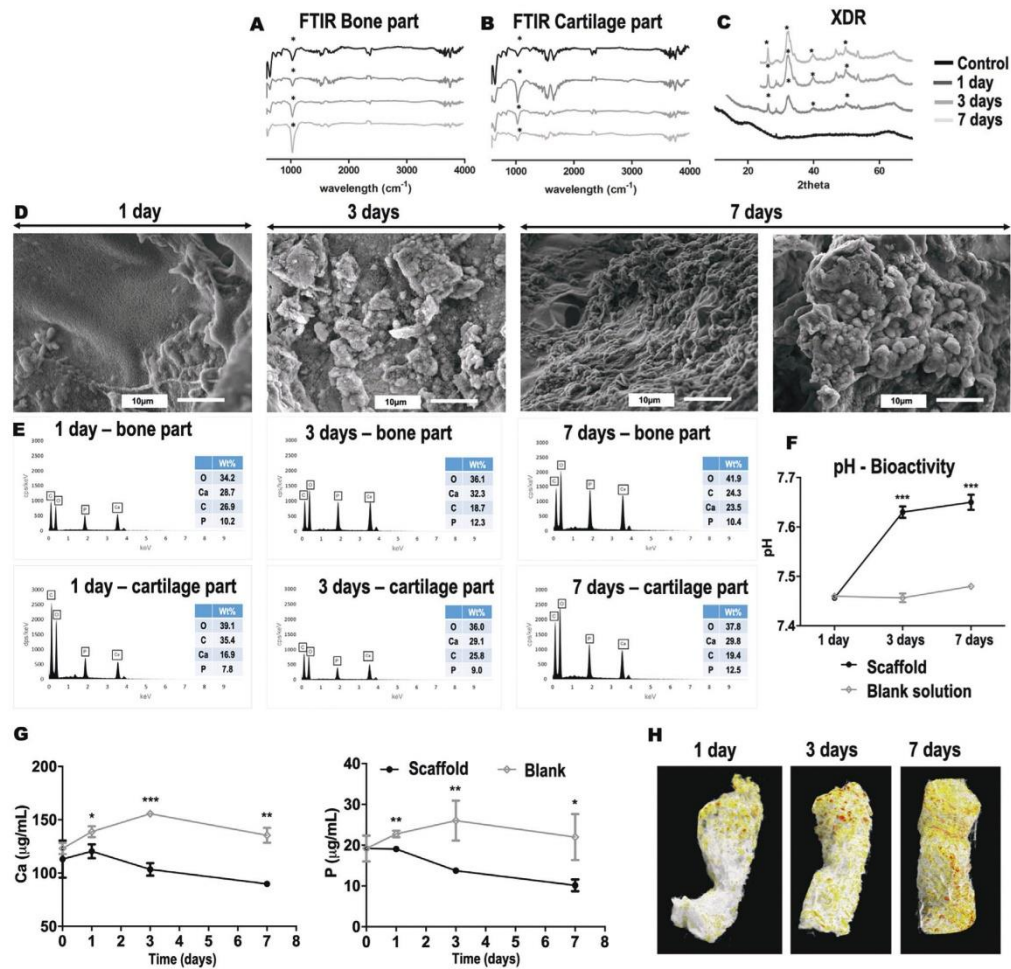


Figure 5. Bioactivity of the chitosan-collagen-octacalcium phosphate (OCP) scaffolds. FTIR spectroscopy showing the chemical composition of the scaffolds before and after immersion in simulated body fluid (SBF). Spectra obtained for A) bony and B) cartilage layers. C) X-ray diffraction spectra showing the crystalline structure of the scaffolds before and after immersion in SBF. Relevant peaks have been identified in FTIR and XRD spectra with an asterisk (*). D) Scanning electron microscopy images of the scaffolds at 1, 3, and 7 days after SBF incubation. E) Corresponding EDS elemental analysis performed for each independent zone of the scaffolds before and after SBF incubation. The different incubation times analyzed (i.e., 1, 3, and 7 days) are depicted in the figure. F) pH of the solutions collected after scaffolds incubation in SBF. Obtained p values are indicated by $***p \leq 0.0003$. G) Ca and P concentrations in the solutions collected after scaffolds incubation in SBF as determined by ICP spectroscopy. Obtained p values are indicated by $*p \leq 0.0243$, $**p \leq 0.0038$, and $***p = 0.0001$. H) Mineral deposit on the scaffolds after SBF incubation as determined by μCT . Material composition have been color coded for better visualization; chitosan-collagen in white, OCP and formed HA in orange to red coloration. Experiments were performed in triplicate (technical replicates = 3). Data are shown as mean value \pm standard deviation. Multiple t -test corrected using Holm-Sidak for multiple comparisons was used for statistical analysis of pH data as well as Ca and P determinations.

SEM-EDS was also performed to characterize the bioactivity (Figure 5D). Because of the distinctive appearance of apatite grains and layers, SEM has been widely used—sometimes as the sole technique—to estimate apatite layer formation. In our study, a significant change in the topography of the scaffold surface was observed after incubation in SBF. Globular aggregates were observed that completely covered the surface of the scaffolds at day 3 post-incubation. Following 7 days in SBF, a compact cauliflower-like coating was observed (Figure 5D, right panel). The presence of Ca, P, C, and O was detected by EDS analysis (Figure 5E). At days 1 and 3 post-incubation, higher wt% of Ca and P were identified in the bony layer of the scaffold. Unexpectedly, at day 7, these elements were slightly higher in wt% in the cartilage zone. The concentration of Ca and P in solution decreased over time (determined by ICP, Figure 5G). This decrease correlated well with a pH increase (Figure 5F) obtained at 1, 3, and 7 days post-incubation.

Specimens collected after SBF incubation were also analyzed by μ CT (Figure 5H). In the reconstructed images, the chitosan-collagen structure is shown in white color. The OCP particles (incorporated in the bony layer) and the HA formed are shown in orange-to-red colors. After 1 day of incubation in SBF, only the OCP particles located in the bony zone of the scaffold were visible. By increasing the incubation time, the number of orange and red particles was elevated, indicating an increase in the amount of HA deposited on the scaffold. These deposits were mostly located in the bony area in agreement with the results obtained by the SEM/EDS analysis. Following 1 week of incubation, the entire scaffold was covered with HA deposits. This also matched the dense apatite-like layer recognized in the SEM for the same observation time. Noteworthy is the occurrence of slight shrinkage in the scaffolds after SBF incubation. This behavior was noticeable mostly in the cartilage part of the multilayered scaffolds.

3.4. Viable Human Adipose-Derived Mesenchymal Stem Cells Proliferated on the Multilayered Scaffolds

Cells were seeded on the scaffolds using a range of cell densities of 10^4 – 10^6 cells per scaffold. Cell proliferation was dependent on the cell number and culture time employed (Figure 6A). Remarkably, only a cell density of 10^5 cells per scaffold displayed a significant elevation of the cell proliferation with increased culture time (3 vs 14 days of culture: $p = 0.0260$ and 7 vs 14 days of culture: $p = 0.0065$). For the lowest (10^4 cells per scaffold) and highest ($\geq 5 \times 10^5$ cells per scaffold) cell densities tested, no significant differences were observed for cell proliferation between 3, 7, or 14 days after cell seeding ($p \geq 0.0658$). This indicated a low proliferative behavior of the cells under these culture conditions. Furthermore, 10^5 cells per scaffold may be optimal for hAMSCs to proliferate in the scaffolds under the culture conditions tested. The toxicity related to the scaffold materials was evaluated for the different cell densities used by quantifying the lactate dehydrogenase (LDH) activity released to the supernatant (Figure 6B). Interestingly, the highest LDH quantities were detected for the highest initial cell density, that is, 10^6 cells per scaffold. Even so, LDH levels still significantly decreased with culture time ($p < 0.0001$). No-

ticeably, lower cell densities resulted in significantly lower LDH production (10^4 vs 10^6 cells per scaffold showed $p < 0.0001$ for days 3 and 7 after culture and $p = 0.0051$ for day 14). Here also, LDH detection significantly decreased from day 3 to day 7 after cell seeding ($p \leq 0.05$ for all cell densities except for 10^6 cells per scaffold) and remained low for the rest of the culture time. This indicated that the cell toxicity observed for 10^6 cells per scaffold was not related to the scaffold material but rather to the high cell density used per scaffold area. Based on the overall results from the cell proliferation and toxicity evaluations, a cell density of 10^5 cells per scaffold was used in subsequent experiments.

From the confocal images displayed in Figure 6C, a good cell attachment and homogenous cell distribution were visible in all layers of the scaffold. In particular, cells could be observed that colonized the entire scaffold structure independently of the tissue-specific zone. By means of a live/dead calcein-AM/PI staining, further insights on cell viability were obtained. All zones of the scaffold were individually observed. At 21 days after seeding, large areas of green stained cells were observed that indicated a high number of viable cells in all zones of the scaffold. Interestingly, a higher cell density was present at the cartilage zone when compared to the bony and interface layers. Cells in the cartilage area appeared rather elongated. The cellular orientation was observed in the direction of the scaffold pores. In the bony layer, the cells displayed a more roundish morphology. In the interface region, a mixture of both morphologies was observed. Cell morphology was analyzed using ImageJ and shape descriptor parameters such as circularity and roundness were calculated (Figure 6D). A value of 1 for both parameters indicates a perfect mathematical circle. Only 5.14% of the cells in the cartilage area featured values of circularity and roundness between 0.7 and 1. Conversely, 18.7% of the cells in the bony part showed values in the same range. In the interface zone, 10.6% of the cells showed circularity and roundness >0.7 in accordance to the microscopic observations. Dead cells were also identified in all three zones of the scaffold (Figure 6C, cell nuclei stained red). However, this was no longer observed at 35 days after seeding. At this observation time, a negligible number of dead cells were identified.

Further effects of the scaffolds on hAMSCs viability were analyzed by qPCR of proliferation and apoptosis markers (Figure 6E). Both minichromosome maintenance complex component 5 (MCM5) and cyclin D1 (CCND1) genes encode for proteins relevant in cell proliferation. Indeed, the protein encoded by MCM5 is involved in the initiation of DNA replication and is thus active in the regulation of the cell cycle. Similarly, CCND1 expression directly alters cell cycle progression. Following 7 days of hAMSCs culture on the scaffolds, a significant upregulation was observed for MCM5 ($p < 0.0001$) and CCND1 ($p < 0.0001$). This upregulation was more pronounced for CCND1 (24.9-fold increased upregulation compared to MCM5). B-cell lymphoma 2 (BCL2) and caspase 3 (CASP3) were investigated as indicators for possible apoptotic effects of the scaffolds on hAMSCs. BCL2, a gene that encodes a protein blocking the apoptotic death of cells, was significantly upregulated already at 3 days post-culture ($p = 0.0013$). Interestingly, also CASP3, which plays a key role in the execution-phase of cell apoptosis, showed a significantly higher expression at 7 days of culture ($p < 0.0001$).

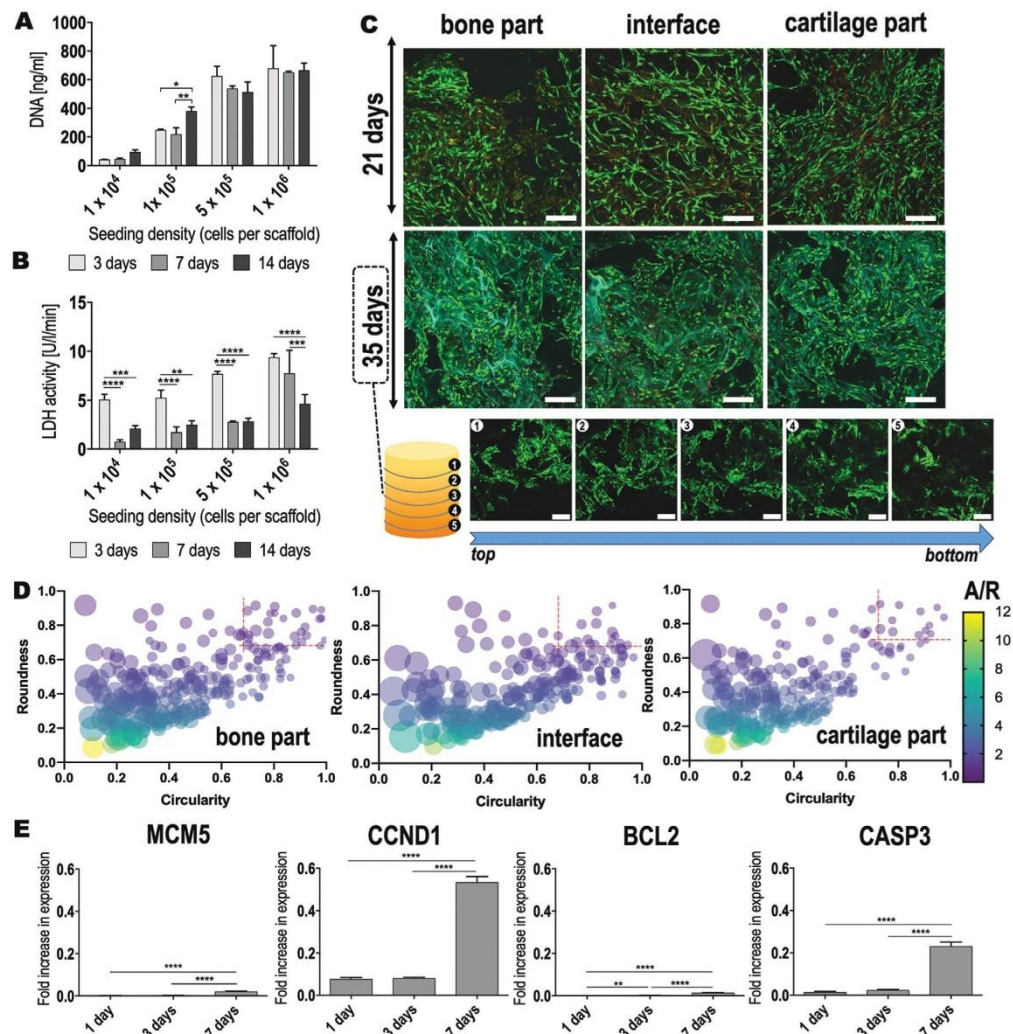


Figure 6. Biocompatibility of the chitosan-collagen-octacalcium phosphate scaffolds using hAMSCs. A) Cell proliferation and B) cell viability of hAMSCs seeded at different densities for up to 14 days of culture on the scaffolds. Two-way ANOVA followed by a Tukey's correction for multiple comparisons was performed. Obtained p values are indicated as follows: DNA $^{*}p = 0.0260$ and $^{**}p = 0.0065$; LDH activity $^{**}p = 0.0013$, $^{***}p \leq 0.0006$, and $^{****}p < 0.0001$. C) Calcein-AM/Propidium iodide live/dead staining performed in each specific zone of the scaffolds after 21 and 35 days of hAMSC culture (10^5 cells per scaffold). Calcein AM stains live cells green, while Propidium iodide stains dead cells red. Scale bar = 200 μm . After 35 days of culture, cell-seeded scaffolds were horizontally sectioned. Each piece (numbered from 1 to 5 in the scheme) was independently imaged in the confocal microscope. Thus, cell colonization in the entire scaffold can be appreciated. Scale bar = 200 μm . D) ImageJ analysis of the cell morphology performed for each specific zone of the scaffolds after 21 days of hAMSC culture. Circularity values of 1 indicate a perfect circle. Round objects also feature high roundness and low aspect-ratio (A/R) values. Over 200 cells were analyzed in each part of the scaffold. Cells that displayed circularity and roundness values between 0.7 and 1 were considered round. This range has been indicated in the graphs using red, discontinued lines. E) Expression of proliferation (MCM5 and CCND1) and apoptosis (BCL2 and CASP3) markers by hAMSCs seeded on the scaffolds (10^5 cells per scaffold) after different culture times. Results are normalized to the housekeeper TUBB. One-way ANOVA followed by a Tukey's correction for multiple comparisons was performed. Obtained p values are indicated as $^{**}p = 0.0013$ and $^{****}p < 0.0001$. Experiments were performed in triplicate (technical replicates = 3). Data are shown as mean value \pm standard deviation.

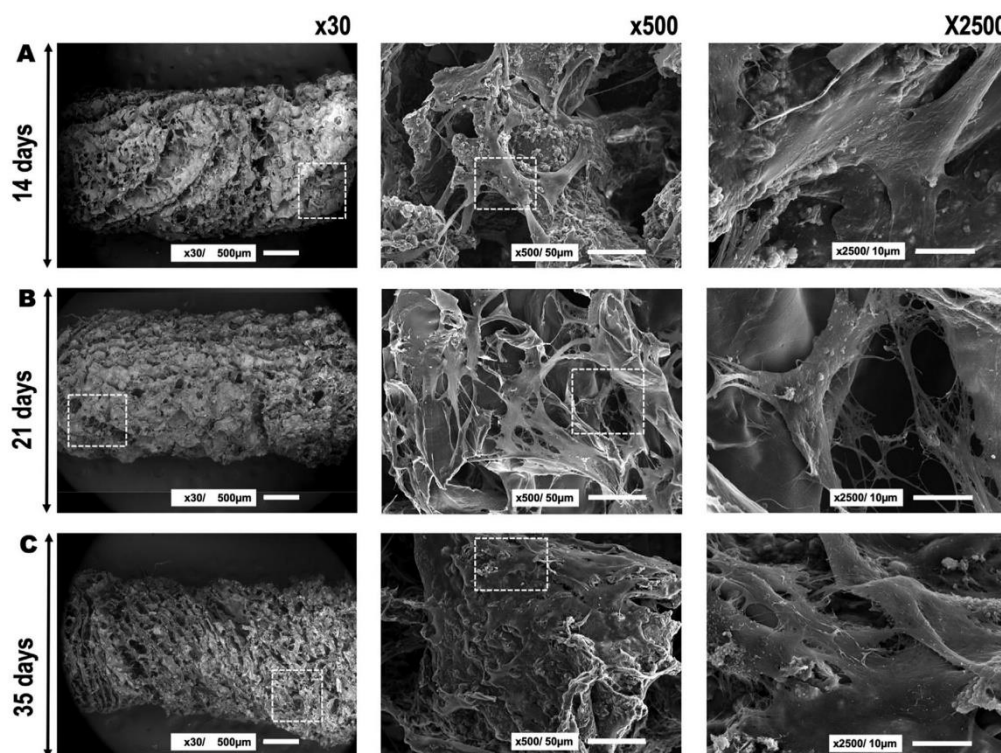


Figure 7. hAMSCs adhesion and morphology after seeding on the chitosan-collagen-octacalcium phosphate scaffolds at A) 14 days, B) 21 days, and C) 35 days of cell culture. The three different panels represent different magnifications used to analyze the samples (i.e., $\times 30$, $\times 500$, and $\times 2500$). From left to right, the boxed area indicates where the magnification was taken that is shown in the next panel.

3.5. Human Adipose-Derived Mesenchymal Stem Cells Colonized the Entire Scaffold Surface, Displayed Multiple Intercellular Connections and Produced Extracellular Matrix

SEM was applied to evaluate cell distribution and morphology after hAMSCs culture on the scaffolds (Figure 7A–C). Interestingly, pores on the scaffold surface appeared to be occupied at 21 and 35 days after culture (overview image taken at $\times 30$, left panel). At these observation times, more cellular material and ECM were visible (Figure 7B,C, image $\times 500$, center panel) that may be occluding the scaffold pores. Good cell distribution and attachment were observed at the scaffold surface. Cells were visible in the bony and cartilage layers of the scaffold. Additionally, the cell density appeared to increase after longer culture periods. Interestingly, at the cartilage area, the scaffold surface had a smooth and flat appearance in which cells were well attached (Figure 7B, $\times 500$, center panel). The morphology of the cells was elongated and abundant cell-cell contact could be observed (Figure 7B, $\times 500$ center panel and $\times 2500$ right panel). At the bony layer, cells were attached surrounded by mineral deposits on a

rougher surface (Figure 7A,C, $\times 500$ center panel). Ample mineral deposition could be observed for the bony layer in images taken at $\times 2500$ (Figure 7A,C, $\times 2500$ right panel). After 35 days of culture on the scaffolds, cells covered the entire scaffold, displaying multiple intercellular connections and ECM production.

3.6. Ionic Composition of the Extracellular Matrix at the Scaffold Bony and Cartilage Layers

SEM-EDS results are depicted for scaffolds without cells (Figure 8A, control scaffolds) and for scaffolds with cells after 14, 21, and 35 days of culture (Figure 8B–D). The bone and cartilage layers were analyzed independently. On the control scaffolds, OCP incorporation in the bony region was detectable, while no Ca or P was measurable in the cartilage region (Figure 8A). With increasing cell culture time, a higher percentage of Ca and of P was detectable for both the bone and cartilage areas. This was particularly noticeable for the bone layer of the scaffolds, featuring

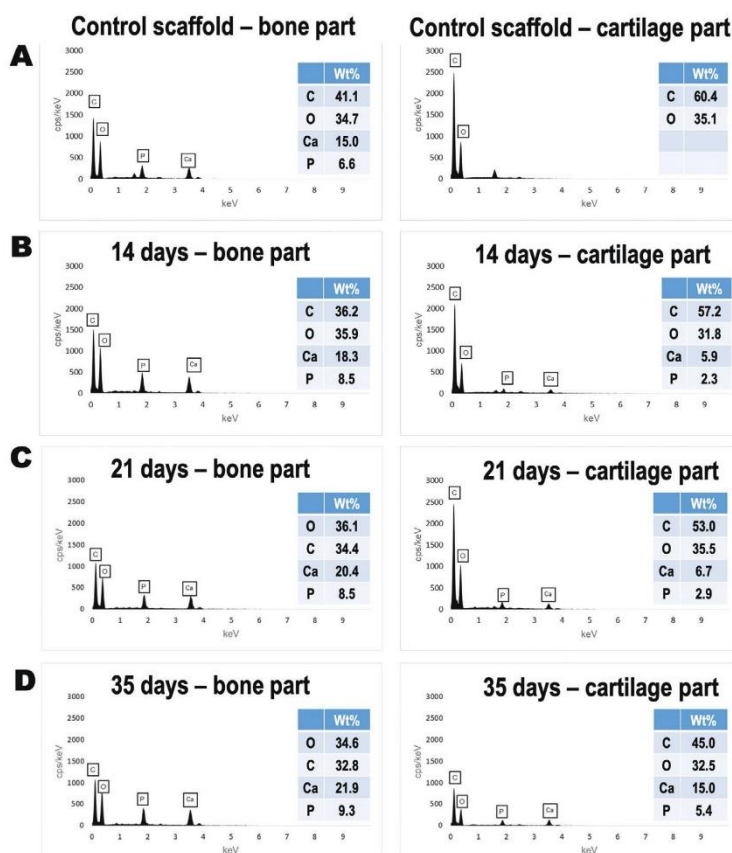


Figure 8. EDS elemental analysis performed for each independent zone of the scaffolds after hAMSCs culture. A) Results before cell culture. Results after B) 14 days, C) 21 days, and D) 35 days of cell culture. Values of wt% are tabulated for C, O, Ca, and P for each experimental condition analyzed.

the highest Ca and P percentages (21.9% and 9.3%, respectively, Figure 8D, left EDS spectrum).

3.7. Specific Differentiation of Human Adipose-Derived Mesenchymal Stem Cells Occurred That was Associated with the Scaffold Zones

All analyzed osteogenic markers showed an increased expression in hAMSCs seeded on the bony layer of the scaffolds (Figure 9A). Upregulation was observed for bone gamma-carboxyglutamate protein (BGLAP, $p = 0.0022$) at 14 days after culture. For the same time of observation, an increase on expression was detected for RUNX family transcription factor 2 (RUNX2) although not significant ($p = 0.0520$). Both, BGLAP and RUNX2 were upregulated at 21 days after culture ($p < 0.05$). Interestingly, collagen type I $\alpha 1$ chain (COL1A1) and collagen type III $\alpha 1$ chain (COL3A1)

expression reached a maximum level at 14 days after culture. Remarkably, secreted phosphoprotein 1 (SPP1) displayed a very early expression at 3 days after culture on the scaffolds. The SPP1 expression levels further increased at 21 days after culture ($p = 0.0190$). ALP activity was also evaluated as an indicator for osteogenesis. ALP increased over culture time, although this increment was not statistically significant (Figure 9B, $p > 0.05$).

SRY-box transcription factor 9 (SOX9) expression was evaluated to gain an insight in early chondrogenesis. Cells seeded on the cartilage layer of the scaffolds displayed a significant upregulation of SOX9 after 14 days of culture (Figure 9C, $p = 0.0005$). Later, at 21 days after culture, SOX9 expression significantly decreased ($p = 0.0022$), such that a peak was observed at 14 days. Other markers, including collagen type II $\alpha 1$ chain (COL2A1) and collagen type X $\alpha 1$ chain, showed expression up to 21 days of hAMSCs culture on the cartilage layer of the scaffolds. Interestingly, aggrecan (ACAN) displayed same levels of expression

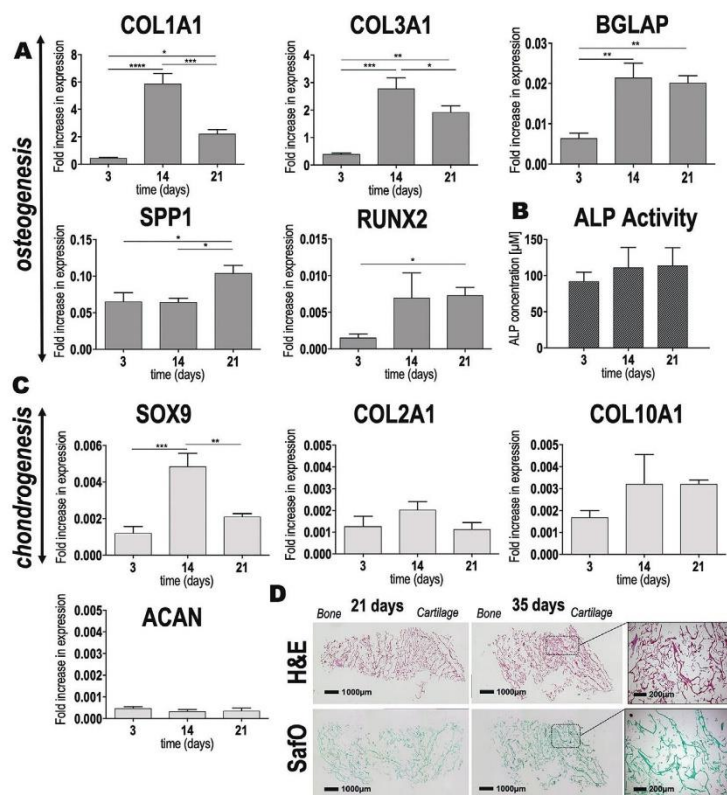


Figure 9. Spatial-specific gene expression and matrix deposition of hAMSCs after seeding on the chitosan-collagen-octacalcium phosphate scaffolds. A) Expression of osteogenic markers (COL1A1, BGLAP, SPP1, and RUNX2) and matrix-related fibrillar COL3A1 were assayed by qRT-PCR after 3, 14, and 21 days of hAMSC culture on the scaffolds. Results are normalized to the housekeeper TUBB. Obtained p values are indicated as $*p \leq 0.0418$, $**p \leq 0.0034$, $***p \leq 0.0007$, and $****p < 0.0001$. B) ALP activity as determined by colorimetric assay ($p > 0.05$). C) Expression of chondrogenic markers (SOX9, COL2A1, COL10A1, and ACAN) assayed by qRT-PCR after 3, 14, and 21 days of cell culture, was normalized to the housekeeper TUBB. Results showed statistical significance only for SOX9 ($**p = 0.0022$ and $***p = 0.0005$). D) H&E and Safo staining of the entire scaffold after extended culture time (i.e., 21 and 35 days of cell culture). Scale bar = 1000 μm . Dashed squares represent the area of the scaffolds where higher magnification images were taken. Scale bar = 200 μm . All data are shown as mean value \pm standard deviation. One-way ANOVA followed by a Tukey's correction was performed for multiple comparisons. Experiments were performed in triplicate (technical replicates = 3).

during the entire cell culture period. Safranin O (Safo) staining after 35 days of hAMSCs culture on the scaffolds revealed a more intense staining pattern when compared to earlier culture times (Figure 9D).

4. Discussion

Functional repair of soft-to-hard tissue transitions remains challenging in orthopedic surgery. Clinical options feature limitations, while current research strives to develop better solutions that are rapidly translatable into patient care. In this respect, the use of tissue-engineered scaffolds may be attractive for the treatment of osteochondral lesions. Generally, one of the problems when designing 3D scaffolds for tissue interfaces is that two dif-

ferent tissue types and the interface must be considered. Frequently, different materials are glued together to recreate individual layers that mimic the different tissue characteristics.^[5b] Such approach clearly presents the limitation of poor integration between the two layers.^[17] In fact, most previous studies present two-layer scaffolds for osteochondral repair^[18] that are obtained by combining individual parts for each specific tissue. Poor integration has been reported as one of the limitations of this combinatorial fabrication strategy.^[5b,17] Gao et al. and Chen et al. introduced the use of fibrin glue to combine a bony and a cartilage scaffold.^[19] Other studies recommend suturing or press fitting both layers.^[20] These studies relied on the eventual formation of ECM produced by the cells initially seeded on the scaffold layers to achieve biological integration. This may be a cumbersome,

hard-to-translate approach lacking proper integration of the bony and cartilage layers, in which the interface is barely considered. In the present study, we developed a single scaffold unit that was fabricated using biomaterial gradients. Our aim was to mimic the structure of articular cartilage and subchondral bone by tailoring the composite material and microstructure. Our scaffold design agrees with that reported by Levingstone et al.^[86,21] The authors developed a multi-layered collagen-based scaffold that was obtained by an iterative layering fabrication. They also considered a cartilage, interface, and bony layer. Our work and that of Levingstone et al. demonstrate that good integration and mechanical stability can be obtained by a layering fabrication approach. In fact, similarly to Levingstone et al., our scaffold did not show any delamination of the different layers during mechanical characterization. Obtained values for G' , G'' , δ , and G^* are within the range of collagen materials^[22] and other biopolymers often used for cartilage regeneration (e.g., alginate gels^[23] and hyaluronan^[24]). Nevertheless, mechanical properties of our scaffolds were found to be lower than those reported for native articular cartilage.^[22b] This is a common problem in scaffolds for cartilage engineering. One possibility will be incorporating proteoglycan-rich materials to the composite. They feature δ of 70° and may increase the typical collagen materials' δ of 3.6° to a more cartilage-like of $\approx 15^\circ$.^[22b] Inorganic compounds have been used with similar aim. The approach followed by Parisi et al. of introducing four different gradient zones using HA showed improved mechanics.^[25] We followed these ideas in that we used a biopolymer-ceramic composite rather than collagen alone. It may be also interesting to crosslink the matrix during fabrication. However, while crosslinking is known to increase matrix stiffness,^[22a] it has been well-documented that scaffolds with minimal crosslinking and low initial stiffness result in beneficial stimulation on the synthesis of cartilage-related molecules by cells.^[22a,26] Crosslinking has been also associated to toxicity.^[22a]

In addition to good integration and mechanical stability, osteochondral scaffolds should feature adequate porosity and biocompatibility.^[5b] Remarkably, porosity has been reported to highly impact cellular behavior in osteochondral constructs.^[27] Our scaffolds were porous, with the pore size ranging mostly from 75 to 240 μm throughout the entire length of the scaffold. Microscopy analysis showed highly interconnected pores. This may have led to the good cellular distribution and extensive cell-to-cell connections observed from 14 days onward. Larger pores were obtained in the cartilage layer of our scaffolds. Pan et al. studied the effect of scaffold porosity on osteochondral repair in vivo.^[27] The authors concluded that the scaffold with greater porosity and a larger pore size of the cartilage layer (i.e., 92% porosity, pores 200–300 μm) exhibited the best repair efficacy. Our results are in agreement with the results of Pan et al.^[27] Larger pores and greater porosity at the cartilage zone of our scaffolds supported good osteochondral features in vitro. To warrant biocompatibility, our scaffolds were designed to feature a material gradient including chitosan, collagen, and OCP. Both, collagen and chitosan are natural-origin biopolymers, highly biocompatible that present bone and cartilage ECM-like features.^[28] The chitosan-collagen-OCP scaffolds developed in our study were biocompatible, promoting good cell adhesion and proliferation. Our results are in agreement with Yan et al., who also demonstrated good cytocompatibility of MSCs with chitosan-collagen

porous scaffolds.^[29] In vivo, their scaffolds supported differentiation of seeded MSCs toward the desired pathway. For bone, to confer additional bone-like features to chitosan and chitosan-blends, diverse biomimetic coating approaches have been investigated. Tuzlakoglu et al.^[30] and Leonor et al.^[31] reported that bioglass spraying and calcium silicate immersion, respectively, enhanced biomimetic mineralization of resulting chitosan biomaterials. Levingstone et al.^[86,21] and Parisi et al.^[25] used HA in the bony layer of their collagen-based osteochondral scaffolds. In our study, we incorporated OCP particles into the chitosan-collagen blend to further improve bioactivity and biomimetic mineralization at the bone layer of the scaffolds. OCP features superior in vitro and in vivo osteogenic properties compared to HA and other inorganic materials.^[32] In vitro, it has been demonstrated that OCP promoted osteoblast differentiation and cell conversion to late osteocytes, while HA and beta-tricalcium phosphate did not.^[33] OCP can be highly resorbed by osteoclasts.^[34] In fact, OCP can be remodeled by new bone in vivo in contrast to HA. The latter is known to be present for years at the defect site.^[32,35] The in vivo superiority of OCP was first described in a pioneer study by Suzuki et al.^[36] The authors reported superior osteoconductive properties of OCP when compared to four different inorganic materials, that is di-calcium phosphate, amorphous calcium phosphate, Ca-deficient HA, and HA. The OCP material had the earliest time of new bone tissue deposition (i.e., 1 week post-implantation). In our study, by incorporating OCP in a gradual manner, bioactivity and mineral deposition increased at the bony end of the scaffolds. Interestingly, cell morphology also appeared to be impacted by the presence of OCP particles in the scaffolds. Expression of osteogenic genes, for example, RUNX2, COL1A1, BGLAP, and SPP1, also increased over time in the OCP-rich layer of the scaffolds. Similar osteogenic features have been reported by other authors for OCP biomaterials. Anada et al. observed an enhanced expression of COL1A1, ALPL, and SP7 in mouse bone marrow stromal cells upon stimulation on OCP coatings.^[37] Kouketsu et al. reported an increased level of RUNX2, COL1A1, BGLAP, and SPP1 in vivo at 4 weeks post-OCP implantation.^[38] Also relevant is the gene expression of cells at the osteochondral interface. Negligible COL2A1 and ACAN expression combined with high collagen type X $\alpha 1$ chain (COL10A1) expression have been reported for the interface area.^[39] Our results on gene expression coincide with these reports. Our osteochondral scaffold facilitated simultaneous expression of markers for differentiated and hypertrophic chondrocyte-like cells.

Limitations of our study are the lack of in vivo validation of the results observed in vitro. These experiments should be performed as part of the preclinical evaluation of this new biomaterial. Further composite optimization may be needed in order to achieve mechanic properties closer to that of the native tissue. Furthermore, an extended in-depth investigation should be conducted to characterize chondrogenesis at the cartilage layer. Importantly, no growth factor or other biologic was used in our study. The chitosan-collagen-OCP scaffolds displayed biocompatibility and specific tissue regeneration potential based solely on microstructural features and biomaterial combinations and gradients. This is advantageous for clinical applications. Growth factor-loaded scaffolds may pose high costs and present considerable side effects for the patients. However, it might be that such biologic is nevertheless needed to achieve robust

chondrogenesis. Furthermore, the chitosan-collagen-OCP scaffolds are produced as soft and flexible sponges of large size (>5 cm; sponge dimensions depend on the mold used during fabrication). The sponges are easy to sterilize and manipulate. Therefore, this offers the surgeon the possibility to cut out the exact size needed with a scalpel directly prior to implantation into the patient defect. No cost-intensive or complex patient-individual production would be required.

5. Conclusion

Collectively, our results demonstrate the feasibility of the multiphasic chitosan-collagen-OCP composite scaffold for osteochondral regeneration. We demonstrated the incorporation of OCP at the top of the bony layer, forming a diminishing gradient toward the cartilage zone, to be a successful approach for osteogenic induction in the bony layer. The porosity and pore size together with the higher concentration of collagen in the cartilage layer resulted stimulative for chondrogenesis. Based on this, we conclude that multiphasic scaffolds designed as a continuous, single unit using composites of materials and gradients thereof may be promising for osteochondral repair. Relevant aspects to consider are selecting materials that mimic the natural ECM of bone and cartilage and following an adequate scaffold design that allows the development of a mechanically and chemically stable scaffold, where the tissue interface is also considered. Moreover, specific pore size for each tissue zone is highly important and this should be carefully considered.

Supporting Information

Supporting Information is available from the Wiley Online Library or from the author.

Acknowledgements

E.A. thanks the TUM Graduate School for funding her research stay at the 3B's Research Group, University of Minho (Guimarães, Portugal). This work was supported by the Portuguese Foundation for Science and Technology (FCT) under the project "ChimericFibre4Tendon" PTDC/BII-BIO/28870/2017.

Conflict of Interest

The authors declare no conflict of interest.

Keywords

bones, cartilage, chitosan-collagen-octacalcium phosphate composites, multiphasic scaffolds, osteochondral differentiation

Received: September 23, 2020

Revised: November 19, 2020

Published online:

[1] R. Wittenauer, L. Smith, K. Aden, WHO Essential Medicines and Health Products Information Portal **2013**.


- [2] R. C. Lawrence, D. T. Felson, C. G. Helmick, L. M. Arnold, H. Choi, R. A. Deyo, S. Gabriel, R. Hirsch, M. C. Hochberg, G. G. Hunder, J. M. Jordan, J. N. Katz, H. M. Kremers, F. Wolfe, *Arthritis Rheum.* **2008**, *58*, 26.
- [3] a) S. J. Newberry, J. FitzGerald, N. F. SooHoo, M. Booth, J. Marks, A. Motala, E. Apaydin, C. Chen, L. Raaen, R. Shanman, P. G. Shekelle, in *Treatment of Osteoarthritis of the Knee: An Update Review*, AHRQ Publication, Rockville, MD **2017**; b) M. Hilgsmann, C. Cooper, F. Guillemin, M. C. Hochberg, P. Tugwell, N. Arden, F. Berenbaum, M. Boers, A. Boonen, J. C. Branco, B. Maria-Luisa, O. Bruyere, A. Gasparik, J. A. Kanis, T. K. Kvien, J. Martel-Pelletier, J. P. Pelletier, R. Pinedo-Villanueva, D. Pinto, S. Reiter-Niesert, R. Rizzoli, L. C. Rovati, J. L. Severens, S. Silverman, J. Y. Reginster, *Semin. Arthritis Rheum.* **2014**, *44*, 271; c) K. M. Jordan, N. K. Arden, M. Doherty, B. Bannwarth, J. W. Bijlsma, P. Dieppe, K. Gunther, H. Hauselmann, G. Herrero-Beaumont, P. Kalamani, S. Lohmander, B. Leeb, M. Lequesne, B. Mazieres, E. Martin-Mola, K. Pavelka, A. Pendleton, L. Punzi, U. Serni, B. Swoboda, G. Verbruggen, I. Zimmerman-Gorska, M. Dougados, *Ann. Rheum. Dis.* **2003**, *62*, 1145.
- [4] C. L. Camp, M. J. Stuart, A. J. Krych, *Sports Health* **2014**, *6*, 265.
- [5] a) E. Kon, G. Filardo, B. Di Matteo, F. Perdisa, M. Marcacci, *Bone Jt. Res.* **2013**, *2*, 18; b) P. Noeaid, V. Salih, J. P. Beier, A. R. Boccaccini, *J. Cell. Mol. Med.* **2012**, *16*, 2247.
- [6] S. Font Tellado, S. Chiera, W. Bonani, P. S. P. Poh, C. Migliaresi, A. Motta, E. R. Balmayor, M. van Griensven, *Acta Biomater.* **2018**, *72*, 150.
- [7] S. Baiguera, L. Urbani, C. Del Gaudio, *Biomed Res. Int.* **2014**, *2014*, 398069.
- [8] a) D. Clearfield, A. Nguyen, M. Wei, J. *Biomed. Mater. Res., Part A* **2018**, *106*, 948; b) T. Kumai, N. Yui, K. Yatabe, C. Sasaki, R. Fujii, M. Takenaga, H. Fujiya, H. Niki, K. Yudoh, *Int. J. Nanomed.* **2019**, *14*, 1283; c) T. J. Levingstone, E. Thompson, A. Matsiko, A. Schepens, J. P. Gleeson, F. J. O'Brien, *Acta Biomater.* **2016**, *32*, 149; d) A. Roffi, E. Kon, F. Perdisa, M. Fini, A. Di Martino, A. Parrilli, F. Salamanna, M. Sandri, M. Sartori, S. Sprio, A. Tampieri, M. Marcacci, G. Filardo, *Int. J. Mol. Sci.* **2019**, *20*, 2227; e) Y. J. Seong, I. G. Kang, E. H. Song, H. E. Kim, S. H. Jeong, *Adv. Healthcare Mater.* **2017**, *6*, 1700966.
- [9] S. M. Bittner, B. T. Smith, L. Diaz-Gomez, C. D. Hudgins, A. J. Melchiorri, D. W. Scott, J. P. Fisher, A. G. Mikos, *Acta Biomater.* **2019**, *90*, 37.
- [10] a) M. L. Lastra, M. S. Molinuevo, A. M. Cortizo, M. S. Cortizo, *Macromol. Biosci.* **2017**, *17*, 1600219; b) A. Oryan, S. Sahviah, *Int. J. Biol. Macromol.* **2017**, *104*, 1003; c) I. Y. Kim, S. J. Seo, H. S. Moon, M. K. Yoo, I. Y. Park, B. C. Kim, C. S. Cho, *Biotechnol. Adv.* **2008**, *26*, 1; d) S. M. Ahsan, M. Thomas, K. K. Reddy, S. G. Sooraparaju, A. Asthana, I. Bhatnagar, *Int. J. Biol. Macromol.* **2018**, *110*, 97.
- [11] a) X. L. Lu, V. C. Mow, *Med. Sci. Sports Exercise* **2008**, *40*, 193; b) H. Muir, *BioEssays* **1995**, *17*, 1039.
- [12] a) D. Algul, H. Sipahi, A. Aydin, F. Kelleci, S. Ozdatli, F. G. Yener, *Int. J. Biol. Macromol.* **2015**, *79*, 363; b) M. T. Islam, R. M. Felfel, E. A. Abou Neel, D. M. Grant, I. Ahmed, K. M. Z. Hossain, *J. Tissue Eng.* **2017**, *8*, <https://doi.org/10.1177/2041731417719170>; c) S. Lewin, A. Barba, C. Persson, J. Franch Serracanta, M. P. Ginebra, C. Ohman, *Biomed. Mater.* **2017**, *12*, 065005; d) G. Thirvikraman, A. Athirasala, C. Twohig, S. K. Boda, L. E. Bertassoni, *Dent. Clin. North Am.* **2017**, *61*, 835.
- [13] V. S. Komlev, I. V. Fadeeva, A. S. Fomin, L. I. Shvorneva, D. Ferro, *Dokl. Chem.* **2010**, *432*, 178.
- [14] a) A. P. Castro, P. Laity, M. Shariatzadeh, C. Wittkowske, C. Holland, D. Lacroix, *J. Mater. Sci.: Mater. Med.* **2016**, *27*, 79; b) I. Gonzalez de Torre, M. Santos, L. Quintanilla, A. Testera, M. Alonso, J. C. Rodriguez Cabello, *Acta Biomater.* **2014**, *10*, 2495.
- [15] T. Kokubo, H. Takadama, *Biomaterials* **2006**, *27*, 2907.
- [16] S. Schneider, M. Unger, M. van Griensven, E. R. Balmayor, *Eur. J. Med. Res.* **2017**, *22*, 17.

- [17] J. F. Mano, R. L. Reis, *J. Tissue Eng. Regener. Med.* **2007**, *1*, 261.
- [18] a) G. Z. Jin, J. Kim, J. H. Park, S. J. Seo, J. H. Kim, E. J. Lee, H. W. Kim, *Tissue Eng., Part C* **2014**, *20*, 895; b) K. Schutz, F. Despang, A. Lode, M. Gelinsky, *J. Tissue Eng. Regener. Med.* **2016**, *10*, 404.
- [19] a) J. Chen, H. Chen, P. Li, H. Diao, S. Zhu, L. Dong, R. Wang, T. Guo, J. Zhao, J. Zhang, *Biomaterials* **2011**, *32*, 4793; b) J. Gao, J. E. Dennis, L. A. Solchaga, A. S. Awadallah, V. M. Goldberg, A. I. Caplan, *Tissue Eng.* **2001**, *7*, 363.
- [20] a) N. H. Dormer, K. Busaidy, C. J. Berkland, M. S. Detamore, *J. Oral Maxillofac. Surg.* **2011**, *69*, e50; b) D. Schaefer, I. Martin, G. Jundt, J. Seidel, M. Heberer, A. Grodzinsky, I. Bergin, G. Vunjak-Novakovic, L. E. Freed, *Arthritis Rheum.* **2002**, *46*, 2524; c) C. Scotti, D. Wirz, F. Wolf, D. J. Schaefer, V. Burgin, A. U. Daniels, V. Valderrabano, C. Candrian, M. Jakob, I. Martin, A. Barbero, *Biomaterials* **2010**, *31*, 2252.
- [21] T. J. Levingstone, A. Matsiko, G. R. Dickson, F. J. O'Brien, J. P. Gleeson, *Acta Biomater.* **2014**, *10*, 1996.
- [22] a) C. R. Lee, A. J. Grodzinsky, M. Spector, *Biomaterials* **2001**, *22*, 3145; b) C. J. Little, N. K. Bawolin, X. Chen, *Tissue Eng., Part B* **2011**, *17*, 213; c) H. Mori, K. Shimizu, M. Hara, *Mater. Sci. Eng. C* **2013**, *33*, 3230.
- [23] H. A. Awad, M. Q. Wickham, H. A. Leddy, J. M. Gimble, F. Guilak, *Biomaterials* **2004**, *25*, 3211.
- [24] J. L. Vanderhooff, M. Alcoutlabi, J. J. Magda, G. D. Prestwich, *Macromol. Biosci.* **2009**, *9*, 20.
- [25] C. Parisi, L. Salvatore, L. Veschini, M. P. Serra, C. Hobbs, M. Madaghiele, A. Sannino, L. Di Silvio, *J. Tissue Eng.* **2020**, *11*, <https://doi.org/10.1177/2041731419896068>.
- [26] S. M. Vickers, L. S. Squitieri, M. Spector, *Tissue Eng.* **2006**, *12*, 1345.
- [27] Z. Pan, P. Duan, X. Liu, H. Wang, L. Cao, Y. He, J. Dong, J. Ding, *Regener. Biomater.* **2015**, *2*, 9.
- [28] a) X. Liu, C. Zheng, X. Luo, X. Wang, H. Jiang, *Mater. Sci. Eng. C* **2019**, *99*, 1509; b) B. Sultankulov, D. Berillo, K. Sultankulova, T. Tokay, A. Saparov, *Biomolecules* **2019**, *9*, 470.
- [29] F. Yan, W. Yue, Y. L. Zhang, G. C. Mao, K. Gao, Z. X. Zuo, Y. J. Zhang, H. Lu, *Neural Regener. Res.* **2015**, *10*, 1421.
- [30] K. Tuzlakoglu, R. L. Reis, *J. Mater. Sci.: Mater. Med.* **2007**, *18*, 1279.
- [31] I. B. Leonor, E. T. Baran, M. Kawashita, R. L. Reis, T. Kokubo, T. Nakamura, *Acta Biomater.* **2008**, *4*, 1349.
- [32] O. Suzuki, in *Octacalcium Phosphate Biomaterials: Understanding of Bioactive Properties and Applications*, (Eds: O. Suzuki, G. Insley), Woodhead Publishing, Sawston, United Kingdom **2019**, Ch. 1, p. 1.
- [33] Y. Sai, Y. Shiwaku, T. Anada, K. Tsuchiya, T. Takahashi, O. Suzuki, *Acta Biomater.* **2018**, *69*, 362.
- [34] H. Imaizumi, M. Sakurai, O. Kashimoto, T. Kikawa, O. Suzuki, *Calcif. Tissue Int.* **2006**, *78*, 45.
- [35] B. Liu, D. X. Lun, *Orthop. Surg.* **2012**, *4*, 139.
- [36] O. Suzuki, M. Nakamura, Y. Miyasaka, M. Kagayama, M. Sakurai, *Tohoku J. Exp. Med.* **1991**, *164*, 37.
- [37] T. Anada, T. Kumagai, Y. Honda, T. Masuda, R. Kamijo, S. Kamakura, N. Yoshihara, T. Kuriyagawa, H. Shimauchi, O. Suzuki, *Tissue Eng., Part A* **2008**, *14*, 965.
- [38] A. Kouketsu, K. Matsui, T. Kawai, Y. Ezoe, T. Yanagisawa, A. Yasuda, T. Takahashi, S. Kamakura, *J. Tissue Eng. Regener. Med.* **2020**, *14*, 99.
- [39] K. Chen, T. K. Teh, S. Ravi, S. L. Toh, J. C. Goh, *Tissue Eng., Part A* **2012**, *18*, 1902.

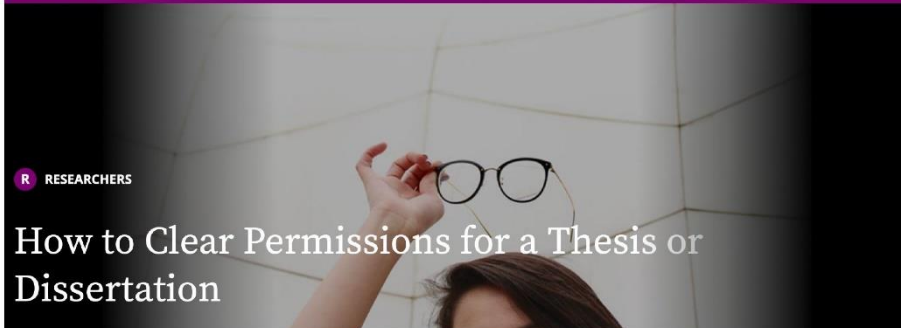
Advance Healthcare Materials permit for reuse

WILEY

THE WILEY NETWORK | INSTRUCTORS & STUDENTS | JOURNAL EDITORS | LIBRARIANS | PROFESSIONALS | **RESEARCHERS** | SOCIETY LEADERS

TOPICS ▾ CONTENT TYPE ▾ 

THE WILEY NETWORK / RESEARCHERS / LATEST CONTENT / HOW TO CLEAR PERMISSIONS FOR A THESIS OR DISSERTATION



R RESEARCHERS

How to Clear Permissions for a Thesis or Dissertation

Leah Alaani, Marketing Manager, Wiley | November 16, 2020

So, you're ready to finish your thesis...

The time has come. You've done the research; you've written the dissertation. You're gearing up to defend your work and your right to scholarly achievement.

But wait: in addition to some last-minute citation formatting, there's one more box you need to tick as you finalize your manuscript. You need to clear permissions.

What are permissions?

Every good scholar knows how to cite her sources. But in cases where someone else's work is directly copied or quoted at length—even with an accurate citation – you may need a license that grants you the legal right to reproduce another person's intellectual property.

The reuse of intellectual property is protected by law. Content creators need to formally request permission to republish or otherwise reuse existing content in new works. This applies to all types of new content, including theses and dissertations. Make sure that you review your manuscript for any quoted content, third-party charts or graphs, and other elements that you have incorporated from existing intellectual property.

When a citation is not enough

Visual content (photographs, videos, images, tables, or charts) will almost always require a formal request for permission in addition to citation. Quoted or excerpted text is less straightforward, and legal requirements differ between countries and regions.

If you're unsure about the legal requirements for permissions clearance in your country, or about your institution's policies, check with your institution's library for resources and guidance.

Wanted: rights holder

Once you've identified the content that will need a reuse license, you'll need to submit requests to the rights holder of each piece of intellectual property and ask them to grant permission for you to use this content in your work.

The rights holder could be the author or the publisher of the content. The rights holder will be specified in the copyright line of a publication. You can also find rights holder information by searching through the [Copyright Clearance Center](#).

Reusing Wiley content

If you're reusing Wiley content in your thesis or dissertation, rights will be granted at no cost to you if the content meets these requirements:

- **Your thesis or dissertation is not being used for commercial purposes.** This means that you're submitting it only for graduation requirements. You don't currently have a deal with a commercial publisher, and you won't otherwise be benefitting financially from the publication of your thesis.
- **Wiley is the rights holder of the content you are seeking to reuse.** Usually, Wiley holds the rights to our content, but occasionally the rights holder will be an author or sponsoring organization. In those cases, Wiley cannot guarantee free reuse.

While Wiley does grant free reuse of content in thesis and dissertation projects, we do still require a record of use so that we can issue you a license agreement.

If you publish your thesis or dissertation through a commercial publisher in the future, you will need to reapply for commercial reuse licenses. The legal rights granted for content reuse in non-commercial publications, such as a thesis or dissertation, are different from the rights required by commercial publishers to legally republish third-party content.

Do I need to request permission to use my own work as my dissertation?

If you are the author of a published Wiley article, you have the right to reuse the full text of your published article as part of your thesis or dissertation. In this situation, you do not need to request permission from Wiley for this use.

If your institution still requires a reuse license in this case, follow the steps below to request your license via RightsLink.

Request permission from Wiley

To request a reuse license, our partner RightsLink is a great place to start. You can request thesis and dissertation permissions through [RightsLink Marketplace](#).

You can also find a link to a RightsLink permissions request form at the point of content on Wiley Online Library. Watch the video below to see how.

If your institution still requires a reuse license in this case, follow the steps below to request your license via RightsLink.

Request permission from Wiley

To request a reuse license, our partner RightsLink is a great place to start. You can request thesis and dissertation permissions through [RightsLink Marketplace](#).

You can also find a link to a RightsLink permissions request form at the point of content on Wiley Online Library. Watch the video below to see how.